DAMAGE DETECTION IN COMPOSITE MATERIALS USING ACOUSTIC EMISSION AND SELF-SENSING FIBRES

by

DAVID JOHN COLLINS

A thesis submitted to The University of Birmingham for the degree MRes in the Science and Engineering of Materials

Department of Metallurgy and Materials
School of Engineering
The University of Birmingham

February 2009

ABSTRACT

The primary objective of this study was to investigate the abilities of acoustic emission testing and self-sensing fibres to detect damage in composite materials. This was achieved by performing acoustic emission testing on fibre samples and resin samples during tensile tests. In parallel to the acoustic emission testing the changes in strain for the resin samples was recorded using electrical resistance strain gauges and fibre Bragg gratings. Acoustic emission testing of Self-sensing fibre composites allowed the recorded changes in the light intensity transmitted by the fibres to be analysed in conjunction with the acoustic emission data.

The fabrication of the three different sample types is presented as is the installation of the electrical resistance strain gauges and fibre Bragg gratings. The experimental procedure and method of data capture is detailed for tensile and acoustic emission testing, strain data and Self-sensing fibre data.

The fabrication and testing of the samples was performed successfully. The testing procedure and analysis of results demonstrates the accurate use of acoustic emission and the potential of self-sensing fibres in detecting damage in composite materials.

DEDICATIONS

My parents have been incredible in supporting me through my writing up period. I love them both very much and will forever be thankful for all they have done for me - Diolch yn fawr iawn.

As a student and now an alumnus of the University of Birmingham I am happy to say that I am honoured to have spent 5 years of my life studying at the University. Many of my friends studied Sports and Material Science and have always been helpful throughout my studies.

The University of Birmingham Rugby Football Club – UBRFC is full of great people who ensured my time at the University was exceptional. The rugby club provided me and all of its members an overwhelming pride to be part of the University and like them I will always say “I love my Birmingham.”

ACKNOWLEDGEMENTS

It was a pleasure to work as part of the Sensors and Composites group and I am grateful to Professor Gerard Fernando who provided me with the opportunity to conduct my research and work with the members of the group. Further thanks to Prof. Fernando who guided me through all stages of my work and offered constant support. His passion for the subject was demonstrated in the lectures of my final year of undergraduate study and it was amazing to see his enthusiasm and dedication continue on every occasion since.

My fellow student colleagues Shoaib Malik and Jon Burns worked with me in the laboratory for long periods and provided help and guidance throughout my studies. It was a pleasure to work with them.

I could not have completed my research without Dr Frank Biddlestone and Dr Ronsheng Chen who taught me how to use all the required equipment and were always available and happy to provide further help and valuable advice.

All the members of the Sensors and Composites group provided an input into my research whether it was in the laboratory or in the office. I am thankful for the help and enjoyment they provided as part of the research group.

TABLE OF CONTENTS

Chapter	Title	Page
-	Title Page	
-	Abstract	
-	Dedications	
-	Acknowledgements	
1.0	**INTRODUCTION**	**1**
1.1	Application of Composites	**1**
1.2	General Structure	**2**
1.3	Fibre and Matrix Properties	**2**
1.3.1	Fibre Properties	**2**
1.3.2	Matrix Properties	**4**
1.4	Damage in Composites	**7**
1.4.1	Matrix Cracking	**7**
1.4.2	Fibre Fracture	**7**
1.4.3	Delamination	**8**
1.4.4	Fibre Debonding / Fibre Pullout	**8**
2.0	**AIMS AND OBJECTIVES**	**9**
3.0	**LITERATURE REVIEW**	**10**
3.1	Damage Detection	**10**

3.2	Optical Fibres	**10**
3.2.1	Fibre Bragg Gratings	**11**
3.2.2	Extrinsic Fabry-Perot Interferometer (EFPI) Sensors	**14**
3.2.3	Optical Fibre Heat Emission	**16**
3.2.4	Intensity Modulated Fibre Optics	**18**
3.3	X-Radiography	**18**
3.4	Ultrasonic, C-Scans	**19**
3.5	Thermography / Infra-Red Imaging	**21**
3.6	Laser Shearography	**22**
3.7	Electrical Resistance	**24**
3.8	Electrical Conductivity Mapping	**25**
3.9	Potential Difference: Direct Current (D.C) Monitoring	**26**
3.10	Acoustic Emission	**28**
3.11	Piezoelectric	**32**
3.12	Self-Sensing Fibres	**34**
3.13	Literature Review Conclusion	**38**
4.0	**METHODOLOGY**	**39**
4.1	Mould Fabrication	**39**
4.1.1	Mould Preparation	**40**
4.2	Resin Sample Fabrication	**40**
4.2.1	Scotchweld Resin Samples	**41**
4.2.2	Epo Tek 305 Samples	**42**

4.2.3	Epo Tek 310M Samples	**42**
4.2.4	Epo Tek 314 Samples	**43**
4.3	End Tabbing	**44**
4.3.1	Resin Samples	**44**
4.3.2	Top-Hat End-Tabs	**44**
4.4	Fibre Samples	**45**
4.4.1	Acoustic Emission Testing	**45**
4.4.2	Self-Sensing Fibre Testing	**47**
4.5	Electrical Resistance Strain Gauge Bonding	**50**
4.6	Fibre Bragg Grating Installation	**53**
4.7	Self-Sensing Composite Samples Fabrication	**54**
5.0	**EXPERIMENTAL PROCEDURE**	**56**
5.1	Tensile Testing	**56**
5.1.1	Fibre Samples	**56**
5.1.2	Resin Samples	**57**
5.2	Acoustic Emission Testing	**58**
5.3	Strain Measurements	**58**
5.3.1	Electric Strain Gauge Data Acquisition	**58**
5.3.2	Fibre Bragg Grating Data Acquisition	**59**
5.4	Self-Sensing Fibres and Composites	**59**
6.0	**RESULTS AND DISCUSSION**	**60**

6.1	Fibre Samples	**60**
6.1.1	Mechanical Testing Results: Load vs. Extension	**60**
6.1.2	Acoustic Emission Results	**63**
6.1.3	Summary of Fibre Sample Results	**66**
6.2	Resin Samples	**68**
6.2.1	Mechanical Testing Results: Stress vs. Strain	**68**
6.2.2	Electrical Resistance Results	**73**
6.2.3	Fibre Bragg Grating Strain Results	**76**
6.2.4	Acoustic Emission Results	**81**
6.2.5	Summary of Results for Resin Samples	**84**
6.3	Composite Samples	**86**
6.3.1	Mechanical Testing Results: Stress vs. Strain	**86**
6.3.2	Acoustic Emission Results	**89**
6.3.3	Summary of Results for Composite Samples	**91**
6.4	Self Sensing Fibre Results	**93**
6.4.1	Self Sensing Fibre Analysis	**93**
6.4.2	Self-Sensing Fibre Images	**94**
7.0	**CONCLUSION**	**98**
8.0	**FUTURE WORK**	**100**
9.0	**APPENDICIES**	**101**
Appendix 1	Finite element modelling of fibre Bragg grating strain sensors and experimental validation.	**101**
10.0	**LIST OF REFERENCES**	**115**

LIST OF FIGURES

Figure	Title	Page
1	A schematic illustration of a Bragg grating on an optical fibre.	**11**
2	A schematic drawing of an extrinsic Fabry-Perot interferometric sensor (Leng & Asundi 2003).	**14**
3	A schematic drawing of an extrinsic Fabry-Perot interferometer sensor (www.netcomposites.com, 2007)	**15**
4	An image of heat loss using the optical fibre heat emission technique (Pevzner *et al.* 2005).	**17**
5	A schematic diagram of a Laser Shearography setup (Toh *et al*. 1990).	**23**
6	The use of silver paint to attach electrodes to a composite specimen.	**24**
7	An acoustic emission signature.	**29**
8	A cross-sectional view of a typical piezoelectric sensor.	**33**
9	Dimensions of the resin dog-bone samples.	**39**
10	Completed silicone mould ready for resin sample fabrication.	**40**
11	Locations that dimensions of the resin were recorded.	**41**
12	A cured Scotchweld Resin sample ready for testing.	**41**
13	A cured Epo Tek 305 Resin sample with attached strain gauge.	**42**
14	A cured Epo Tek 310M Resin sample ready for testing.	**42**
15	A cured Epo Tek 314 Resin sample with attached strain gauge.	**43**
16	Schematic illustration indicating the dimensions of the top-hat end tab.	**44**
17	The setup used to fabricate carbon and uncoated E-glass samples for Acoustic Emission testing.	**45**
18	A carbon sample ready for Acoustic Emission testing.	**46**

19	An uncoated E-glass sample ready for Acoustic Emission testing.	**46**
20	The wooden jig used for fabrication of uncoated E-glass and small diameter optical fibres.	**48**
21	A small diameter optical fibre sample ready for self-sensing testing.	**49**
22	Electrical contacts and electric strain gauge in formation for transfer to resin sample at x25 magnification.	**50**
23	Schematic of a generic resin sample with dimensions and locations of the electrical resistance strain gauge and fibre Bragg grating.	**52**
24	An attached Fibre Bragg Grating indicated by the arrows, running parallel to the electric strain gauge at x25 magnification.	**53**
25	A cross section and dimensions of the silicone mould used to fabricate the self-sensing samples.	**54**
26	A carbon fibre sample inserted into the load cells ready for tensile testing.	**56**
27	Load vs. extension graph for a carbon fibre sample.	**60**
28	Load vs. extension graph for an un-coated E-glass fibre sample.	**61**
29	Load vs. extension graph for a small-diameter optical fibre sample.	**61**
30	The maximum loads of fibre samples during tensile testing.	**66**
31	The amplitude of acoustic emission hits for fibre samples during tensile testing.	**67**
32	The average frequency of acoustic emission hits for fibre samples during tensile testing.	**67**
33	Load vs. Extension graph for a Scotchweld resin sample.	**68**
34	Load vs. Extension graph for a 305 resin sample. The horizontal regions represent the time when the extension was paused to record strain values.	**69**
35	Load vs. Extension graph for a 310M resin sample.	**69**

36	Load vs. Extension graph for a 314 resin sample. The horizontal regions represent the time when the extension was paused to record strain values.	**70**
37	Strain recordings for tensile testing of 305 resin sample.	**73**
38	Strain recordings for tensile testing of 310M resin sample.	**73**
39	Strain recordings for tensile testing of 314 resin sample.	**74**
40	The changes in FBG peak shift for Epo Tek sample 314_04 before and during tensile testing.	**76**
41	The changes in FBG peak shift for Epo Tek sample 310_03 before and during tensile testing.	**77**
42	A comparison between electrical strain resistance gauges and Fibre Bragg Grating strain recordings for Epo Tek 305 samples.	**78**
43	A comparison between electrical strain resistance gauges and Fibre Bragg Grating strain recordings for Epo Tek 310M samples.	**78**
44	A comparison between electrical strain resistance gauges and Fibre Bragg Grating strain recordings for Epo Tek 314 samples.	**79**
45	The maximum load applied for resin samples during tensile testing.	**84**
46	The amplitude of acoustic emission hits for resin samples during tensile testing.	**85**
47	The average frequency of acoustic emission hits for resin samples during tensile testing.	**85**
48	Stress vs. strain graph for a small diameter optical fibre / 305 resin composite sample.	**86**
49	Stress vs. strain graph for a small diameter optical fibre / 310M resin composite sample.	**87**
50	The maximum load applied for composite samples during tensile testing.	**91**
51	The amplitude of acoustic emission hits for composite samples during tensile testing.	**92**

52	The average frequency of acoustic emission hits for composite samples during tensile testing.	**92**
53	The change in normalised light intensity with a changing load during tensile testing.	**93**
54	The initial image captured with the first AE hit for sample SDO_4.	**94**
55	Image 6900 captured when maximum load was achieved during tensile testing of for sample SDO_4.	**95**
56	Image 15748 captured when 3.00 mm extension was achieved and the last image captured for sample SDO_4.	**95**

LIST OF TABLES

Table	Title	Page
1	Mechanical properties of specified fibre types. (Hull & Clyne, 1996)	**4**
2	Mechanical properties of different matrix types. (Hull & Clyne, 1996)	**6**
3	A list of Acoustic Emission terminology.	**30**
4	The resin and fibre contents of the self-sensing composites.	**54**
5	The loads at which samples were held to record strain values during tensile testing.	**57**
6	A list of extension rates that were used for self-sensing samples during tensile tests.	**59**
7	A comparison of the average mechanical testing values for the fibre samples.	**62**
8	A comparison of the acoustic emission parameters for fibre samples.	**63**
9	The change in the average Secant moduli for Scotchweld samples during tensile testing.	**68**
10	A comparison of the average mechanical testing values for the resin samples.	**70**
11	A comparison of further mechanical testing values for the resin samples.	**70**
12	A comparison of the Acoustic Emission parameters for the resin samples.	**81**
13	A comparison of the average mechanical values for the composite samples.	**87**
14	A comparison of further mechanical values for the composite samples.	**88**
15	A comparison of the Acoustic Emission parameters for the composite samples.	**89**
16	The average change in light intensity compared to the change in load and duration of the tensile test for the SDO fibre samples.	**94**

1.0 INTRODUCTION

1.1 Application of Composites

The use of composite materials has seen a remarkable increase in recent years. The major advantages of fibre reinforced polymer composites is their specific properties, in particular the specific strength and specific stiffness. It is these properties that have seen their extensive use in the aeronautical, aerospace and sports equipment industries become dominated by composite materials.

Since 1970, the aerospace industry has seen a rise in the use of composites in civil aircraft from 1 % to an estimated 50 % in 2010. Military aircrafts such as the American F-35 are made from 45 % composite material (http://ir.gknplc.com, 2007). Composite use in the sports sector has developed into nearly all sports including archery cycling, fishing, golf, tennis, squash and skiing. Marin have constructed a racing bike predominantly made from composite that weighs 7 Kg, considerably less than similar bikes constructed from metallic alloys. The design requirements of golf clubs require high bending and torsional stiffness and strength, lightweight, optimal weight distribution and damping effects. Millions of golf clubs have been made from composites all around the world to satisfy these design requirements resulting in the replacement of metallic clubs (Harris, 1999 & McConnell, 2000).

The ability to detect damage in composites is a major disadvantage of using composites as load bearing applications or applications where safety is paramount.

1.2 General Structure

The general structure of fibre reinforced composites can be divided into three parts: reinforced fibres, matrix resin and an interfacial region that joins the fibre and resin. By altering the types and ratios of fibre and matrices the properties of the composite can be tailored to match the requirements of the end user.

1.3 Fibre and Matrix Properties

1.3.1 Fibre Properties

Carbon, glass and aramid fibres are the main fibres used in polymer matrix composites; Table 1 provides a summary of mechanical properties for different fibre types covered in this section. The choice of fibre and its specific properties are designed to complement a specific matrix, the addition of fibres in different volumes allows composites to be customised for specific applications.

Carbon fibres can be split into three categories depending on their production method: Polyacrylonitrile (PAN) fibres, Mesophase pitch and Pyrolytic deposition. The majority of commercially used fibres are produced from the PAN method developed in Farnborough, UK by Rolls-Royce and the Royal Aircraft Establishment from 1966-67 (Dunham & Edie, 1992).

PAN based carbon fibres exhibit a higher tensile strength but a lower moduli than mesophase pitch based carbon fibres (Edie, 1997). Mesophase pitch based carbon fibres are suited more to use in high temperature applications. Fibres manufactured by pyrolitic deposition tend to be of

short length and varying diameters, because of these issues these fibres have found little use in commercial applications. Carbon fibres have the disadvantage of lower impact strength than aramid and glass fibres but have a higher fatigue resistance (Hull & Clyne, 1996).

"Glass fibres are the most used reinforced material in structural reinforced thermoplastics" (Giraldia *et al*, 2005). Glass fibres are based on silica (SiO_2) with additions of oxides such as calcium and sodium. E-glass (electrical) fibres are the most commonly used and have good strength, stiffness and electrical properties. C-glass (corrosive) fibres have less strength but are better suited to corrosive environments whilst S-glass (strength) fibres have higher strength than E-glass they have a higher price (Hull & Clyne, 1996). General advantages of fibre glass include low cost, high tensile strength, high chemical resistance and excellent insulating properties (Nam-Jeong & Jang 2000).

Organic fibres are considered the most important high modulus fibres and were developed from aromatic polyamides and are called aramid fibres. The disadvantage of aramid fibres is the low compressive strength but this is outweighed by the advantages. Aramid fibres have a low density and a high tensile strength in the range of 2-3 GPa (Meier, 1995).

A Self-senesing fibre is a fibre that is used as a reinforcing fibre that can also be used as a light guide; they are also referred to as reinforcing fibre light guides (RFLG). Reinforcing fibre types such as E-glass and Quartz have the ability to transmit light whilst utilising their specific fibre properties in their required application.

The name Self-sensing fibres was coined when it was proved that the fracture of E-glass fibres could be tracked in real time by monitoring the transmitted light intensity (Kister *et al.* 2003).

	Property			
Type of Fibre	Tensile Strength	Relative Density	Youngs Modulus	Failure Strain
	GPa	Kg/m^3	GPa	%
Carbon HS	3.5	1.8	220-240	1.5-2.2
Carbon HM	3.5	1.8	290-300	1.3-2.0
Carbon UHM	3.4-5.5	2.0	350-450	0.7-1.0
Aramid	2.0-3.0	1.4	60	4.4
Kevlar	3.0	1.5	130	2.3
E-glass	2.4	2.6	73	3.0
S-glass	3.4	2.5	86	3.9

HS: High Strength
HM: High Modulus
UHM: Ultra High Modulus

Table 1: Mechanical properties of specified fibre types. (Hull & Clyne, 1996)

1.3.2 Matrix Properties

Matrix materials for polymer composites can be broken down into two groups thermoplastics and thermosetting resins, both have been widely used as matrices in high performance composite applications (Meyer *et al.* 1995). The important difference between the two materials is where the forming and the shaping of the thermosetting plastic take place in a simultaneous irreversible chemical reaction. Whereas thermoplastics have the advantage of being able to be softened and shaped when heated, if necessarily the process can be repeated without chemical degradation (Ford, 2004)

Thermosetting epoxy resins are the preferred choice of matrix material in polymer matrix composites opposed to other thermosets such as polyesters or vinyl esters. Thermosets are produced when a liquid resin is turned into a solid by chemical cross-linking which cures into a tightly bound three dimensional network resulting in a solid (Neffgen, 1985). The mechanical properties depend on the length of chains and the density of cross-links. Epoxies have good resistance to heat distortion and shrink less during curing than other thermosets; they can also be semi-cured allowing pre-pregs to be made (Mimura & Ito, 2002).

The disadvantages of thermosetting resins are high moisture absorption and brittleness (Feldman, 1990 & Stenzenberger, 1993). Thermosets have the advantage of a much greater resistance to solvents than thermoplastics and are commonly used because of their simple processing abilities and excellent mechanical properties (Meyer *et al*. 1995).

The thermoplastic Poly-ether-ether-ketone (PEEK) has found extensive use in aeronautical applications and a variety of structures when in a composite containing carbon fibres (Rae *et al*. 2007). PEEK has a high chemical resistance and high fracture toughness even at elevated temperatures; these properties make PEEK a desirable material for load bearing applications (Zhang *et al.* 2004) .

Advantages of thermoplastics include good stiffness, toughness and good impact absorbance (Belbin, 1985). The high viscosity of thermoplastics is a disadvantage as it decreases the ability to impregnate fibres whilst laying up composites (Gabriel *et al.* 1995) Table 2 details properties for two thermosetting resins and two thermoplastic resins.

	Property			
Type of Matrix	Tensile Strength	Relative Density	Youngs Modulus	Failure Strain
	MPa	Kg/m^3	GPa	%
Thermosetting				
Epoxy	40-80	1.1-1.4	2.0-5.0	1.0-20.0
Polyester	40-90	1.2-1.5	2.0-4.5	2.0
Thermoplastic				
PEEK	90-170	1.26-1.32	3.6	50
Polypropylene	20-40	0.9	1.0-1.4	300

Table 2: Mechanical properties of different matrix types. (Hull & Clyne, 1996)

1.4 Damage in Composites

The following sections provide a brief overview of the different types of damage in composites.

1.4.1 Matrix Cracking

Matrix cracking is the regularly the initial mode of failure and if severe enough will lead to delamination of the plies and eventual failure of the laminate. Although matrix cracking is very localised it can be very difficult to detect (Lafarie-Frenot *et al.* 2001). The energy required for matrix cracking is relatively low, for a brittle carbon / epoxy composite the energy needed could be as low as several hundred J/m^2 (Cantwell & Morton, 1992).

1.4.2 Fibre Fracture

It is commonly known that at the point of fibre fracture during loading the composite material will generally fail catastrophically. If large enough, local stress concentrations at the tip of a matrix crack are able to initiate cracking of the adjacent reinforcing fibres (Hull & Clyne, 1996). Fibre failure is largely dependent on the materials characteristics and can occur through many types of damage initiation, i.e. transverse impact loading or compression fatigue cycling (Cantwell & Morton, 1992).

1.4.3 Delamination

Delaminations in fibre reinforced polymer composites (FRPC) are commonly caused by bad manufacturing or impact damage and result in a significant reduction of compressive strength (Pan *et al*. 2006). Dependant on the initiation point of delamination within a material there can be two modes of delamination. If the initiation point is near to the surface of the sample local delamination can occur, in this case the plies above and below the initiation point separate. Global delamination is a result of internal delamination where the plies move in the same direction, if the composite is under compression loading this can result in the composite buckling (Short *et al*. 2002).

1.4.4 Fibre Debonding / Fibre Pull Out

Fibre debonding / pull out are attributed to the frictional sliding between the interface of the fibre and matrix (Huang & Liu, 1994). At the tip of an advancing crack fibres can fracture and fail, if the crack continues to advance along the length of the fibre the fibre is pulled away from the surrounding matrix. If the stresses around the debonding site are large enough and frictional forces are exceeded then this can result in the fibre being completely pulled out of the matrix (Short *et al*. 2002).

2.0 AIMS AND OBJECTIVES

There are 4 preliminary objectives for this project, these objectives will provide substantial information for the completion of the final objective.

1: Characterisation of acoustic emission caused by fibre fracture during tensile testing.

2: Characterisation of acoustic emission caused by resin fracture during tensile testing.

3: Characterisation of acoustic emission caused by composite failure during tensile testing.

4: Determination of the extent to which self sensing fibres can detect damage.

5: Comparison of the ability to detect damage in composites by acoustic emission and self-sensing fibres.

This thesis will provide a Literature review covering a variety of different applications and methods used to detect and monitor damage in composite materials. The methodology of producing fibre, neat resin and composite samples will be detailed as will the installation of fibre Bragg gratings and electrical resistance strain gauges. The experimental section will detail how the samples were tested and the methods of data capture.

The results will be combined with the discussion and cover the achieved results in their sample types. The discussion will continue to comment on the results from the testing of self-sensing fibres.

3.0 LITERATURE REVIEW

3.1 Damage Detection

Damage detection in composites can be split into two methods: destructive testing and non-destructive testing. Destructive testing can include using laboratory methods and on-site to test samples to failure e.g. tensile, compression and fracture toughness tests. Sectioning, de-plying and fractography are methods of destructive testing which analyse damaged composites. Examples of popular non-destructive techniques include: Acoustic Emission (AE) (Cole, 1985), Thermography (Avelidis *et al.* 2003), Ultrasonic C-Scanning (Burke *et al*. 1994) and X-Ray Radiography (Prakash, 1980). This literature review will consider some examples of destructive and non-destructive techniques: the types of damage they can detect, their advantages and disadvantages.

3.2 Optical Fibres

There are many methods of detecting damage in composites using optical fibres that are now commonly used and are very effective in detecting damage and health monitoring. “A system of thin, light-conducting fibres, integrated into a composite structure during its manufacturing process, can serve as a reliable, automatic and remote working long-term monitoring device for structural damage” (Hofer, 1987). The methods of optical fibre damage detection that will be discussed include fibre Bragg gratings and Fabry-Perot interferometric sensors. The optical fibre can also be used to detect damage by recording the heat emission of cracks in the optical fibre and intensity modulated fibre optics.

3.2.1 Fibre Bragg Gratings

The first Fibre Bragg Grating (FBG) was demonstrated by Hill *et al.* in 1978, it was then during the 1980's that initial experiments using FBGs were performed. Hill demonstrated the photosensitivity of germanium-doped glass fibres and their ability to support gratings. Over the last 20 years they have attracted particular attention from the aerospace industry, manufacturing process monitoring, structural health monitoring and non-destructive testing (Tsuda, 2006). FBG sensors have proved to be well suited for single and multiplexed strain measurements in composite materials and structures whilst being able to detect temperature change within $\pm$ 1 ^{o}C (Rao *et al*. 2002). FBG sensors have several advantages over conventional electrical and piezoelectric sensors, they are generally smaller (i.e. a 125 mm diameter for a standard telecom fibre) more flexible, light weight, resistance to corrosion, higher temperature capability, and immunity to electromagnetic noise and radio frequency interference (Burke *et al*. 1994).

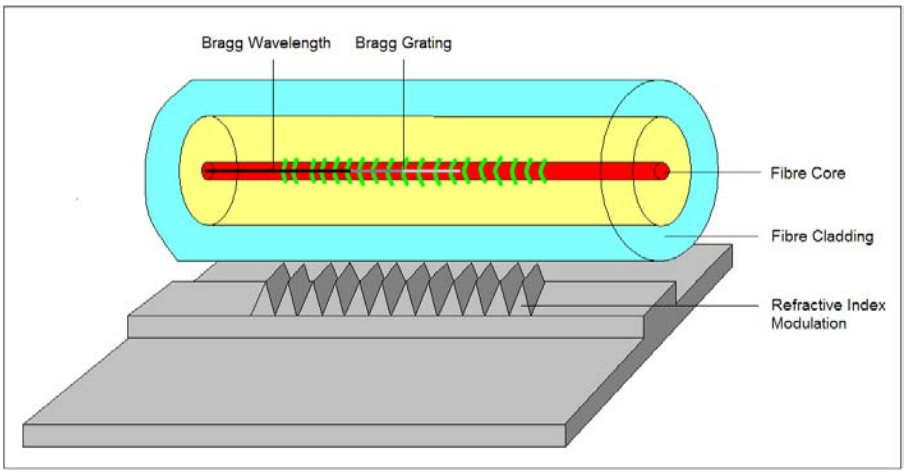

Fig 1: A schematic illustration of a Bragg grating on an optical fibre.

The fibre core of an optical fibre has a spatially periodic modulation of the refractive index created along its length (Fig. 1). This process is possible due to the photosensitivity property of

the doped silica glass fibre core; normally a germanium dopant is used and then a grating is inscribed into the photosensitive fibre core when exposed to ultraviolet (UV) light (Cole *et al.* 1995). Bragg gratings were first fabricated using the internal writing technique (Hill *et al*. 1978) and the holographic technique (Poumellec *et al.* 1996). These techniques have taken a back seat to the phase mask technique (Hill *et al.* 1993). The phase mask technique is dependant on a flat slab of silica glass which is transparent to the UV light. On the lower surface a one dimensional periodic surface relief structure is etched using photolithographic techniques, this is known as the grating corrugations. The optical fibre is drawn close to the corrugations; UV light is diffracted by the periodic corrugations of the phase mask. Most of the light is then contained in the 0, +1 and -1 diffracted orders. The beams from these diffracted orders then interfere to produce a periodic pattern that photo-imprints a corresponding grating in the optical fibre. Any change in the fibre property such as strain or temperature will alter the Bragg wavelength; this in turn will alter the volume of reflected light (Hill & Meltz, 1997).

It is the gratings that cause reflection, when a fibre is illuminated with a light source Fresnel reflections occur. It is these reflections that produce the Bragg wavelength. The peak signal of the Bragg wavelength is determined by Equation 1 (Hill & Metz, 1997):

$$\lambda_B = 2\, n_{eff}\, \Lambda_1 \qquad \text{[Equation 1]}$$

Where:
λ_B = Wavelength of the Bragg peak signal
n_{eff} = Modal index of the fibre core
Λ_1 = Period between two gratings

The spacing between the gratings will change depending on the type of loading and/or temperature applied. Under a compressive load the distance between the gratings will decrease and under tension they will increase. The wavelength of the Bragg signal will change in accordance with the type of loading; using Equation 2 (Yang *et al.* 2000) the strain can be calculated.

$$\frac{\Delta\lambda_B}{\lambda_B} = (1 - P_{eff})\,\varepsilon \qquad \text{[Equation 2]}$$

Where:
λ_B = Wavelength of the Bragg peak signal
$\Delta\lambda_B$ = Change in wavelength of the Bragg peak signal
P_{eff} = Strain-optic constant = 0.78
ε = Strain

Assumption: Temperature is constant

FBG are used commonly for strain measurements as the Bragg wavelength varies with the strain that a FBG is subjected to. In 2007 Tsuda and Lee used a FBG sensor to measure strain and monitor damage during impact testing of a CFRP measuring 300 mm x 300 mm x 1mm. The FBG sensor was attached 50 mm away from the sensor and the plate was impacted at 2.7 J. A resistive strain gauge was placed next to the FBG for reference. Experimental results proved that FBG sensors could measure strain correctly and was more effective than the conventional resistive strain gauge. FBG were determined to be suitable for long-term strain measurements because of its self-referencing and immunity to electromagnetic interference.

3.2.2 Extrinsic Fabry–Perot Interferometric (EFPI) Sensors

Some fibre optic sensors have been successfully commercialised and are widely in use for structural health monitoring of composite materials, large civil engineering structures, space craft and aeroplanes. EFPI sensors are one of the sensor systems deployed for structural health monitoring in these applications and is primarily used for strain and temperature monitoring (Taylor, 2002).

This sensor design is fabricated from two single mode fibres fixed at a specific distance "d" inside a glass capillary (Fig 2). The EFPI sensor utilises the variations in cavity length "d" between two cleaved optical fibres for sensor operation. Upon light source illumination, Fresnel reflections occur at the interfaces (a & b) at either ends of the cleaved fibres. Such reflections have an observed optical path difference and therefore produce fringes of interference. The change in the length of the cavity is calculated from a change in the interference pattern of the fringes as demonstrated in Equation 3 (Machavaram et al, 2006)

.

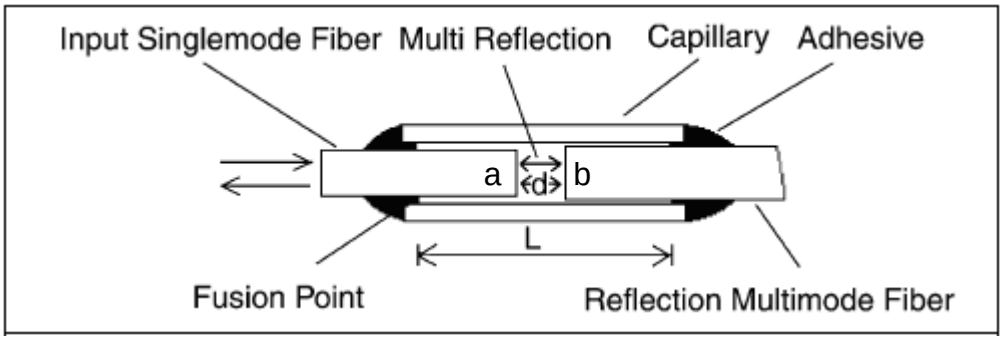

Fig 2: A schematic drawing of an extrinsic Fabry-Perot interferometric sensor (Leng & Asundi 2003).

$$d = \frac{n\lambda 1\lambda 2}{2(\lambda 1-\lambda 2)} \qquad \text{[Equation 3]}$$

Where:
n = Integer
λ1 = Wavelength 1 – Fig: 3
λ2 = Wavelength 2 – Fig: 3
d = Cavity length

When the distance changes so does the phase difference between the reflected waves. These phase differences produce a variety of fringe patterns as a function of displacement (Hare & Moore, 2000). The cavity length of the EFPI can be measured from the modulation in the reflection spectrum by counting the number of fringes over a specified wavelength range (Leng & Asundi 2003).

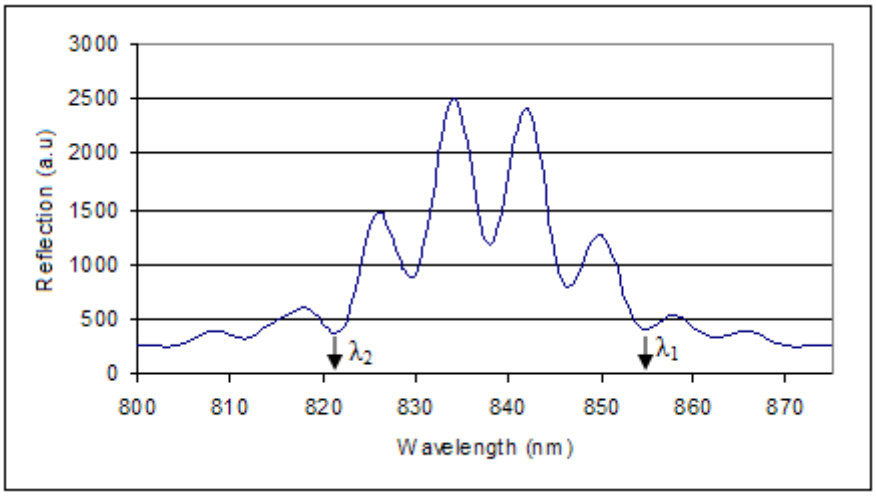

Fig 3: A schematic drawing of an extrinsic Fabry-Perot interferometer sensor. (www.netcomposites, 2007)

Strain (ε) is then calculated by comparing the difference of the original cavity length (L) compared to that of the change in cavity length (l-L) as indicated in Equation 4.

$$\varepsilon = \frac{l - L}{L} \qquad \text{[Equation 4]}$$

Where:
ε = Strain
l = Final length between bonded capillary section
L = Original length between bonded capillary section

3.2.3 Optical Fibre Heat Emission

The detection of damage in composites using heat emission is relatively new. In 2005 Pevzner *et al.* embedded some weakened fibre optics that had been stripped of their jackets into a composite plate structure. When cracks and delaminations occurred within the structure the optical fibre broke, at the location of a crack in a fibre, the transmitted laser-light energy was converted into thermal energy. This resulted in the area around the damage rising in temperature. The experiment was tested on a 16-ply graphite epoxy plate, 8 stripped optic fibres were glued to the face of the composite 20 mm apart. To inflict damage a 13 mm diameter steel ball bearing was used to impact the composite plate with an incident speed of 40 m/s. The detection of damage was performed by connecting a helium-neon laser with a range of 300-400 mW at one end of the fibre, another laser was connected to the other end of the fibre with a range of 300-400 mW. Infra-red images were taken of the composite surface (Fig. 4) the differences between the crack point and the background were highlighted by dark spots at points of energy “leakage”. The difference in temperature at the dark spot compared to the background temperature ranged form 10 ^{o}C to 16 ^{o}C.

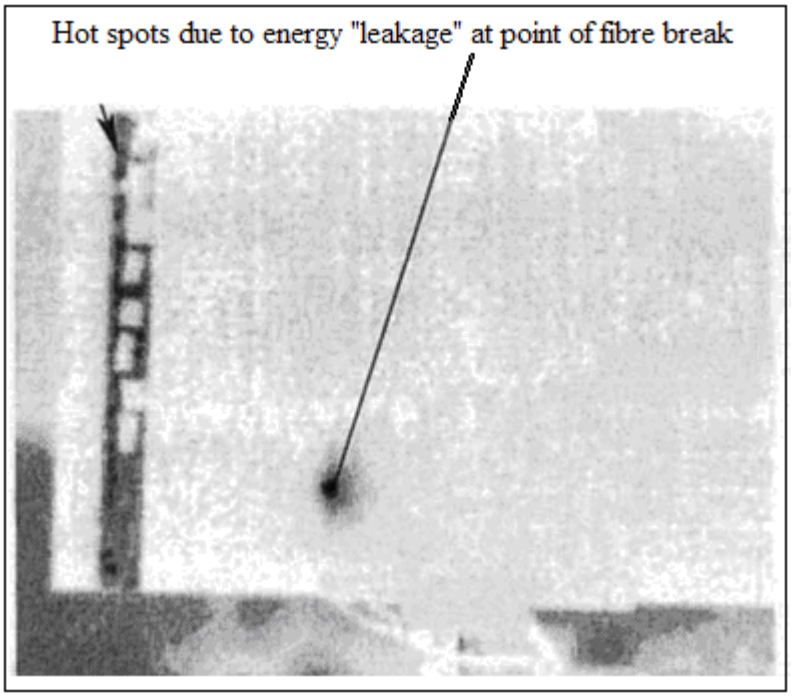

Fig 4: An image of heat loss using the optical fibre heat emission technique (Pevzner *et al.* 2005).

The results of this new method of damage detection in composites were confirmed by ultrasound scanning. The tests performed provided a large enough heat change to be recorded by infra-red cameras to provide an accurate detection of local damage (Pevzner *et al.* 2005).

A considerable advantage of this method is the ability to make use of optical fibres that have already been attached or embedded into a structure whether they are there for frequency, strain or temperature measurements. The degree of change in temperature i.e. 10 ^{o}C to 16 ^{o}C is a limitation of this detection method, applications where the composite structure itself is in a hotter environment will increase the difficulty to distinguish between the location of damage and the background temperature.

3.2.4 Intensity Modulated Fibre Optics

Intensity modulated is perhaps the most basic form of fibre optic sensors, it is based on the modulation of light intensity in a multimode optical fibre. When any portion of the optical fibre is strained it is reflected by the loss of light intensity transmitted by the fibre. Intensity modulated sensors are relatively easy to construct and do not require complex instrumentation and signal processing. The main problem is that intensity-modulated sensors provide only limited information, as they require knowledge on the location of damage (Zhou & Sim, 2002)

3.3 X-Radiography

Dye-enhanced x-radiography is a less commonly used NDT and only requires an x-ray source and photographic x-ray film to obtain a radiograph although real time x-ray detectors are available and are the preferred method (Prakash, 1980). Whilst radiography has the ability to easily detect voids and porosity within structures on its own it is not possible to detect matrix cracking, delaminations, debonding among other forms of damage. Detection of these forms of damage requires the introduction of a penetrant die such as di-iodomethane or zinc iodide. Where there is surface cracking within a structure this can be easily achieved and is highly effective (www.netcomposites.com, 2007).

Cantwell and Morton (1985) demonstrated the ability of radiography to detect impact damage in (CFRP laminates. CFRP plates of 1, 2, and 4 mm thickness were impacted using a 6 mm diameter steel ball fired from a gas powered gun. The samples were subjected to impact energies ranging from 0.4 J to 23.5 J. Zinc iodide was used as a dye penetrant, this allowed damage to be

observed in greater detail. X-Radiography proved to be a very useful technique for identifying areas of delamination and matrix cracking. Detection of fibre fracture presented a greater challenge since at lower energies damage only extended a few milimeters and was consistently surrounded by larger areas of delamination and matrix cracking (Cantwell & Morton, 1985).

X-Radiography has the advantages of being simple to use, effective on thick composites and can produce good images of impact damage. The disadvantages may outnumber the advantages depending upon the scenario in which it is used. Some disadvantages are: there always needs to be access to both sides of the structure and the absorption characteristics of the matrix are similar to that of carbon fibres, there are no specific composite standards to compare results to and with radiation there are always health and safety implications.

3.4 Ultrasonic, C-Scans

Ultrasonic C-Scanning is the measurement of attenuation of ultrasound through a material. The fundamental principle of ultrasonic detection relies on ultrasonic pulses with a frequency ranging from 1 MHz to 1.5 GHz. These pulses are either transmitted through a material or reflected back to the detector by material abnormalities i.e. internal damage (Burke *et al.* 1994). There are two common methods: through transmission scanning where there is a probe on either side of the test structure or pulse echo scanning where there is a receiver on one side and a reflective plate on the other side of the structure. The data is output in the form of a C-scan which resembles a planar view looking through the top surface of the structure. By using Ultrasonic C-scanning it is

possible to detect delaminations and dis-bonds as well as volumetric defects including voids within the structure (Aymerich & Meili, 2000).

Ultrasonic testing was used by Okafor *et al.* to determine the extent of damage in a 48-ply composite laminate. The laminate was impacted with a 95 mm steel ball fired from a gas gun. The impact energies were: 0.87 J, 1.47 J, 3.17 J, 4.92 J and 6.39 J. The ultrasonic C-scan was able to identify all damages above 2.0 J and was able to show the increase of the damaged area with the increase of impact energy (Okafor *et al.* 2001).

A limitation of conventional ultrasonic C-scanning is the high attenuation caused by absorption in porous resin and scattering by the fibres. A further limitation of ultrasonic C-scanning is the shadow effect; the shadow effect is caused by large delaminations close to the transducer. This results in the closest delamination reflecting the ultrasonic beam allowing only parts of delaminations below that are not covered by the closest delamination to be observed (Shang-Lin & Jang-Kyo, 1998).

The main disadvantage is one of the main requirements: water coupling. This has traditionally been achieved by immersing the structure in a water bath. Recent advances in using wheel coupled and air coupled sensors have increased the speed of testing and simplifies in service inspections. This is a major advantage for the aerospace industry where C-scanning is often mandatory (Imieli´nskaa *et al*. 2004).

3.5 Thermography / Infra-red imaging

Thermography techniques use infra-red sensitive camera detectors and film or recording methods, to monitor the surface temperature of a structure whilst in use. Heat is injected into the structure using heat lamps or hot air guns and reflected by the structure. When damage occurs or a defect is detected the thermal output from the structure is altered. Thermography is now widely used in detection of defects in sandwich composites such as airframes (Avdelidis *et al*. 2003). As well as the aforementioned equipment, a television setup or monitor is required as is a computer for data analysis.

Toubal *et al.* demonstrated the ability of thermography to detect damage in composite laminates. They performed fatigue tests on a carbon fibre epoxy fabric. The infrared camera recorded the temperature and heat sources on the specimen, from studying the results it was possible for Toubal *et al*. to identify three different stages of damage during fatigue testing. The damage rapidly grew in the initial testing period. The second stage saw damage grow steadily and the third stage saw damage occur rapidly until failure occurred (Toubal *et al.* 2006).

There are many advantages of thermography, these include the fact that no coupling is required, it can be performed *in-situ*, it can cover large areas and it is a quantitative method. The disadvantages are that there is a limit on the thickness of the structure being monitored, it is a much better method for monitoring glass fibre composites than carbon composites and it is perceived as an expensive option (www.netcomposites.com, 2007).

3.6 Laser Shearography

Shearography is a laser based technique that is non-contact and measures surface deformation in the form of displacement (Hunga & Ho, 2005). Shearography can be likened to a full-field strain gauge which allows strain to be monitored over a large area without the use of a strain gauge. Shearography has already received considerable acceptance from industry, in particular non-destructive testing of composites in the aerospace industry (Hung, 1996).

Figure 4 is a schematic diagram of laser Shearography. As illustrated a laser is used to illuminate the test object. The test object is imaged by a video imaging image-shearing camera consisting of a charge-coupled device (CCD) camera and an imaging shearing device. The shearing device is a birefringent crystal which splits one image point into two in the image plane. This is the integral part of the setup, the shearing crystal brings two non-parallel beams scattered from two different points to become nearly co-linear and interfere with each other. The CCD sensor then resolves the resulting low spatial frequency of the interference fringes. Damage can then be assessed by comparing the in-situ interference fringes to the original interference fringes of the structure (Hung, 1999).

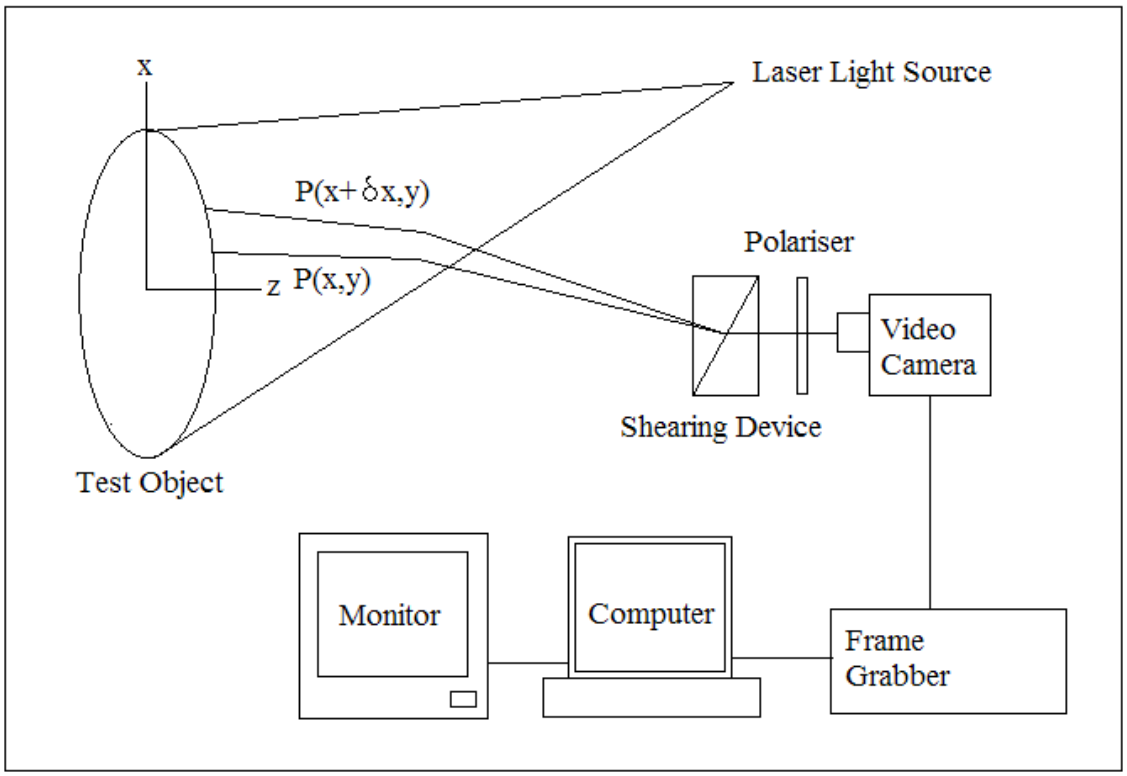

Fig 5: A schematic diagram of a Laser Shearography setup (Toh *et al*. 1990)

Toh *et al.* used laser shearography to measure the size of dis-bonds in glass fibre reinforced plastic plates. The composite plates were fabricated using the usual hand lay up method; during the fabrication mylar sheets of different dimensions were placed in between the glass fibre sheets to represent delaminations. The composite plate measuring 260 mm x 240 mm had 5 delaminations 1.9 mm from the surface randomly situated inside and was subjected to vacuum stressing at various pressures. Shearography was used to accurately determine the position and dimensions of the delaminations. The authors were also able to determine the criticality of the defects after comparison with a uniform composite plate (Toh *et al.* 1990).

3.7 Electrical Resistance

The ability of carbon fibres to conduct electricity has resulted in the electrical resistance of a sample being used as a parameter for in situ damage detection of carbon fibre reinforced polymer (CFRP) laminates (Seo and Lee, 1999). The basic principle of using electrical resistance is that fibre breakage or delamination will cause a decrease in the electrical conductivity in the damaged region leading to resistance or voltage change. The change can be monitored using electrode pairs at a remote distance from the damaged region (Shen *et al*. 2006).

For the electrical resistance to be recorded, a pair of electrodes need to be attached to the composite and contact with the carbon fibre is required. Figure 5 is a diagram of copper electrodes attached to the composite using silver paint; this is the most common method of testing electrical resistance. This is a widely used method; the silver paint ensures that the electrical resistance loss through the contact method is minimal (Abrya *et al.* 1999, Angelidis *et al.* 2004, Wang & Chung, 2006). The method of contact between the probe and the composite is one of the major disadvantages when electrical resistance is used to detect damage.

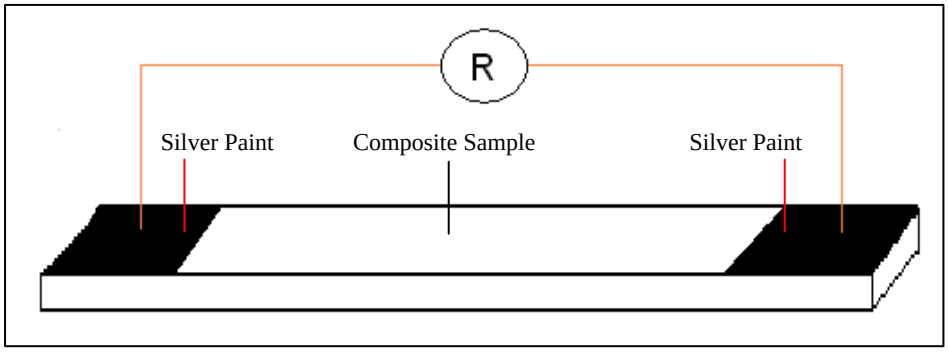

Fig 6: The use of silver paint to attach electrodes to a composite specimen

The detection of delaminations in composites by electrical resistance has been widely researched and proven to be a reliable technique (Todoroki *et al*. 2002). Work by Todoroki *et al.* into the detection of delaminations in composite plates demonstrated the ability to determine the size of delaminations within the plates but concluded that further work on the method must be done to improve the determination of the location of the delaminations for practical applications (Todoroki *et al*. 2005).

As well as the previously mentioned disadvantage further disadvantages can be attributed to the need for Artificial Neural Networks (ANN) for in-depth data analysis. The advantages of using the electrical resistance technique to detect damage revolve around the simplicity of using the carbon fibres. Electrical resistance testing has the advantage that there is no need for extra sensors or large amounts of instrumentation (Angeledis *et al*. 2005) and only low input current and low resolution voltage meters are required (Seo & Lee, 1999).

3.8 Electrical Conductivity Mapping

Electrical conductivity mapping (ECM) uses the same principle as electrical resistance, the fibres act as sensors themselves due to their ability to conduct electricity. Electrical conductivity mapping maps the specimen electrical resistivity or impedance information; this is more commonly known as electrical impedance tomography (EIT).

For electrical conductivity mapping to work electrodes are placed around the edge of the test sample, two of the electrodes are used to input a voltage into the sample. The potential difference

is then measured by all of the other electrodes. By using different combinations of input electrodes in different sequences and repeating the potential differences information can be recorded. This information is then analysed to extract resistivity distributions within the sample, hence areas of low resistivity indicate areas of damage (Scheuler *et al*. 2001).

In 2001 Scheuler *et al*. used electrical conductivity mapping for damage detection in composite laminates. A carbon fibre pre-preg 0.16 mm in depth measuring 52 mm x 52 mm had 16 electrodes attached every 13 mm. A hole 5 mm in diameter was drilled into the sample. They were able to calculate the location and size of the hole using simple FEA calculations, despite the simple calculations the results demonstrated that electrical conductivity mapping has a promising future.

3.9 Potential Difference: Direct Current (DC) Monitoring

As in the two previous mentioned techniques Potential Difference monitoring of damage relies on the carbon fibres ability to conduct electricity. Potential Difference is defined as: The voltage difference between two points which will cause current to flow in a closed circuit. The electrical potential difference technique measures the potential field on the surface of a current carrying composite laminate, any changes in the potential field indicates the presence of damage (Angelidis & Irving, 2007).

For a circuit to be completed the sample requires two electrodes to be attached to the surface of the composite plate. An input and an output electrode are required to introduce the current and for

the current to leave the sample to be recorded by the instrumentation. Electrical contacts / electrodes are then place on both sides of the composite plate systematically spaced typically in a grid formation. To attach the electrical contacts emery cloth or a similar abrasive material is used to reveal the outermost layers of carbon fibres then a high conductance paint containing silver to hold them in place.

This setup was used by Angelidis and Irving to monitor impact damage on the composite plate. The plate was a quasi-isotropic plate and had had dimensions of 280 x 280 x 2 mm. The plate was subjected to impacts ranging from 2 J to 12 J. The study found that electrical potential changes both on the top and bottom surfaces correlated well with delaminations in between the 1st and 2nd layers of the composite. Delaminations in between other layers had little effect on the potential difference. Whilst this method of damage detection has the ability to detect delaminations the influence of the additional failure modes must be included before accurate predictions of damage can be made.

3.10 Acoustic Emissions (AE)

"Acoustic emission (AE, sometimes called stress wave emission) is the term used to describe the resulting acoustic stress waves when energy is released rapidly due to the occurrence of micro structural changes in a material" (Cole, 1985)

The use of AE to detect damage can be traced back as early as 6500 BC where potters were known to listen for audible sounds during the cooling of their ceramics, signifying structural failure. Whilst there have been many references made to craftsmen using sounds to identify damage the first documented observation of AE was made in the 8th century where the Arabian alchemist Jabir ibn Hayyan wrote that tin and iron gave off different sounds during forging (Gautschi, 2002). The modern day study of AE testing is widely acknowledged to have begun when in 1950 Joseph Kaiser wrote his PhD thesis: "Results and Conclusions from Measurements of Sound in Metallic Materials under Tensile Stress" (Drouillard, 1996).

AE has the potential to detect and locate damage and damage sites continuously in a non-destructive manner (Marin-Francha *et al.* 2002). To detect AEs, sensors are attached to the structure that is being tested. Traditionally AE sensors have been made from piezoelectric materials but recently optical fibre sensors have been used to detect AE (Pevzner *et al.* 2005). In composite materials the AE release is due to one or more of the following: debonding, delamination, fibre cracking and/or matrix cracking (Yeun-Ho *et al.* 2006)

One of the main advantages of the AE techniques is linear location. Linear location requires two sensors to be placed in a line on the structure (Chen *et al.* 2006). It is also necessary for the

distance between the sensors to be recorded and the velocity of wave propagation within the material of the structure. Using this information it is possible to calculate a spatial source location based on the arrival times of an AE signal at the sensors (Surgeon & Wevers, 1999).

An AE event is recorded in a waveform (Figure 7). It is the analysis of waveforms that provides information about the event that has occurred within a sample or structure. The waveform is plotted as Voltage against Time and it is possible to use all of the terms mentioned in Table 3 to analyse and account for damage occurring in a material.

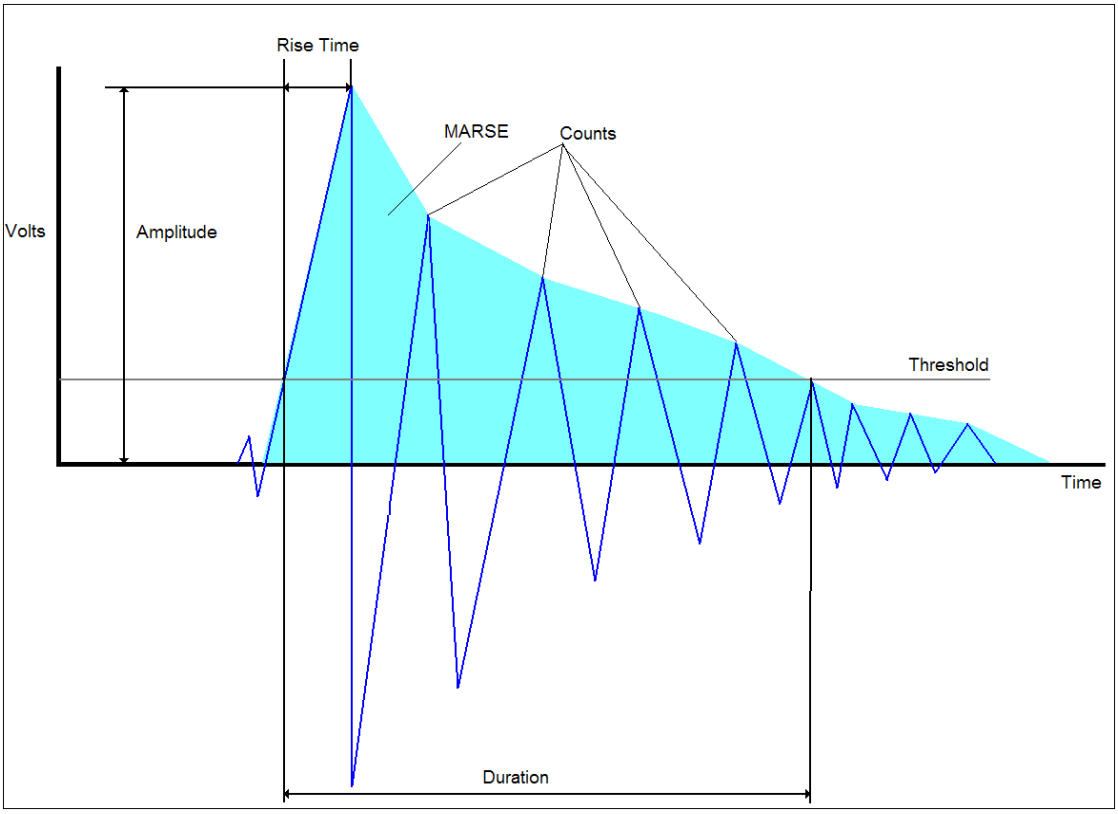

Fig 7: An acoustic emission signature

Table 3 provides a list of key terminology involved in deciphering an AE waveform

Key Term	AEWin Definition
Amplitude	The largest peak voltage in the AE signal waveform; customarily expressed in decibels relative to 1 microvolt.
Counts	The number of times the AE signal crosses the detection threshold.
Frequency	For an oscillating signal or process, the number of signals occurring in unit time.
Average Frequency	Calculated in KHz, determines an average frequency over the entire AE hit.
Rise Time	The time from an AE signal's first threshold crossing to its peak.
Duration	The time from the first threshold crossing to the end of the last threshold crossing of the AE signal from the AE threshold.
MARSE	The strength of the absolute value of a detected AE signal. Also known as "relative energy" and "signal strength".
Rise Time	The time from an AE signal's first threshold crossing to its peak.
Threshold	A pre set amplitude that needs to be exceeded for data to be recorded.

Table 3: A list of Acoustic Emission terminology.

The sensitivity of AE can be affected by the magnitude of background noise. Noise represents undesirable signals detected by the sensors. This can be due to the machine that is being used to perform the test, the material itself or a poor contact between the structure and the sensor. The amount of noise recorded can be determined by setting a threshold value, (Fig. 7) any emissions under the threshold will not be recorded (Wevers, 1997).

Johnson and Gudmundson performed a set of tensile tests on glass fibre epoxy composites with the aim of characterising AE signals to see if it was possible to discriminate between different types of damage. There were 4 different types of composite laminates used, three cross-ply samples and one unidirectional sample. The samples were 25 mm in width and either 235 mm or 280 mm in length depending on the lay-up. The samples were end-tabbed using aluminium rectangles measuring 30 mm in length and 25 mm in width. 6 Piezoelectric sensors were attached using vacuum grease as a couplant and tape to hold them in place, there were four on one side and two on the other. The samples were extended at 0.6 mm/s.

Due to the different types of lay-up used different forms of damage were more present in certain samples. Johnson and Gudmundson were able to characterise the AE signatures and relate them to different forms of damage within the composite (Johnson & Gudmundson, 2001).

3.11 Piezoelectric Sensors

Piezoelectric materials undergo a change in dimension when they are subjected to an applied voltage. They also undergo the reverse effect, the development of electric polarization when they are strained (Moulson & Herbert, 1992). It is this effect that allows piezoelectric materials to be incorporated into sensors. Piezoelectric sensors are solid-state electronic devices which respond to changes in pressure, temperature and changes in physical properties. It is the change of physical properties at the interface between the device surface and the structure that it is monitoring that develops the electric polarization (Chang *et al.* 2000). The electric polarization is recorded by a specific software program that allows analysis of the change in physical properties.

Piezoelectric sensors are commonly used for monitoring force, pressure, strain, temperature and acoustic emission. They have the advantage of being stable, highly reliable, rugged and have an unlimited life (Marschall & Gautschi, 1994). The disadvantages of piezoelectric sensors are their bulky size and that it is not possible to use them in areas of electromagnetic interference.

Figure 8 is a cross-sectional view of a piezoelectric sensor. The piezoelectric element is housed inside a metal - usually aluminium case. Either side of the piezoelectric element are electrodes that connect the element to the computer, this part of the sensor is surrounded by a damping material to facilitate in reducing unwanted noise.

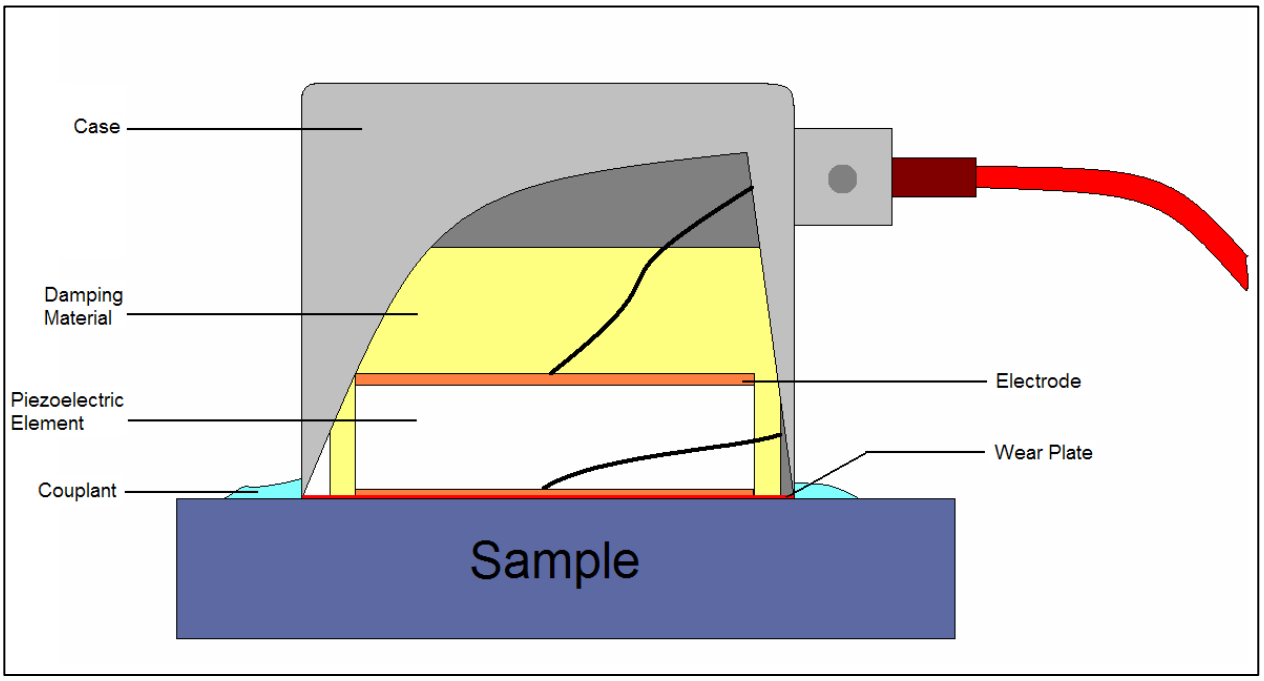

Fig 8: A cross-sectional view of a typical piezoelectric sensor

As mentioned in the Acoustic Emission section piezoelectric sensors are widely used for the detection of AE (Dong & Mistry, 1998).

3.12 Self-Sensing Fibres

Optical fibre sensors have some disadvantages in monitoring the structure of fibre reinforced composites. One of the main disadvantages is the size of the optical fibre. The diameter of the fibres in sensors such as Bragg gratings and Fabry-Perot sensors is in the range of 125-230 µm. When optical fibre sensors of this diameter are embedded in fibre reinforced composites there is no apparent effect due to the diameter mismatch whilst tensile testing on the samples is carried out. When a sample is subjected to a long term compression or tension test the larger diameter of the optical fibre has a detrimental effect on the reinforced composite (Hayes *et al.* 1997). The advantage of reinforcing fibres is that their diameter is in the range of 7-9 µm. The aforementioned advantages of optical fibre sensors over conventional sensors are also relevant for self-sensing fibres.

In 1997, Hayes *et al*. used commercially available Quartz reinforcing fibres in the development of a novel composite system in which some of the reinforcing fibres acted as the light guide. The quartz fibres were identified as they had comparable mechanical properties to E-glass fibres. The coating that was applied to the fibres during manufacture was de-sized. The fibres were then re-coated with a silicone resin. “A basic requirement for a conventional light guide is that the refractive index of the core (E-glass fibres) be higher than that of the cladding or coating” (Kister *et al.* 2003). Composite panels were produced by a vacuum assisted hand lay-up technique, 300 mm square panels with a ply sequence of 16 plies in the sequence (0*;* 90*;* 90*;* 0*;* 0*;* 90*;* 0*;* 90)s. There was one reference composite plate, one sample consisting of self-sensing fibres, and three samples with conventional optical fibres, one with 30 µm one with a diameter of 50µm and one with a 125 µm diameter. These fibres were introduced between plies 1 and 2 and plies 15 and 16

at a spacing of 10 mm. Different samples of each lay-up were impact tested at 2, 4, 6, 8 and 10 J using a 20 mm hemispherical tup. The results indicated that the self-sensing fibres were able to detect impact damages as low as 2 J and they were more sensitive than the conventional optical fibres. The use of Quartz fibres overcame the problem of diameter mismatch when using optical fibres (Hayes *et al.* 1997).

The problem with Quartz fibres is that they are expensive. Instead of using Quartz fibres the use of E-glass fibres which are significantly cheaper and extensively used in the electrical, aerospace automotive and marine industries as reinforcing fibres was investigated (Wang *et al.* 2004).

In 2004, work by Kister *et al*. used reinforcing E-glass fibres as light guides to detect damage induced by the composite by impact, indentation and flexure. E-glass fibre-reinforced epoxy resin composite were made from unidirectional E-glass/epoxy prepregs, the prepregs were stacked into a 16 ply composite using the lay-up sequence (0, 90, 90, 0, 0, 90, 0, 90)s and then processed in an autoclave. Conventional E-glass fibres were de-sized and coated with an epoxy and a polyurethane resin so they could act as reinforced fibre light guides (RFLGs). The refractive index of the E-glass fibres was 1.56 and the refractive index of the epoxy and polyurethane resins were 1.49 and 1.36 respectively. The RFLGs were placed on the surface of the panels, or between the 4^{th} and 5^{th} plies or between the 12^{th} and 13^{th} plies. The RFLGs were illuminated using a 100 mW solid-state laser operating at 532 nm or a white light source. A photodiode was used to record the output light intensity and a CCD camera was used to image the ends of the light guides.

- The samples for the impact test were 300 mm x 150 mm and were impacted at 2 J and 10 J using a 20 mm hemispherical tup. The light transmission was measured before and after the experiment using the green laser and photodiode.

- The indentation tests were performed on samples with dimensions of 300 mm x 100 mm. The samples were indented using the same 20 mm hemispherical tup at a rate of 0.5 mm/min. The light transmission characteristics were recorded using the photodiode and the CCD camera was used for visualization.

- The flexure experiment was performed as a 3-point bend experiment. The samples were 60 x 20 x 20 mm and were loaded at a speed of 0.5 mm/min. The intensity of light transmission output was recorded using the photodiode. In all cases the damaged area of the composites was located by finding the bleeding light from the damaged RFLGs.

The impact testing revealed that the two different claddings used were similar in the transmitted light intensity after impacts of 2 J and 10 J. The light transmission of the light guides was attenuated after impact, despite a significant increase in delamination there was only a slight decrease in light transmission due to the hemispherical head being much larger than the diameter of the fibres. The main conclusion from impact testing was that the surface mounted RFLGs can provide an effective means for detecting damage in composites.

The indentation test was stopped at 3.5 kN. In both cases of epoxy and polyurethane cladding the light transmission through the RFLG bundles in the top half of the composite was attenuated

before the bundles in the bottom half as the load increased. A slight recovery of the attenuation was noted as the load was removed but overall this experiment demonstrated that permanent damage in terms of fibre fracture can be detected using RFLGs.

Light transmission was continuously attenuated throughout the 3-point bend test. The light transmission in the RFLGs on the top surface was attenuated almost immediately when loading commenced. All other bundles of RFLGs began to attenuate at 50% of the failure load. There was no recovery of light transmission as the sample was tested to failure.

The authors successfully demonstrated the ability of the RFLGs to detect the presence of damage by monitoring the transmission characteristics.

3.13 Literature Review Conclusion

Whilst this literature review has covered common well established methods that are routinely applied to detect damage in composite materials such as acoustic emission, there are more specialised and developmental methods that will become more commonly used. At the present time it is suitable to claim that self-sensing fibres is a specialised method of damage detection that is under development. The advantages of self-sensing fibres over other damage detection methods include the ability to deploy the fibres into composite structures; this allows monitoring of the internal structure as well as the external surface. Self-sensing fibres are immune to electro-magnetic interference; do not require a coupling agent such as water for ultrasonic C-scans or silicone for acoustic emission.

It is evident from the literature that individual methods are more than capable of accurately detecting damage in composites. Complications arise when the need to record multiple forms of damage is required with only a single method available, for example the detection of impact damage whilst recording changes in strain. At the present time for multiple parameters to be recorded multiple sensors are required, development of current methods or further research into the ability of a single sensor to record multiple parameters would increase the accuracy and efficiency of detecting damage in composite materials.

4.0 METHODOLOGY

4.1 Mould Fabrication

Fabrication of the dog-bone resin samples was performed using a silicone mould. The silicon used was Silax from Replication Technologies Limited, the mixing ratio was 10 parts base to 5.5 parts catalyst, the total volume of silicone was 62 g. The silicone was used to cast a mould around 2 pre cut dog bone Teflon samples. Figure 9 is a schematic of the dimensions of the sample surface; the samples have a depth of 4.5mm.

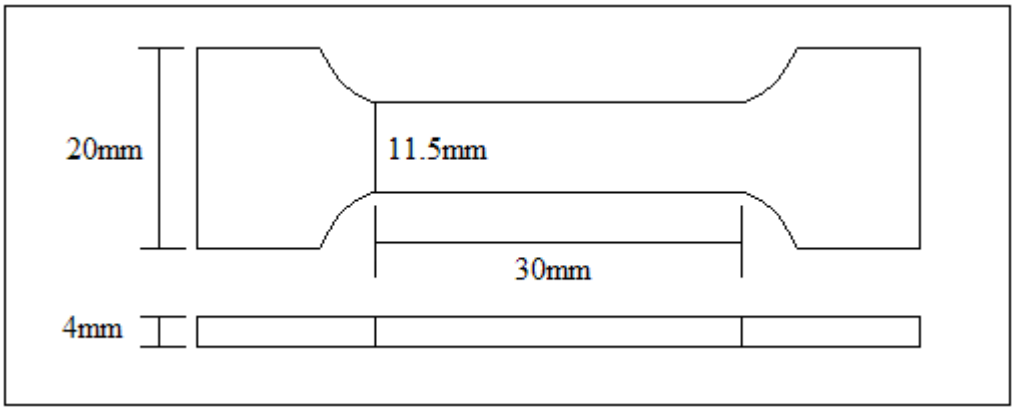

Figure 9: Dimensions of the resin dog-bone samples.

The Teflon samples were laid face down on a glass plate and a 100mm x 70mm wooden wall was placed around the samples. The Silicone was poured over the Teflon samples ensuring they were completely covered and then allowed to cure for 24 hours. The mould was then removed from the wooden walls and glass plate. Figure 10 presents a diagram of the cured mould.

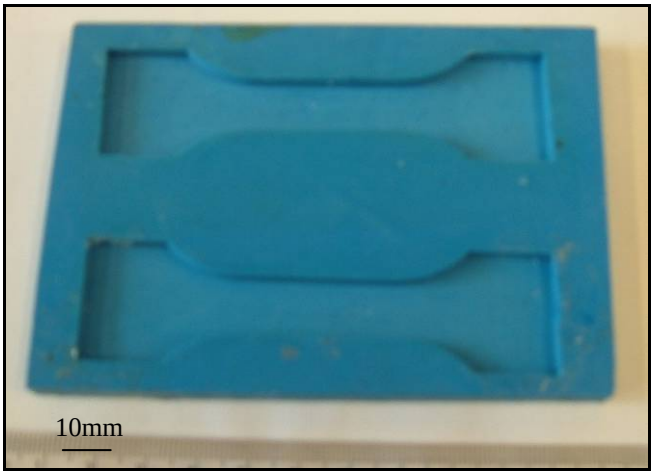

Figure 10: Completed silicone mould ready for resin sample fabrication.

4.1.1 Mould Preparation

Before the resin systems were poured into the mould impurities were removed from the surface, large visible impurities were removed using an artists brush. The mould was then cleaned using lint free tissue and isopropanol, the mould was then left to dry for 2 minutes.

4.2 Resin Sample Fabrication

All resins were subjected to the same mixing and casting process, this section will describe the process. Each resin system will have the curing process and final preparation individually reported. All samples had the width and depth measured at 3 points as indicated in Figure 11. Six Samples of each resin system were fabricated.

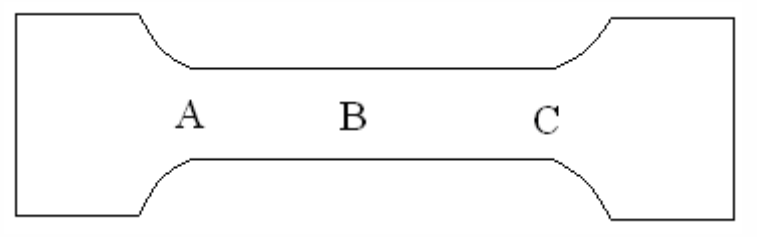

Figure 11: Locations that dimensions of the resin were recorded.

Each single sample required a total of 10g resin. The hardener and resin were poured into an aluminium tray and mixed together with a wooden spatula. The mixed resin was then place in a vacuum for 30 minutes to remove any air bubbles.

4.2.1 Scotchweld Resin Samples

The Scotchweld resin was mixed at a ratio of 4 parts resin to 1.4 parts hardener and then left to cure at room temperature for 24 hours. Figure 12 is an image of a cured Scotchweld sample.

Figure 12: A cured Scotchweld Resin sample ready for testing.

4.2.2 Epo Tek 305

Epo Tek 305 was mixed at a ratio of 10 parts resin to 2.8 parts hardener and cured at 65^{o}C for 1 hour. Figure 13 is an image of a cured 305 sample.

Figure 13: A cured Epo Tek 305 Resin sample with attached strain gauge.

4.2.3 EpoTek 310M

Epo Tek 310M was mixed at a ratio of 10 parts resin to 5.5 parts hardener and left to cure for 24 hours at room temperature. Figure 14 is an image of a cured 310M sample.

Figure 14: A cured Epo Tek 310M Resin sample ready for testing.

4.2.4 EpoTek 314

Epo Tek 314 was mixed at a ratio of 100 parts resin to 6 parts hardener and cured at 120^{o}C for 3 hours. During curing the exposed surface of the samples developed a rough film due to shrinkage, to remove this film the samples were ground down and polished to a finish of 3 µm. Figure 15 is an image of a cured 314 sample.

Figure 15: A cured Epo Tek 314 Resin sample with attached strain gauge.

4.3 End-Tabbing

4.3.1 Resin Samples

Aluminium end-tabs with dimensions of 25 mm x 20 mm x 1 mm were used to end tab the 305, 310M and 314 samples. The Scotchweld samples did not require end tabbing. The end-tabs were attached to the resin samples using Scotchweld Resin. Due to stress concentrations along the edges of the end-tabs on the 310M samples 4mm holes were drilled through the centre of the end tab after the Scotchweld resin had cured. The samples then had a 160 mm length of wire looped through the hole; the wire was then used to secure the sample during tensile testing.

4.3.2 Top-Hat End-Tabs

Figure 16 is a schematic of the Top Hat end tab dimensions. The end-tabs were machined from 25 mm x 25 mm x 3 mm steel blocks. A 10 mm channel through the middle of the end tab allowed the fibres to rest and be held in place without crushing them thus reducing the volume of light travelling through the fibres during self-sensing testing. 1 mm diameter holes were drilled in the corners allowing pins to be placed through the end-tabs to ensure they stayed parallel to each other during curing.

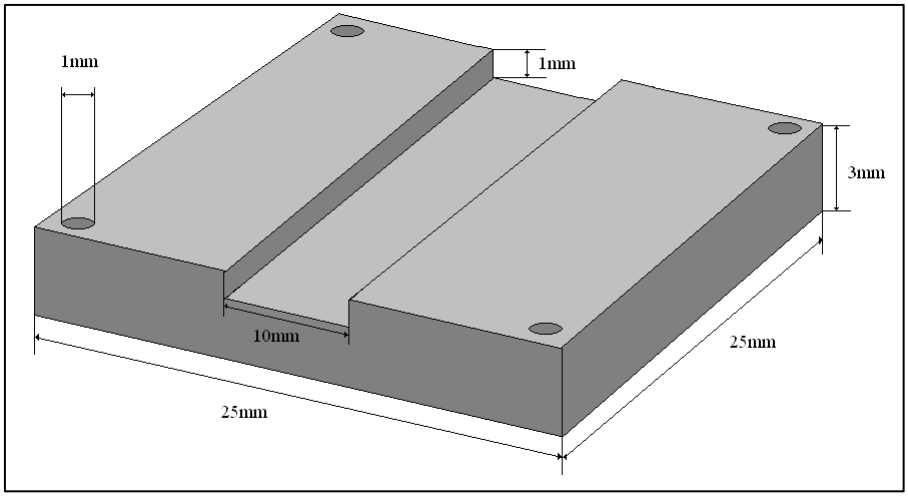

Figure 16: Schematic illustration indicating the dimensions of the top-hat end tab.

4.4 Fibre Samples

4.4.1 Acoustic Emission Testing

The fibres used to fabricate samples for acoustic emission testing were carbon and uncoated E-glass fibres. The carbon fibres were supplied by Tenax UK Limited and consisted of 24 000 filaments. The uncoated E-glass fibres were supplied by PPG Industries and consisted of 12 000 filaments. The samples were 250 mm in total length with a gauge length of 200 mm and each end tab being 25 mm long.

A PTFE covered steel plate was used to lay up the fibre samples. A 200 mm length was measured and marked out. Figure 17 is an image of the set up used to fabricate the samples.

Figure 17: The setup used to fabricate carbon and uncoated E-glass samples for Acoustic Emission testing.

At each end an end-tab was secured in place and lined up so it was parallel to the opposite end tab. Scotchweld resin was used to secure the fibre bundles in place, a small amount was place in the end-tab groove. The fibre bundle was then placed on top of the resin and bull dog clips were used to hold the fibres in place. A small amount of Scotchweld resin was placed on top of the bundle to ensure the fibres remained in the middle of the end tab. Another end-tab was place on top of the fibre and pins were placed through the holes in the corners of the end-tabs to ensure that the end-tabs were set square. The samples were left to cure for 24 hours and had the excess fibres removed.

Figures 18 and 19 are images of cured carbon and uncoated E-glass samples ready for testing.

Figure 18: A carbon sample ready for Acoustic Emission testing.

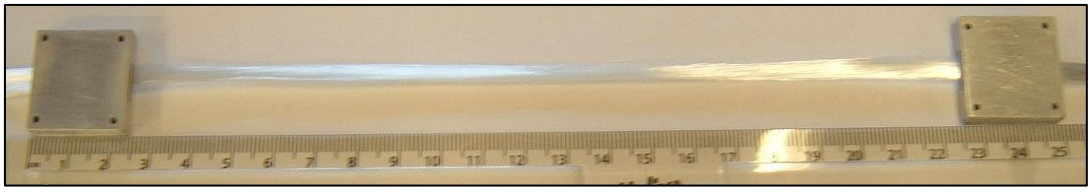

Figure 19: An uncoated E-glass sample ready for Acoustic Emission testing.

4.4.2 Self-Sensing Fibre Testing

The fibre samples for the self-sensing experiments were shorter measuring 150 mm in total length with a 100 mm gauge length. The fibres used were small diameter optical (SDO) fibres with a diameter of 10 – 12 µm were provided by Admolin Ltd. and consisted of 1200 filaments.

For self-sensing experiments to be performed a light source is required to be connected to the fibres. For this to happen Sub-Miniature version A (SMA) connectors need to be attached to either end of the sample. Epo Fix resin was used to attach the connectors. After the fibres had been threaded through the SMA connectors they were cleaved to remove as much of the excess fibres as possible. The ends were then polished to a 0.5 µm diamond finish. The polishing was performed using An ANC 8000 polisher, this allowed up to 12 samples to be polished at a time ensuring that each sample had a close to identical finish. Before end-tabs could be applied to the uncoated E-glass fibres a silicone coating was applied to the length of the fibres that would be in contact with the end tab. The coating was allowed to cure for 6 hours at room temperature. To attach the end-tabs a jig was made that allowed all the fibres in the bundle to be under the same tension. Figure 20 is an image of the jig.

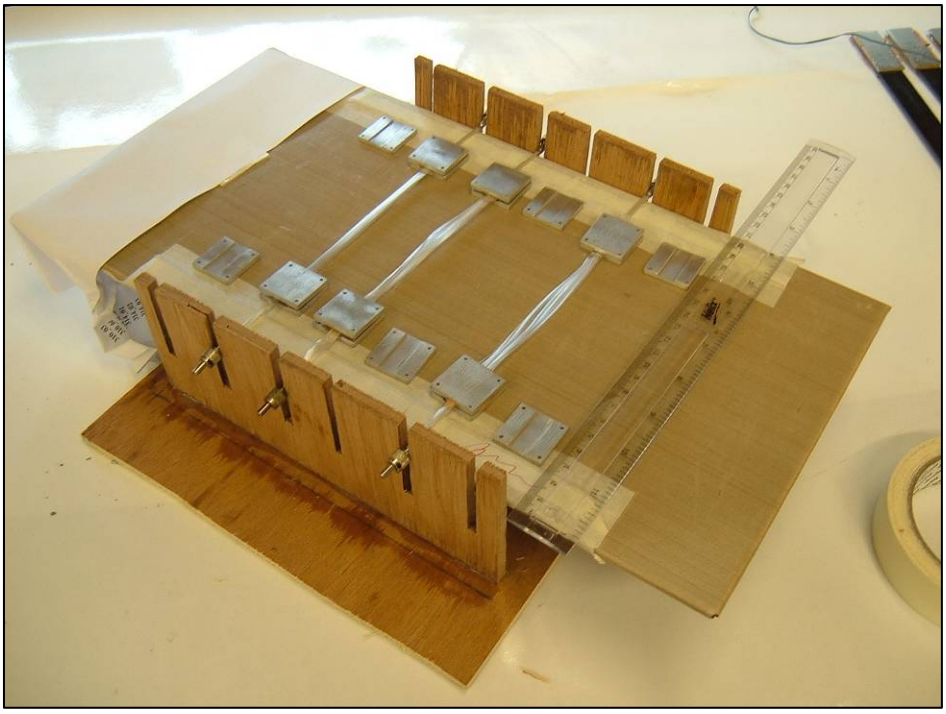

Figure 20: The wooden jig used for fabrication of uncoated E-glass and small diameter optical fibres.

The jig consisted of a PTFE covered steel sheet with a 100 mm length marked using masking tape. The fibre bundles were lined up using the grooves in the jig to ensure the fibres were parallel through the end-tabs. Scotchweld resin was used to secure the fibre bundles in place, a small amount was place in the end tab groove. The fibre bundle was then placed on top of the resin and bull dog clips were used to hold the fibres in place. A small amount of Scotchweld resin was placed on top of the bundle to ensure the fibres remained in the middle of the end tab. Another end tab was place on top of the fibre and pins were placed through the holes in the corners of the end-tabs to ensure that the end-tabs were set square.

The samples were left to cure for 24 hours. Figure 21 is an image of a SMA connected self-sensing Small Diameter Optical fibre sample.

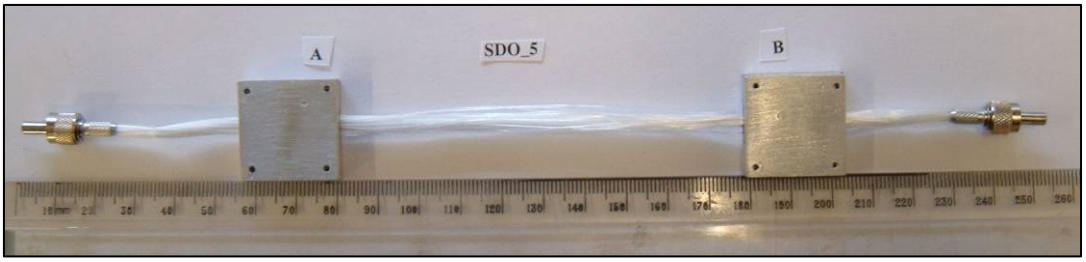

Figure 21: A small diameter optical fibre sample ready for self-sensing testing.

4.5 Electric Resistance Strain Gauge

Electrical strain gauges were attached to Epo Tek 305, 310M and 314 samples. The strain gauges were purchased from Tokyo Sokki Kenkyujo Co. Ltd.

To ensure the work was carried out in a clean environment an acetone cleaned glass plate was stuck using masking tape to a table top. All equipment that was used to attach the strain gauges i.e. scissors and tweezers were cleaned with isopropanol. As well as the equipment being cleaned the surface of the sample was cleaned using lint free tissue and isopropanol. Each sample was attached to the glass plate using masking tape placed over the end-tabs. The midpoint of each sample was measured out and marked on either side of the sample.

Tweezers were required to remove the strain gauge and electrical contact from their casing and placed on the glass plate facing up as in Figure 22.

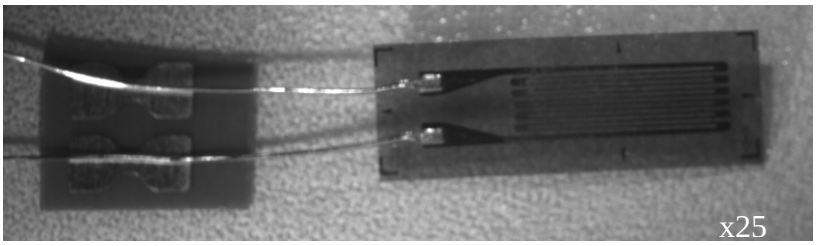

Figure 22: Electrical contacts and electric strain gauge in formation for transfer to resin sample at x25 magnification.

M-line cellophane tape was used to cover the contact and the gauge, to ensure there were no air bubbles medical gauze was used to apply pressure and wipe across the surface as the tape was lowered from the strain gauge end. The strain gauge and electrical contact were removed from

the glass plate with the gauge end firstly being peeled off at a 45^{o} angle. The tape was place on the sample with the midpoint of the strain gauge aligned with the previously marked points on the samples. The electrical contact and strain gauge were covered in 1 stroke of blue catalyst and two drops of M-Bond adhesive were placed on the resin surface below the strain gauge. The tape was lowered at a 45^{o} angle and medical gauze was used to ensure an even covering of M-Bond over the surface of the sample.

Immediately after the gauge and electrical contact have been lowered into place a Teflon sheet, rubber block and aluminium block were placed on top of the gauge and electrical contact with pressure being applied for 2 minutes. After the pressure had been applied the tape was left on for 5 minutes. Finally the tape was removed at an angle of 180^{o} to leave the sample ready for soldering.

For the strain gauge data to be recorded they needed to be attached to the Cambridge Electronic Systems DMM4 electric strain gauge indicator. The surface of the contacts and strain gauge wires were first cleaned with M-Line rosin solvent. The strain gauge wires were formed with a zigzag in them to allow the contacts and strain gauge to move apart during testing without breaking the circuit. 1 Metre long pieces of strain gauge wire were soldered to the electrical contacts. The wire was initially tinned and then soldered to the other half of the electrical contact. The resistance of the strain gauge was then recorded, to ensure the soldering had connected the strain gauge to the contacts the displayed resistance needed to be 120 Ω, +/- 1 Ω.

Figure 23 is a schematic of a generic resin sample with attached end-tabs, fibre Bragg grating and electrical strain gauge.

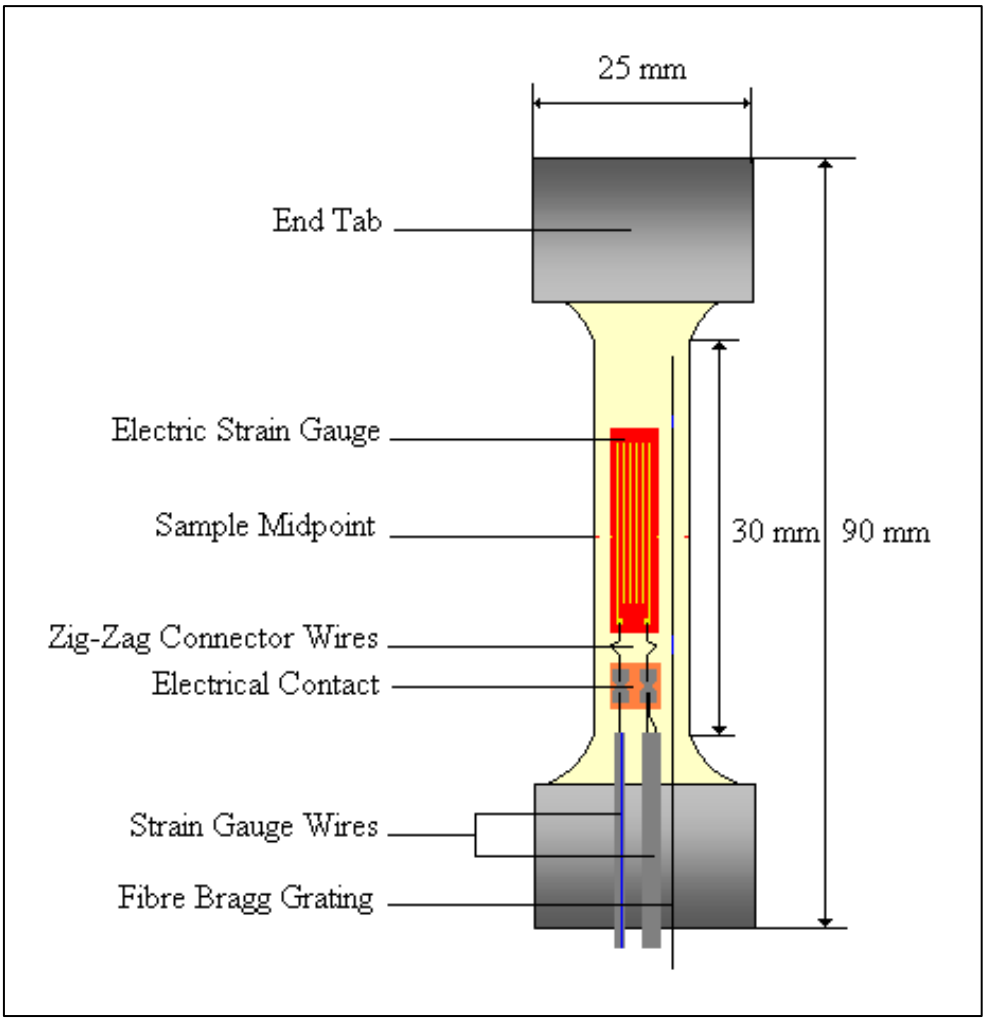

Figure 23: Schematic of a generic resin sample with dimensions and locations of the electrical resistance strain gauge and fibre Bragg grating.

4.6 Fibre Bragg Grating Installation

The Fibre Bragg Gratings (FBGs) were written onto a single mode fibre by Dr. Rajanikanth Machavaram. Single mode fibres were chosen as there was less light loss when the fibre was bent during tensile tests. A 10 mega Joule laser shot 3000 shots at the fibre to write the grating. The Bragg wavelength of the FBG was recorded before it was attached.

The surface of the resin sample was cleaned using isopropanol. The FBG was placed on the sample lying parallel to the electric strain gauge with the grating covering the same distance as the strain gauge. Using masking tape the coating at either end of the grating temporarily held the FBG parallel to the electric strain gauge before mounting. To attach the FBG M-Bond 2000 was applied to the length of the grating using a hypodermic needle. After 5-10 minutes of applying the M-bond 2000 the Bragg wavelength was recorded again to ensure there was no change in the wavelength or strain applied during the mounting. Figure 24 is an image of a mounted FBG running parallel to the electric strain gauge.

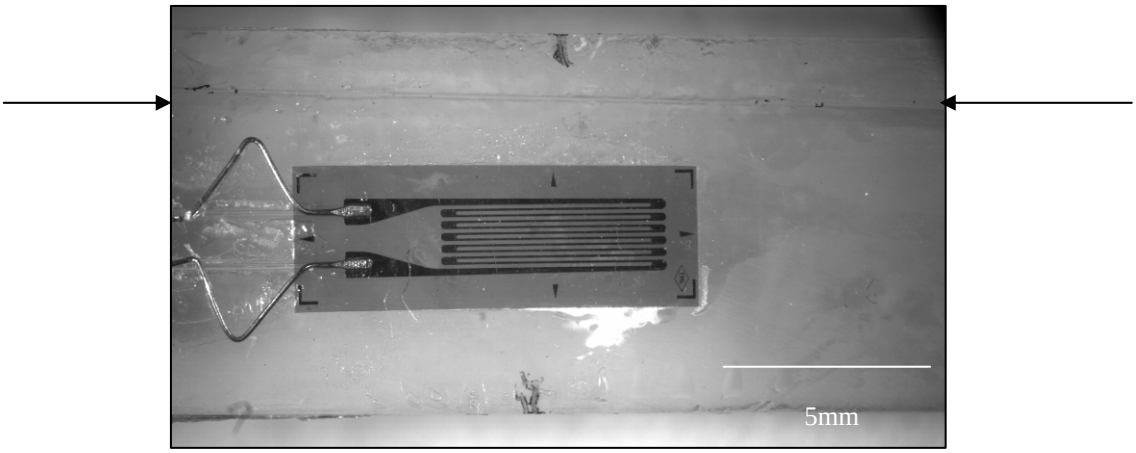

Figure 24: An attached Fibre Bragg Grating indicated by the arrows, running parallel to the electric strain gauge at x25 magnification.

4.7 Self-Sensing Composite Samples Fabrication

The self-sensing composites consist of a mixture of the aforementioned resins and fibres. Table 4 is a list of the types of fibres used and the resin systems used to impregnate them.

Fibre Type	Resin System	
	Epo Tek 305	Epo Tek 310M
Small Diameter Optical	6	6

Table 4: The resin and fibre contents of the self-sensing composites.

Another silicone mould was cast from Silax, 150 g were required to fabricate the mould. This was poured over a 110 mm x 10 mm x 2mm aluminium strip onto a glass plate. Either end of the strip a piece of smooth PTFE tape with dimensions 20 mm x 10 mm x 0.5 mm was stuck to the glass plate to create a step in the mould. The Silax was left to cure for 24 hours and removed from the glass plate and wooden walls.

Figure 25 is a schematic cross section of the silicone mould used to fabricate the self-sensing composite samples.

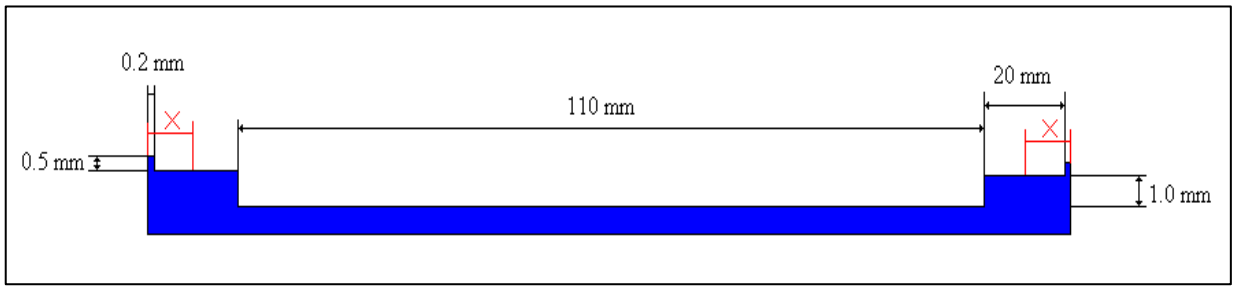

Figure 25: A cross section and dimensions of the silicone mould used to fabricate the self-sensing samples.

The mould was placed on a steel plate, 250 mm lengths of fibres were laid down in the mould and the excess lengths of fibres were clamped to the steel sheet using bulldog clips.

For each individual sample 1.5 g resin was required. The resin was poured into the 110 mm channel and a paintbrush was used to impregnate the fibres. The same ratios used to mix the neat dog bone resin samples were used and all samples were left to cure for the same aforementioned time.

SMA connectors were attached to either end and polished to the same degree of accuracy as the fibre samples. The wooden jig (Fig. 20) was again used as was the same procedure for end tabbing. Once the end-tabs had been laid out in the correct alignment and a small amount of resin had been placed in the end tab channel the composite was put in place. The dimensions and shape of the samples were designed to facilitate end tabbing, this resulted in 0.5 mm of the composite being placed in the composite and the other 20 mm of depth 0.5 mm also in the end tab. This enabled the fibres of the sample to pass through the centre of the end-tabs ensuring axial loading.

5.0 EXPERIMENTAL PROCEDURE

5.1 Tensile Testing

All samples were tensile tested on an Instron 5566 machine with the data being recorded on Merlin software. The machine can produce a maximum load of 10 kN and is screw driven thus keeping background noise to a minimum. The Instron 5566 has a load accuracy of +/-0.5 % of the indicated load.

5.1.1 Fibre Samples

Before testing of the fibre samples could begin an engraving pen was used to roughen the surfaces of the end-tabs to provide more grip between themselves and the Instron grips. The sample was always placed into the upper load cell first then the lower load cell. Figure 26 is an image of a carbon fibre sample inserted into the grips and ready to be tested.

Figure 26: A carbon fibre sample inserted into the load cells ready for tensile testing.

The initial extension and stress of the sample was zero and the load was set between 0 and 1 N. The test was performed at an extension rate of 1 mm/min. Merlin software was used to record the time / sec, extension / mm, load / N and stress / MPa for the duration of the experiment. The experiment was run until there was a continuous extension at no increase of load and was finally stopped at 2.2% extension.

5.1.2 Resin Samples

The method to setup the experiment for the resin samples was the same as fibre samples. Instead of an extension rate of 1 mm/min a rate of 0.5 mm/min was used. This allowed a longer testing time to record a greater number of acoustic emissions. Merlin software was used to record the time / sec, extension / mm, load / N and stress / MPa for the duration of the experiment, the experiment ended when resin fracture occurred.

For strain measurements to be recorded a ramp and hold method was used to record at predetermined loads. This method was used for the 305 and 314 samples. Figure 23 is a table indicating the loads at which samples were held during tensile testing. Due to the slow increase in load there was no need to ramp and hold the 310M samples.

Sample Type	**Load (N)**			
305	50	100	150	N/A
314	200	400	600	800

Table 5: The loads at which samples were held to record strain values during tensile testing.

5.2 Acoustic Emission Testing

Acoustic Emission (AE) testing was performed using two Micro 80s piezoelectric sensors supplied by Physical Acoustics Corporation. The sensors were attached to the samples using silicone rubber, this acted as an adhesive and as a couplant. Masking tape was used to secure the sensors to the resin samples, for the fibre samples the sensors were held in place using clamp stands. The AE data acquired by the sensors was recorded on an adjacent computer using AEWin software.

5.3 Strain Measurements

Strain measurements were recorded for the 305, 310M and 314 resin samples. Each resin system had its own testing procedure. This was dependant on the duration of the test and the ability to record data. The previous mentioned method of ramp and hold allowed strain data from electric strain gauges and Fibre Bragg Gratings to be recorded at set loads

5.3.1 Electric Resistance Strain Gauge Data Acquisition

A Cambridge Electronic Systems DMM4 electric strain gauge indicator was used to record change in strain. The strain gauge has the ability to record up to + / - 20 000 micro strain i.e. + / - 2% strain.

Strain was recorded using two methods. At a set load the value was manually recorded by reading directly off the strain gauge indicator display. Strain was recorded directly by the Acoustic Emission system. This was achieved by inputting the strain values directly into the AE system as a hit based parametric value. Each time a hit was recorded the strain value was recorded.

5.3.2 Fibre Bragg Grating Data Acquisition

Strain recordings were recorded by using an IS 7000 Interrogation System. The FBG was spliced to a multimode fibre that was connected to a Fiberpro.

The Bragg wavelength was recorded before the start of the experiment i.e. 0 N and then recorded at the same loads as the electric strain readings were recorded.

5.4 Self Sensing Fibres and Composites

Testing of the self-sensing samples was dependant on the memory size of the high speed camera. The recording time of the camera was directly affected by the resolution and the number of frames per second. For a minute of recording time it was possible for 250 frames per second to be recorded at a resolution of 486 x 512. Table 6 is a list of tensile testing speeds to ensure samples could be fully tested in 1 minute.

Sample Type	Extension rate (mm / min)
Small Diameter Optical Fibres	3
SDO / 305 Composite	2
SDO / 310M Composite	2

Table 6: A list of extension rates that were used for self-sensing samples during tensile tests.

6.0 RESULTS AND DISCUSSION

6.1 Fibre Samples

6.1.1 Mechanical Testing Results: Load vs. Extension

Mechanical Testing was performed on all samples; this section will present typical traces for each sample type. Further results from the mechanical testing will be presented to provide a comparison between the different fibre samples.

Figures 27, 28 and 29 are typical traces of Carbon, Un-coated E-glass and small-diameter optical fibres respectively. The red lines imposed on Figure 27 represents the point at which the maximum extension and time the maximum tensile load was reached for all samples. The area inside the imposed red circle on Figure 29 indicates the lag where the Instron machine took up the tension of the sample.

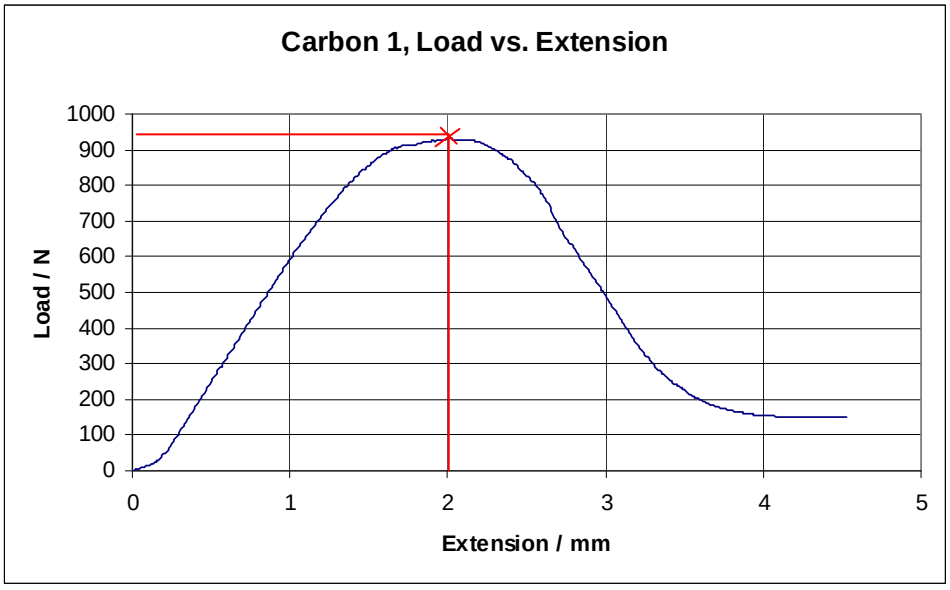

Figure 27: Load vs. extension graph for a carbon fibre sample.

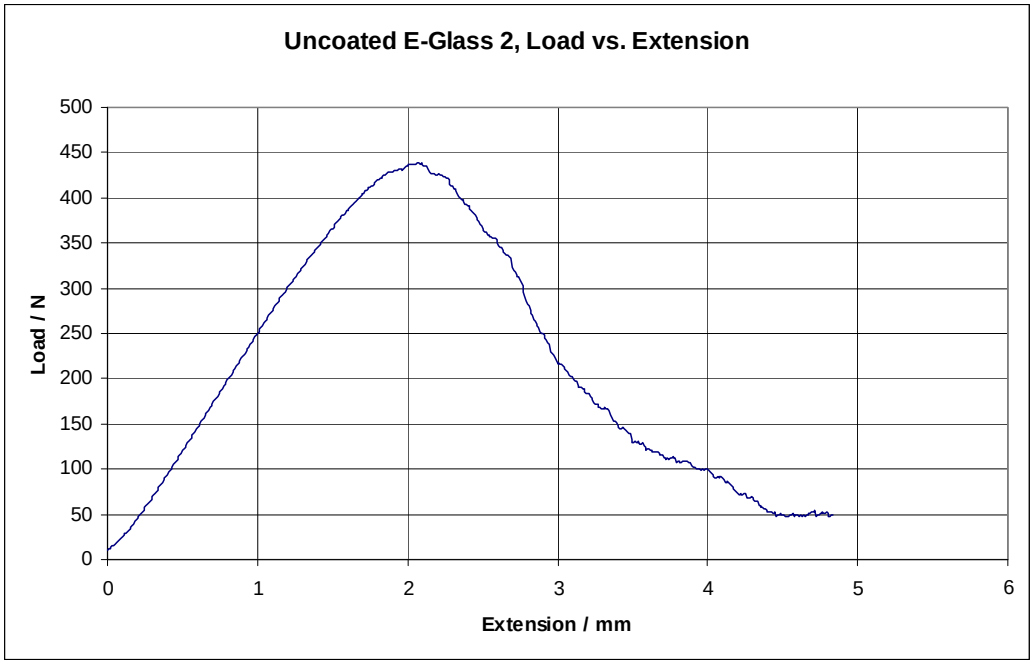

Figure 28: Load vs. extension graph for an un-coated E-glass fibre sample.

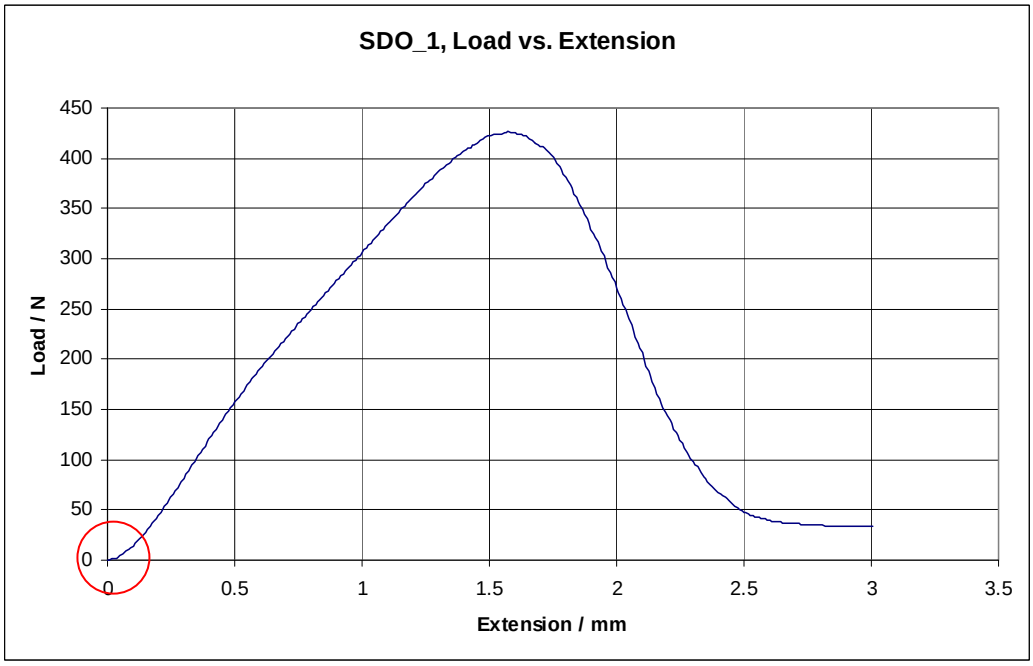

Figure 29: Load vs. extension graph for a small-diameter optical fibre sample.

Fibre Bundle Type	Number of Samples	Time at Maximum Load (sec)		Maximum Load (N)		Extension at Maximum Load (mm)	
		Average	S.D.	Average	S.D.	Average	S.D.
Carbon	12	116.92	6.87	1147.53	107.81	1.94	0.12
Uncoated E-Glass	12	124.90	20.50	358.70	73.20	2.14	0.48
Small-diameter Optical	6	31.16	3.50	558.94	138.84	1.55	0.18

Table 7: A comparison of the average mechanical testing values for the fibre samples.

The carbon fibre samples had an average maximum load of 1147.5 N, Table 7 shows this is double the maximum load applied to the small-diameter optical (SDO) fibre samples and over three times that of the E-glass fibre samples. The extension at maximum load values for the fibre samples were 0.97 % for the Carbon samples and 1.07 % for the E-glass samples. The SDO fibres had the greatest extension of all the fibre samples with an average extension of 1.56 %. The consistency of the results was demonstrated with a 6 % standard deviation (SD) for the Carbon samples and 10.1 % SD for the SDO samples.

Hayes *et al*. used Quartz fibres for reinforcing fibre light guides as they had comparable mechanical properties to E-glass fibres. Table 7 provides a comparison between mechanical testing of SDO fibres and E-glass fibres, the SDO fibres had a larger tensile failure load and a greater extension at maximum load than the E-glass fibres. Combined with their diameter of 10 - 12 µm they are suitable to be considered as reinforced fibre light guides.

Figures 28 – 30 display curved regions at the area of maximum load on the Load vs. Extension traces. This would suggest that the fibres in the bundle were not all under the same tension when the samples were fabricated. This would result with different fibres within the bundle failing at different loads during the tensile test. If all the fibres were parallel and uni-directional there would be a more defined maximum load.

6.1.2 Acoustic Emission Results

Fibre Bundle Type	Number of Samples	Number of Hits		Amplitude (mV)		Peak Frequency (kHz)		Average Frequency (kHz)	
		Average	S.D.	Average	S.D.	Average	S.D.	Average	S.D.
Carbon	12	35970	2675	42.43	1.23	475.21	20.76	164.37	4.97
Uncoated E-Glass	12	4785	1233	36.08	2.46	354.58	20.36	126.91	16.32
Small Diameter Optical	6	6497	1236	62.63	3.25	344.92	35.08	285.76	13.75

Table 8: A comparison of the acoustic emission parameters for fibre samples.

For all of the samples the number of hits, amplitude, peak frequency and average frequency were recorded and are presented in Table 8. The number of hits and amplitude has been the most widely adopted parameters for describing damage in composites materials due to the simplicity of recording and analysis (Sung-Choong & Nak-Sam, 2007). Frequency parameters of AE signals were chosen as they are known to differ according to failure mechanisms in laminated composites (Groot *et al.* 1995 & Barre, 1994). For all sets of samples the average values were

presented and all standard deviation values calculated, these values helped to demonstrate the consistency of the testing procedure.

The AE results for the carbon fibres were the most consistent recorded, Table 8 presents an average of 35,965 hits recorded with a standard deviation (SD) of 8 %. The average amplitude of 42.4 mV with a SD of 1.2 mV for the carbon samples. The peak frequency of the AE hits had an average value of 475 kHz and a SD of 20.7 kHz. Frequencies above 300 kHz in an AE hit for unidirectional carbon fibre represent fibre failure; frequencies for fibre pull out in unidirectional composite can range from 180 kHz and 240 kHz (Sung-Choong & Nak-Sam, 2007). Table 8 shows the average frequency recordings had an average value of 164.3 kHz this is lower than values recorded by Sung-Choong & Nak-Sam.

Results for the uncoated E-glass samples in Table 8 show an average of 4874 hits, a SD of 1232.8 hits highlights the range in number of hits recorded. The recorded parameters were far more consistent; the Amplitude values had an average of 36 mV and a SD of 2.4 mV. These amplitude values are in agreement with previous analysis of AE hits that has demonstrated amplitudes of greater than 35 mV in glass fibre composites are associated with fibre fracture (Short & Summerscales, 1984). Table 8 presents the different frequencies recorded, an average peak frequency of 354.6 kHz and an average frequency of 126.9 kHz were recorded. The peak frequency recordings were the least consistent of the parameters with a SD of 12 %, the average frequency results were more consistent with a SD of 5.6 %. Tensile tests performed on unidirectional glass fibre composites and consistently demonstrated AE hits with frequencies in

two distinct groups 100 kHz – 120 kHz and the majority of frequencies recorded from 250 kHz – 300 kHz (Ramirez-Jimenez *et al.* 2004).

The number of hits recorded for the SDO fibres ranged from 5325 hits to 8042 with an average of 6497 hits recorded per sample. An average amplitude of 62.6 mV was recorded for the SDO fibres with a SD of 3.2 mV again proving the consistency of the results. The most consistent parameter recorded was the average frequency, an average frequency of 285.7 kHz was recorded with a SD of only 13.7 mV. An average peak frequency of 344.9 kHz was recorded, the SD was 35 kHz.

6.1.3 Summary of Results for Fibre Samples

Figure 30 provides a summary of the maximum load applied to the fibre samples. Figure 31 and 32 provide a summary of the amplitude and average frequency of the acoustic emission hits recorded respectively. These figures provide a graphical presentation of the tabulated results from the mechanical and acoustic emission testing. The amplitude and average frequency of the acoustic emission hits were chosen as they were the parameters with the lowest SD.

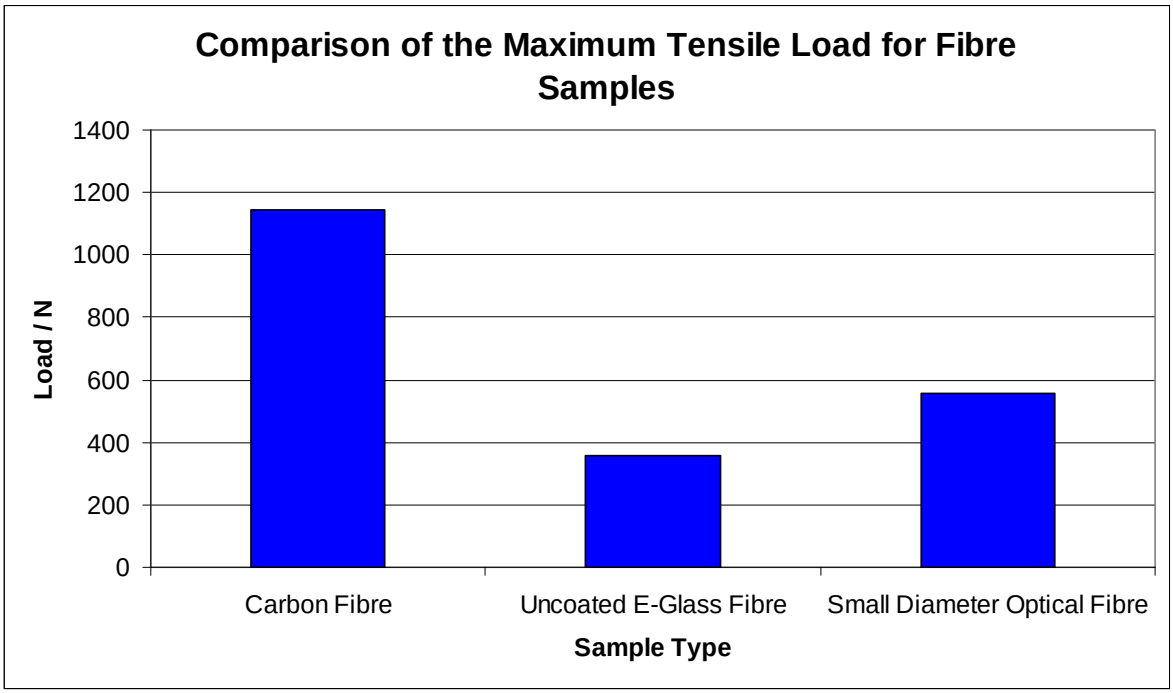

Figure 30: The maximum loads of fibre samples during tensile testing.

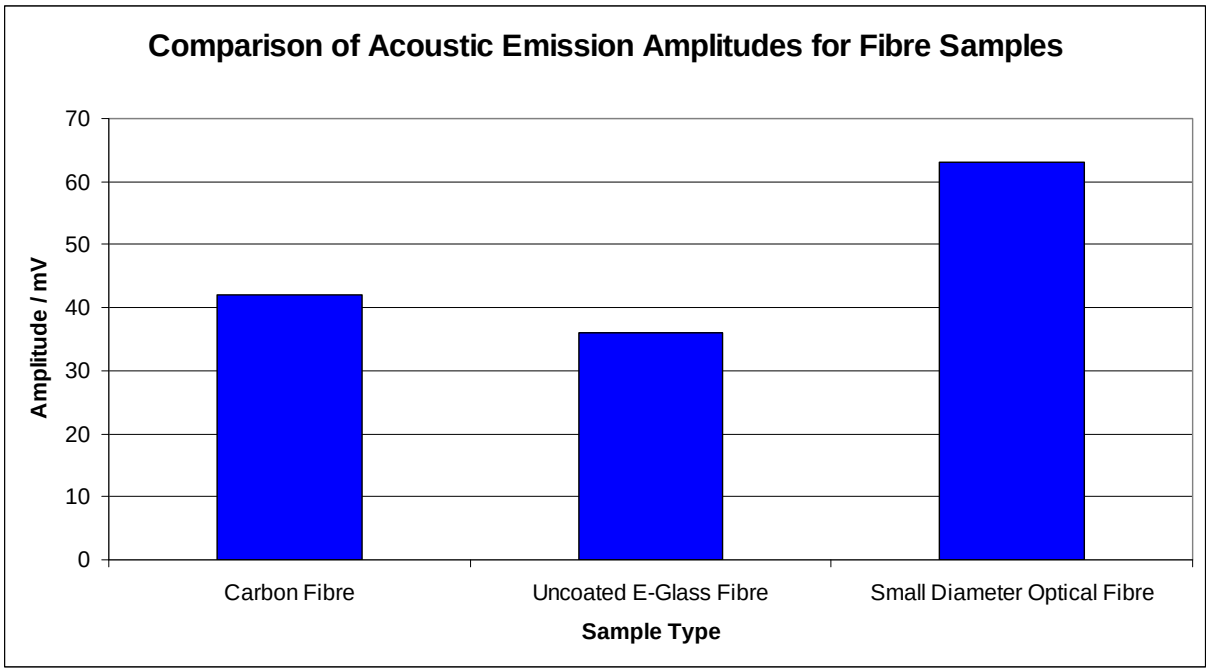

Figure 31: The amplitude of acoustic emission hits for fibre samples during tensile testing.

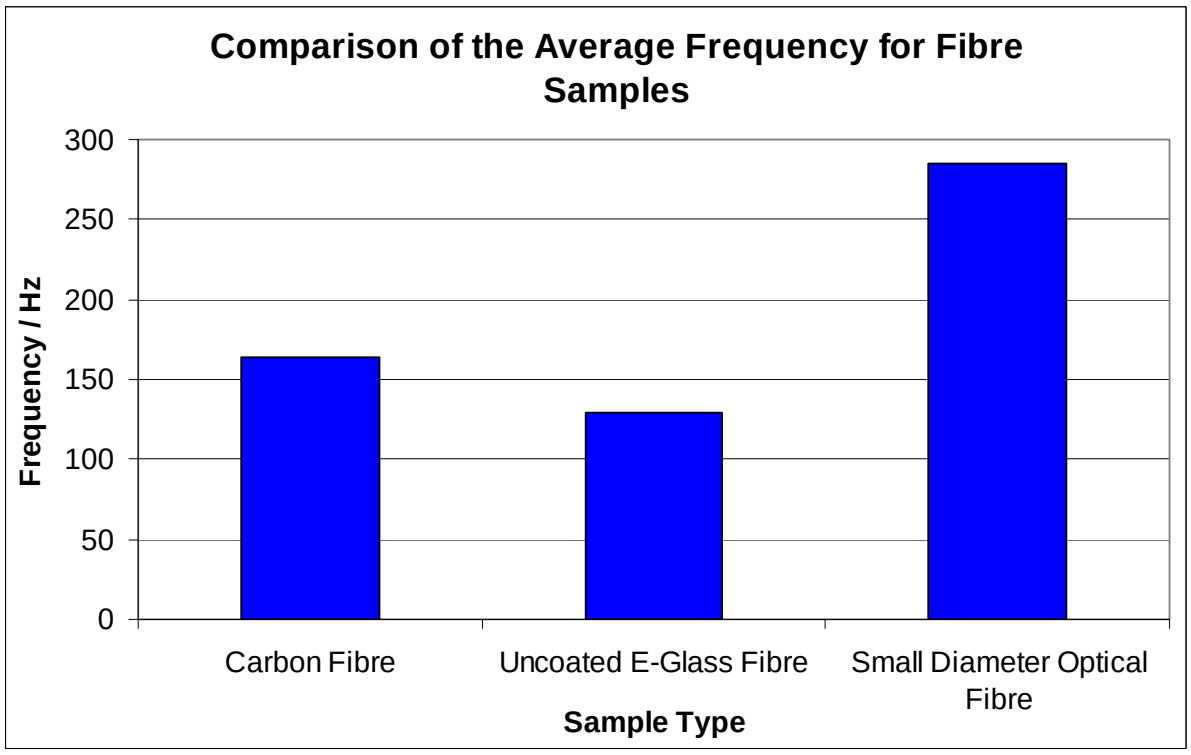

Figure 32: The average frequency of acoustic emission hits for fibre samples during tensile testing.

6.2 Resin Samples

6.2.1 Mechanical Testing Results: Stress vs. Strain

The results from the tensile testing of the resin samples have been summarised in the form of Stress vs. Strain graphs. Figures 33 through 37 present a typical plot for each of the four resin systems. Figure 33 highlights the use of a red line on the stress strain graph to represent the Secant modulus which was calculated at strain values of 1.5, 3 and 5 %, the imposed red line was used to calculate the Secant modulus at 3 %. The changes in the Secant modulus are presented in Table 9.

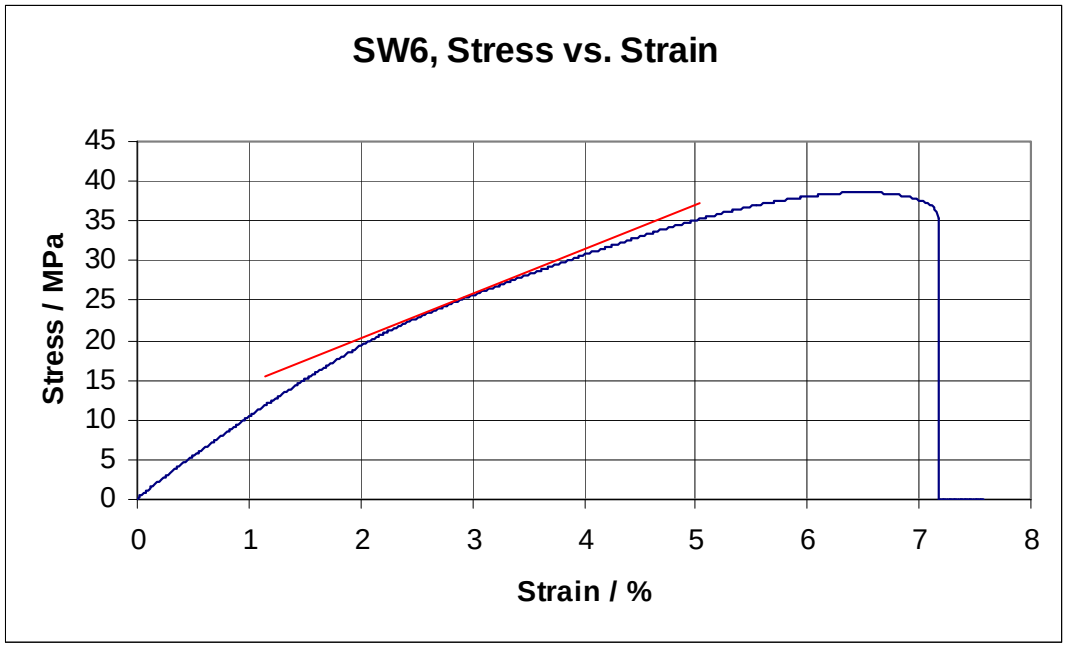

Figure 33: Load vs. Extension graph for a Scotchweld resin sample.

Strain (%)	Secant Modulus (GPa)
1.5	11.23
3	7.29
5	4.07

Table 9: The change in the average Secant moduli for Scotchweld amples during tensile testing.

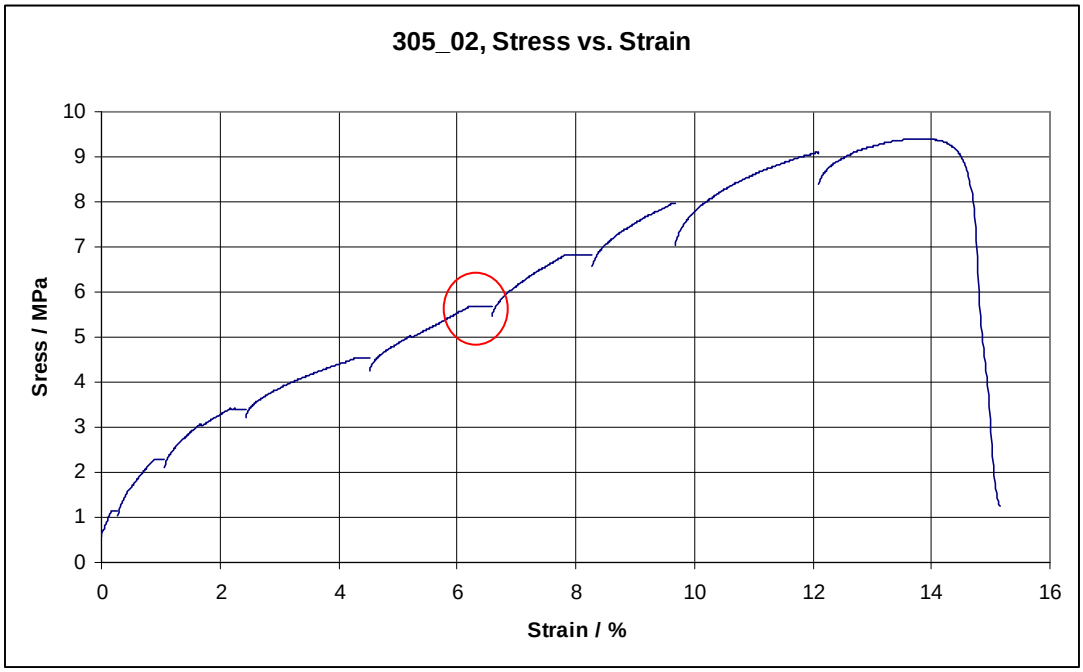

Figure 34: Load vs. Extension graph for a 305 resin sample. The horizontal regions represent the time when the extension was paused to record strain values.

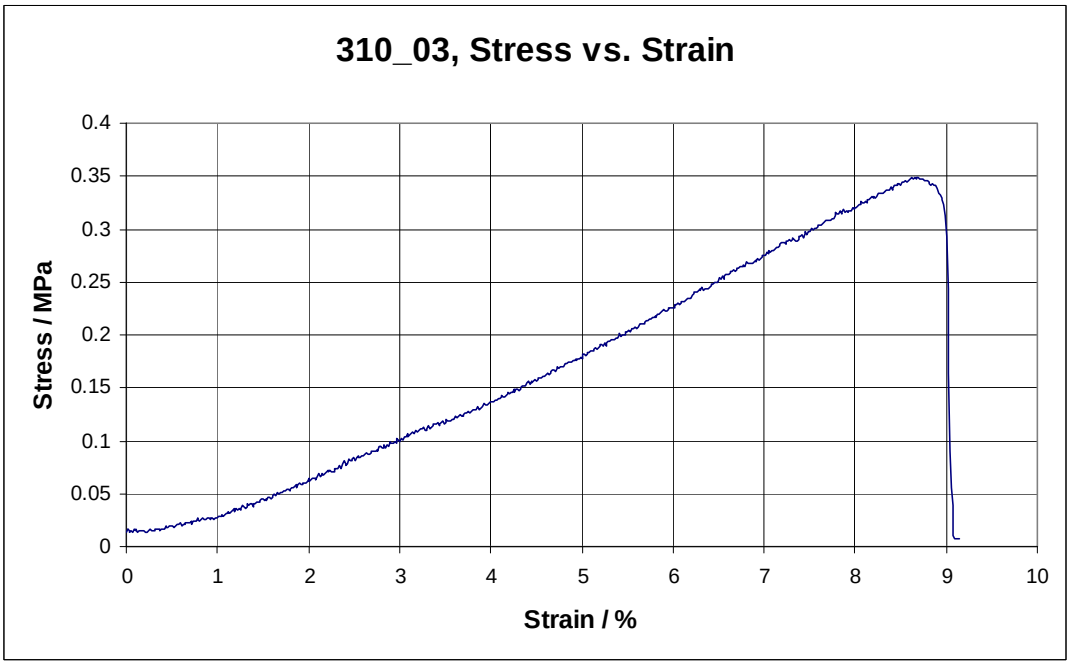

Figure 35: Load vs. Extension graph for a 310M resin sample.

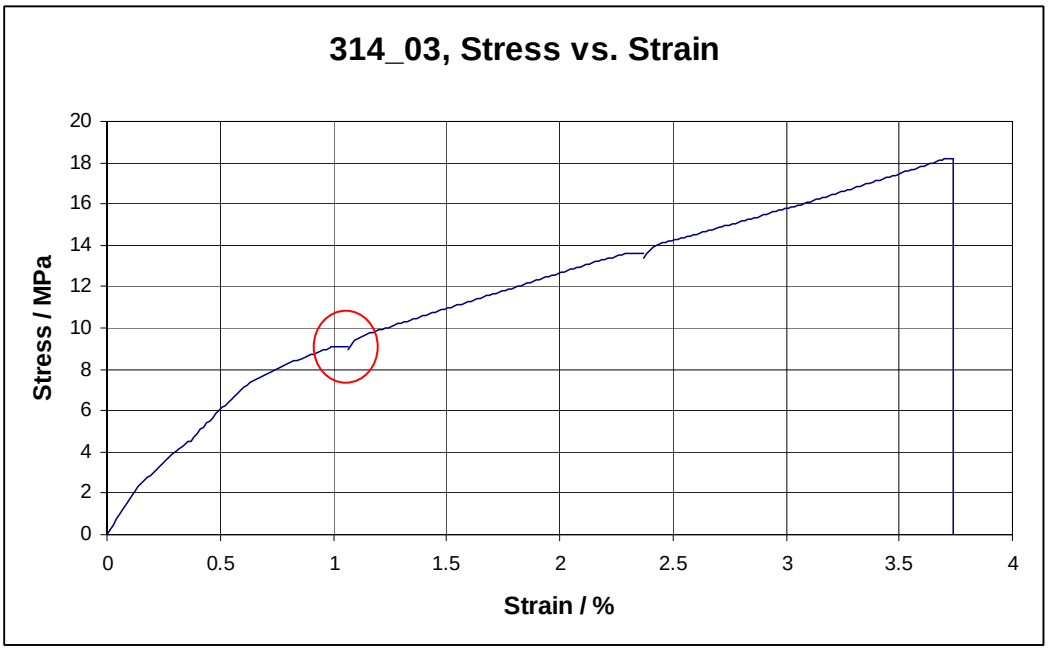

Figure 36: Load vs. Extension graph for a 314 resin sample. The horizontal regions represent the time when the extension was paused to record strain values.

Resin Type	Number of Samples	Time At Maximum Load (sec)		Maximum Load (N)		Extension at Maximum Load (mm)	
		Average	S.D.	Average	S.D.	Average	S.D.
Scotchweld	6	213	29	1685	136.5	1.67	0.25
Epo Tek 305	6	422	74	363	78.12	3.28	0.46
Epo Tek 310M	6	269	36	16	2.1	2.24	0.29
Epo Tek 314	6	169	68	842	109.7	1.06	0.61

Table 10: A comparison of the average mechanical testing values for the resin samples.

Resin Type	Number of Samples	Young's Modulus (GPa)	Ultimate Tensile Strength (MPa)
		Average	Average
Scotchweld	6	10.01	36.33
Epo Tek 305	6	7.22	7.88
Epo Tek 310M	6	4.62	0.35
Epo Tek 314	6	7.28	19.06

Table 11: A comparison of further mechanical testing values for the resin samples.

The three Epo Tek resin system samples proved difficult to test. The varying stiffness of the samples was the main obstacle; the Epo Tek 310M samples were ductile with a Young's Modulus of 4.62 GPa as presented in Table 11. Whilst the Epo Tek 314 samples had a higher Young's Modulus of 7.28 GPa the brittle nature of the samples resulted in a high accuracy being implemented the testing procedure being required. The testing procedure was different from the reported experimental procedure for the Epo Tek 310M , the samples required 2mm diameter holes to be drilled through the end-tabs and Steel wire to be looped through to ensure the sample were not crushed in the jaws of the Instron. This was a un-forseen obstacle but the changes in the testing procedure enabled the tensile tests to be successfully performed. The testing procedures were carefully implemented to achieve the results presented in Tables 10 & 11.

Table 11 provides a comparison between the ultimate tensile strength (UTS) of the samples. The Epo Tek 310M samples had the lowest UTS of 0.35 MPa this was not even 5 % of the UTS for Epo Tek 305 which was 7.88 MPa. The Epo Tek 314 had the largest UTS of the EpoTek samples at an average of 19.06 MPa, this range in UTS reinforces the need for different testing procedures to ensure the samples could be accurately tested.

As previously mentioned the Secant modulus was recorded at 1.5, 3 and 5 % strain. This was due to the curved slope in Figure 33 of the stress / strain graph for the Scotchweld samples. Table 11 presents an average Young's modulus of 10.01 GPa for the 6 samples. In Table 9 the Secant modulus varies from 4.07 GPa – 11.23 GPa throughout the tensile tests.

Figure 34 presents a Stress vs. Strain graph for sample 305_02, the horizontal part of the trace at 5.65 MPa is the point at which the tensile test was held for the strain to be recorded. In most tests the increase in strain at the held point was minimal as highlighted in Figure 36, for some of the samples such as 305_06 when the load was applied after the held state the Instron did not increase the load as the sample was extending at the required rate of 1.5 mm/min at the current load.

6.2.2 Electrical Resistance Results

305 Electrical Resistance Strain Gauge Data

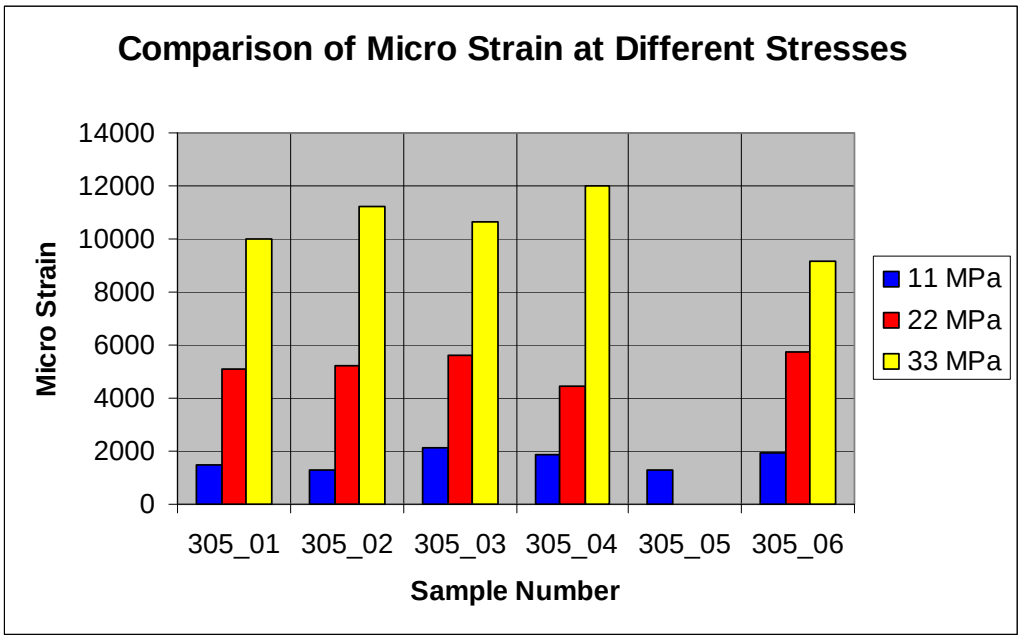

Figure 37: Strain recordings for tensile testing of 305 resin sample.

310M Electrical Resistance Strain Gauge Readings

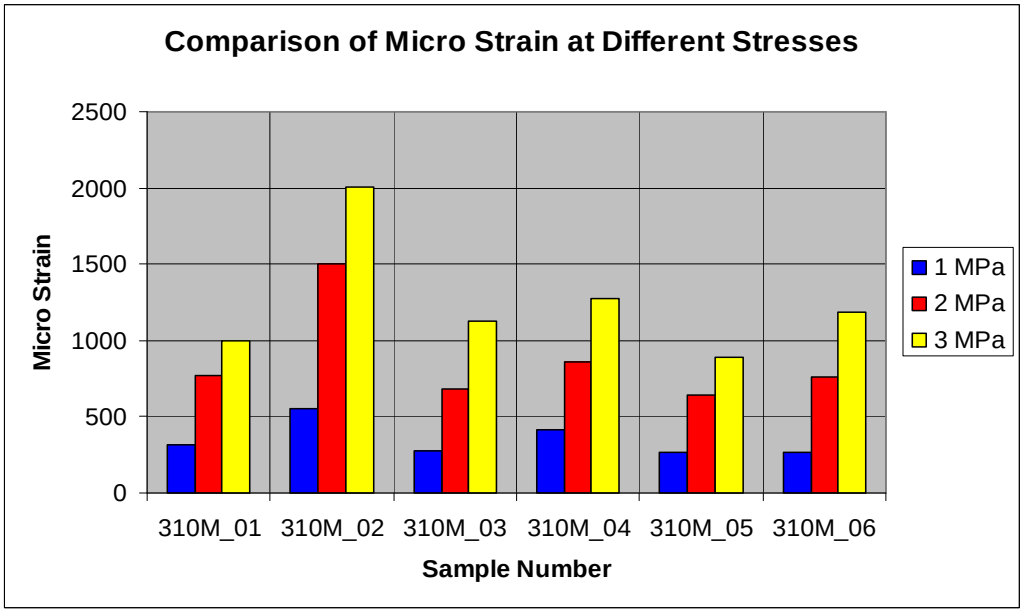

Figure 38: Strain recordings for tensile testing of 310M resin sample.

314 Electrical Resistance Strain Gauge Readings

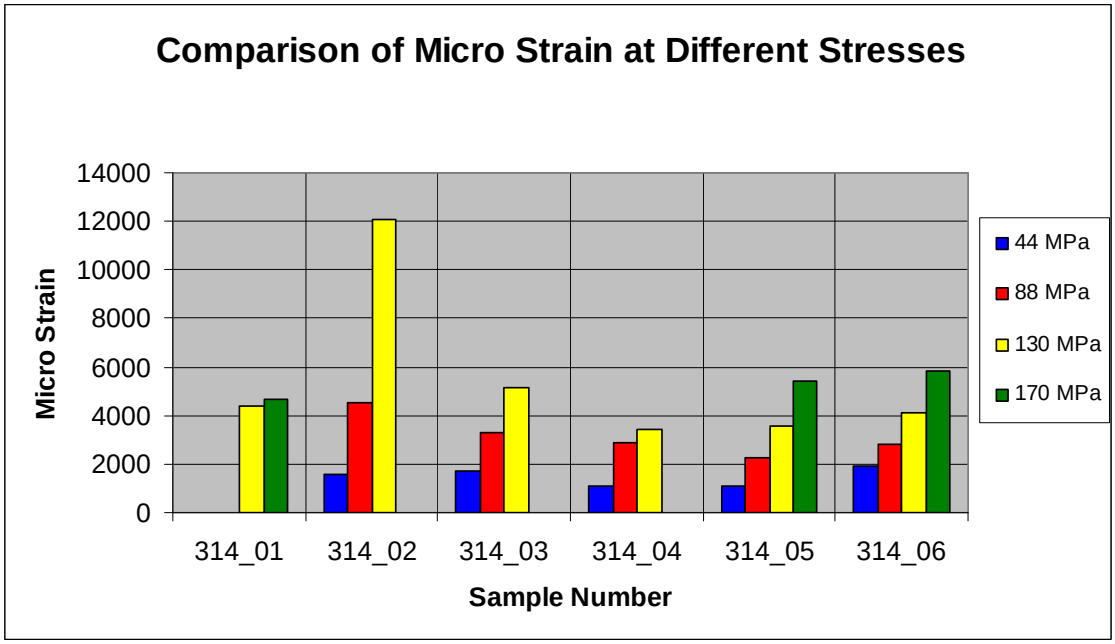

Figure 39: Strain recordings for tensile testing of 314 resin sample.

Strain data were recorded on each Epo Tek sample using an electrical resistance strain gauge and a surface mounted fibre Bragg grating (FBG). Electric strain gauge data was successfully recorded for all 305 samples apart from 305_05 sample as indicated in Figure 37, this was due to the strain gauge peeling off the surface of the sample. Figure 37 demonstrates a consistent recording of strain data for stresses of 11 MPa, 22 MPa and 33 MPa. These stresses were calculated from the loads at which the samples were in the hold part of the ramping procedure i.e. 50 N, 100 N and 150 N.

With such a low failure load recording strain data for 310M samples proved hard as the time for the test to complete was much shorter than that of all other samples. Figure 38 shows recordings were taken at 5 N, 10 N and 15 N, stresses calculated from these loads meant that the strain

values were plotted against stress values of 1 MPa, 2 MPa and 3 MPa. Sample 310M_02 is an anomalous result with both the readings taken at 2 MPa and 3 MPa being around double of the recordings taken for the other 310M samples.

Micro strain values for Epo Tek 314 samples were recorded at 200 N, 400 N, 600 N and 800 N, Figure 39 presents the changes in strain plotted against the stresses at these loads: 44 MPa, 88 MPa, 130 MPa and 170MPa. Figure 39 shows results were recorded for all samples at 130 MPa and three samples had micro strain values recorded at 170 MPa. Apart from an anomalous result for sample 314_02 where the micro strain greatly increases at 130 MPa the consistent increase in strain can be clearly seen as the stress increases. Figure 39 has no data plotted for sample 314_01 at 44 MPa and 88 MPa but data was recorded for 130 MPa and 170 MPa. This was due to the contact between the strain gauge wires, contacts and connecting leads not having a consistent and reliable enough connection.

6.2.3 Fibre Bragg Grating Strain Results

The installation of Fibre Bragg Gratings (FBG) onto the surface of the three EpoTek resin systems allowed strain data to be recorded in conjunction with data recorded by the electrical resistance strain gauges. Figures 40 presents a successful recording of the changes in wavelength recorded, disappointingly traces of this clarity were only recorded for a third of all samples. Despite some splitting of the peak for loads above 400 N; Figure 40 present's seven clear peaks with a high reflectivity percentage where calculation of the changes in strain is possible.

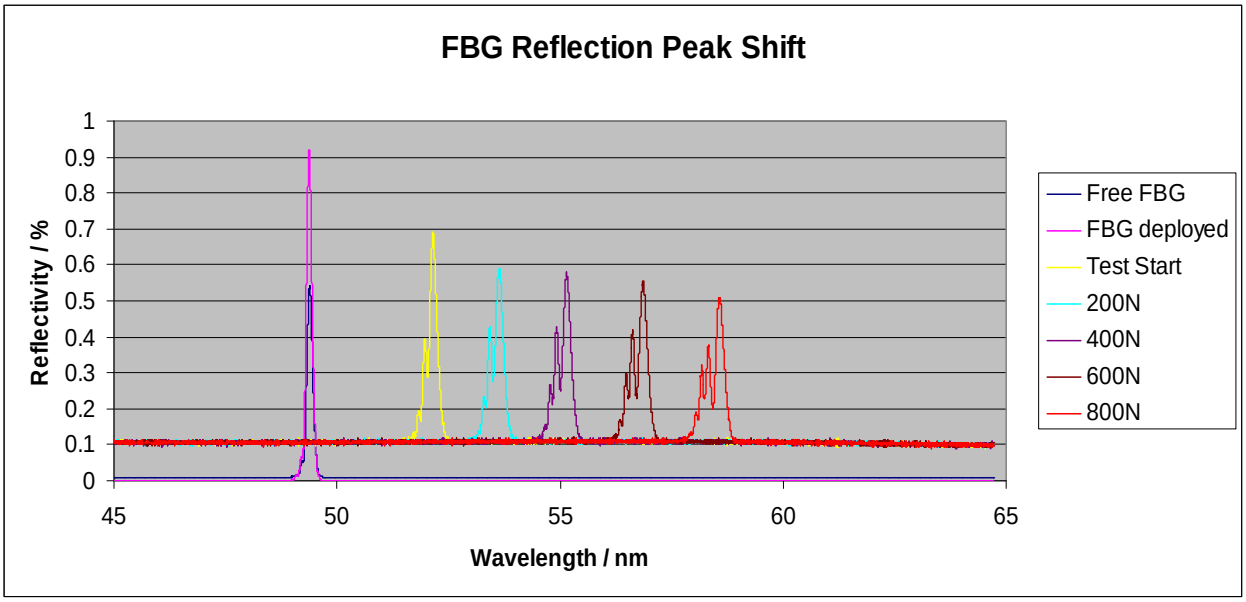

Figure 40: The changes in FBG peak shift for Epo Tek sample 314_04 before and during tensile testing.

Due to the dimensions of the resin samples the hardest task was mounting the FBG alongside the electrical resistance strain gauge. It was necessary to ensure that the FBG was securely mounted onto the sample, whilst at the same time allowing the remainder of the optical fibre to pass out of the Instron grips and connect to the Fibrepro to allow the wavelengths to be recorded. The method applied for this attempted for as little as possible of the cladding to be stripped from the

fibre. This resulted in the fibre being able to bend but not alter the Bragg wavelength that was being recorded. When the methodology was successfully implemented the shifting of the peak was easily analysed as in Figure 40. When the FBG was not successfully attached to the sample or the fibre was not able to reach the Fibrepro without distorting the reflectivity of the peaks was severely decreased; Figure 41 is such an example.

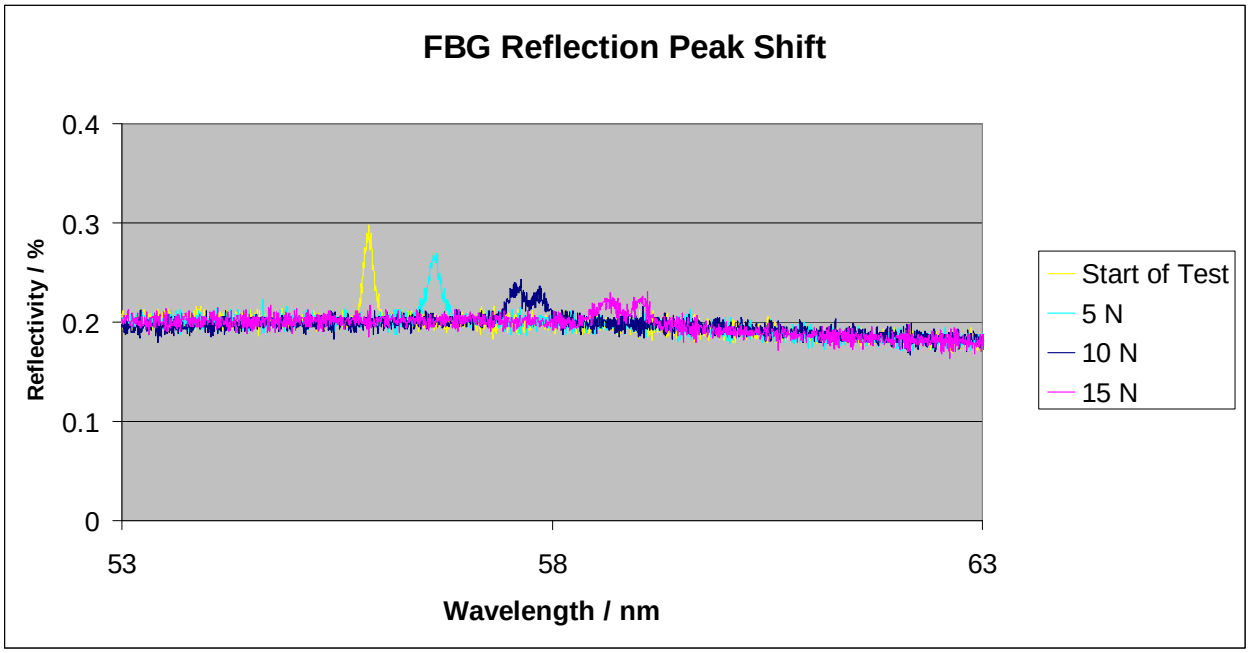

Figure 41: The changes in FBG peak shift for Epo Tek sample 310_03 before and during tensile testing.

The most successful results were for the Epo Tek 310M samples, with an improved reflectivity percentage it was easier to distinguish peaks and all bar one sample had wavelengths recorded at multiple loads. The improved reflectivity was due to the resin samples being tensile tested using wire extensions. The wires ensured a greater distance between the grips and allowed the optical fibre to connect to the Fibrepro without bending.

Figures 42 – 44 present a comparison between the average micro strain values recorded by Electrical Resistance Strain Gauges (SG) and FBGs against stress.

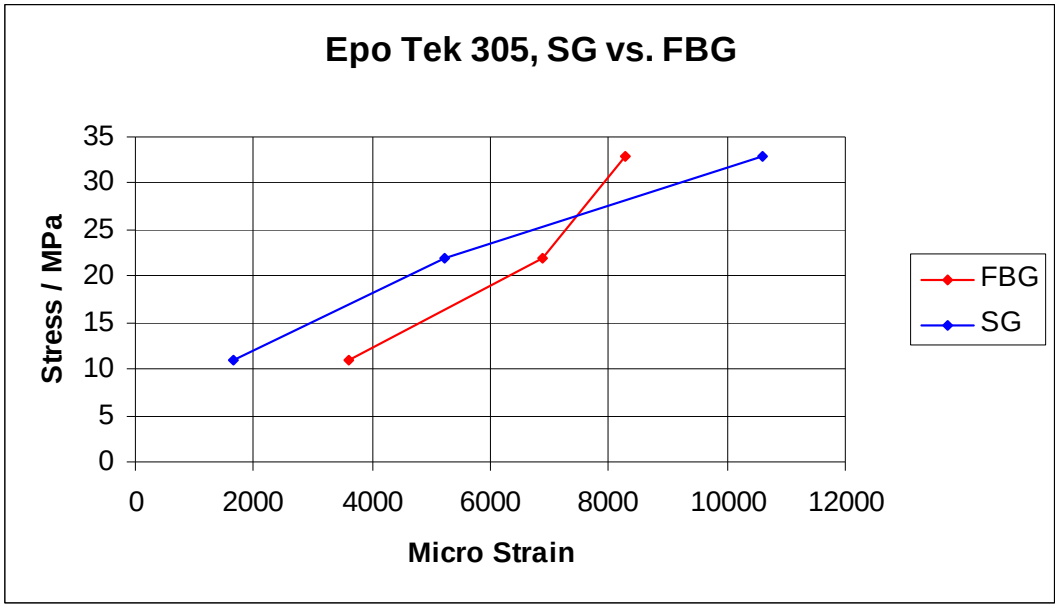

Figure 42: A comparison between electrical strain resistance gauges and Fibre Bragg Grating strain recordings for Epo Tek 305 samples.

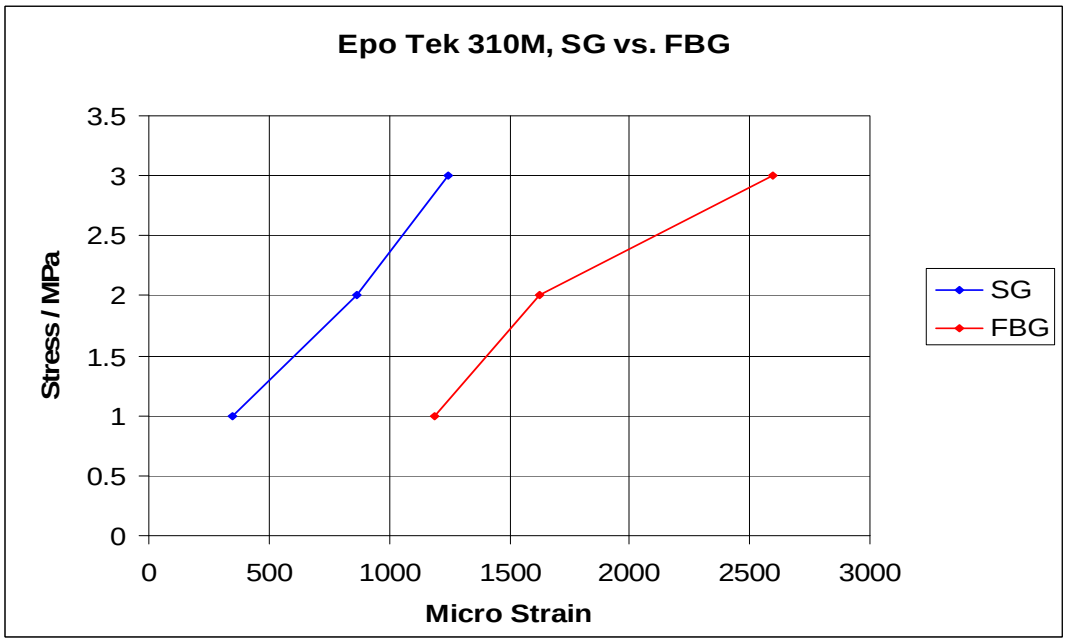

Figure 43: A comparison between electrical strain resistance gauges and Fibre Bragg Grating strain recordings for Epo Tek 310M samples.

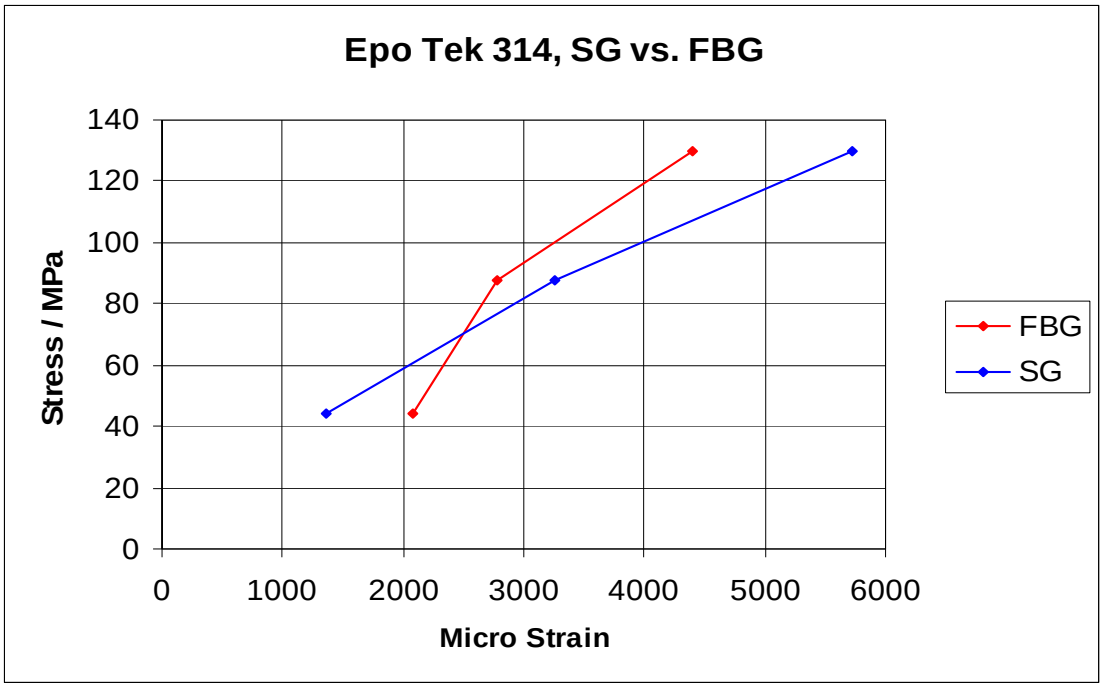

Figure 44: A comparison between electrical strain resistance gauges and Fibre Bragg Grating strain recordings for Epo Tek 314 samples.

Figures 42 & 43 present a similar increase in strain from the first recording to the second recording for both the SG and FBG. For both sample types the SG demonstrates a greater increase in strain from the second to third reading than the increase from first to second reading. For the same readings the FBG demonstrate a smaller increase in strain than the first to second reading. Figure 43 presents a consistent increase in strain throughout the test as recorded by the SG; the FBG shows a greater increase in strain from the second to third reading than the increase from first to second reading. There is not a consistent difference between the strain values recorded by the two methods for any sample set or between sample types. This suggests that the difference between the methods is not associated with an off set or calibration factor between the two methods.

The differences in micro strain recorded can be associated with the adhesion of the FBG and the SG to the surface of the sample. It was recorded during experiments that the components were prone to peeling away from the sample at higher loads. This in turn limited the ability of the components to provide accurate wavelengths and peaks or digital readouts for the strain to be recorded. Figures 42 - 42 demonstrate their largest difference in recording at the final measurement i.e. at the highest stress.

6.2.4 Acoustic Emission Results

The Acoustic Emission results for the resin sample are presented in Table 12; the average values for the different parameters are presented as are the Standard Deviations of the results.

Sample Type	Number of Samples	Number of Hits		Amplitude (mV)		Peak Frequency (kHz)		Average Frequency (kHz)	
		Average	S.D.	Average	S.D.	Average	S.D.	Average	S.D.
Scotchweld	6	29	8	58	1.91	283.04	73.63	120.94	39.87
Epo Tek 305	6	191	74	39.4	2.6	118.67	82.05	118.48	54.62
Epo Tek 310M	6	26	25	22.4	4.73	214.4	85.69	240.36	184.65
Epo Tek 314	6	238	179	36.93	2.2	94.72	28.17	138.6	30.03

Table 12: A comparison of the Acoustic Emission parameters for the resin samples.

Acoustic Emission results for pure matrix samples during tensile testing have been found to have a maximum amplitude of 60 mV for matrix cracking (Haselbach & Lauke, 2003). The Scotchweld samples had an average amplitude of 58 mV, with a threshold set at 25 mV all amplitude recordings lower than this value were excluded, if a lower threshold value had been implemented the average amplitude would have been lower. This would have still resulted in all recordings being lower than the reported maximum of 60 mV for matrix cracking. The authors also recorded peak frequencies for matrix cracking ranging from 100 kHz – 200 kHz Table 12 shows that the average frequency of 120.9 kHz falls into the aforementioned frequency range. The average peak frequency presented in Table 12 was 283 kHz, these recordings were the least consistent of the parameters with a SD of 26 %. As previously stated there were less hits recorded

for the resin samples, an average of 29 hits per sample were recorded for the Scotchweld samples. These recorded parameters agree favourably with the AE parameters recorded by Haselbach & Lauch.

The Epo Tek resin samples proved to be the least consistent set of samples in terms on number of hits recorded. Table 12 prove the amplitude to be the most consistent results for the 305 samples with an average amplitude of 39 mV and SD of 2.6 mV. The average frequency and peak frequency had close to identical values of 118.48 kHz and 118.67 kHz as presented in Table 12. Again all these values fall into the ranges specified by Haselbach & Lauch.

Epo Tek 310M samples provided the fewest hits on average of all sample the sample types. The amplitude recordings were the most consistent of the recorded parameters with an average amplitude of 22.4 mV and a SD of 4.73 mV this was well below the maximum 60 mV associated with matrix cracking. An average frequency of 240.4 kHz and a peak frequency recording of 214 kHz were the least consistent parameters recorded as demonstrated with SD's of 184.65 and 85.69 kHz.

The amplitude recordings for Epo Tek 314 proved to be the most consistent of the recorded parameters, an average amplitude of 36.9 mV was recorded with a SD of 2.2 mV. An average of 138.6 kHz was recorded for the average frequency. The peak frequency was the least consistent parameter recorded with a SD of 29 %, the average peak frequency was 94.7 kHz. Whilst the SD of the average frequency – 22 % and peak frequency – 29 % for the Epo Tek 314 samples they were considerably less than the SD of Epo Tek 310 M and 305.

The analysis of the AE results for the resin samples has highlighted the varying levels of consistency especially for Epo Tek 305 and Epo Tek 310M. It has been documented that AE testing of polymers has particular difficulties resulting from the properties of the material such as low Young's modulus and high damping. This results in the AE sensor needing to be located near the zone of due to the low rate of energy release in polymers (Leps *et al.* 1986). The Epo Tek 305 and 310M samples were extremely ductile and had much lower Young's modulus values than those of the Epo Tek 314 and Scotchweld samples. Whilst there was a greater range in the hits recorded for the Scotchweld and 314 samples the analysis of the parameters for these sample sets as previously stated revealed a greater consistency.

6.2.5 Summary of Results for Resin Samples

Figure 45 provides a summary of the maximum load applied to the fibre samples. Figure 46 and 47 provide a summary of the amplitude and average frequency of the acoustic emission hits recorded respectively. The same parameters have been chosen to be presented for the same reaons as the figures presented in the summary of the fibre results.

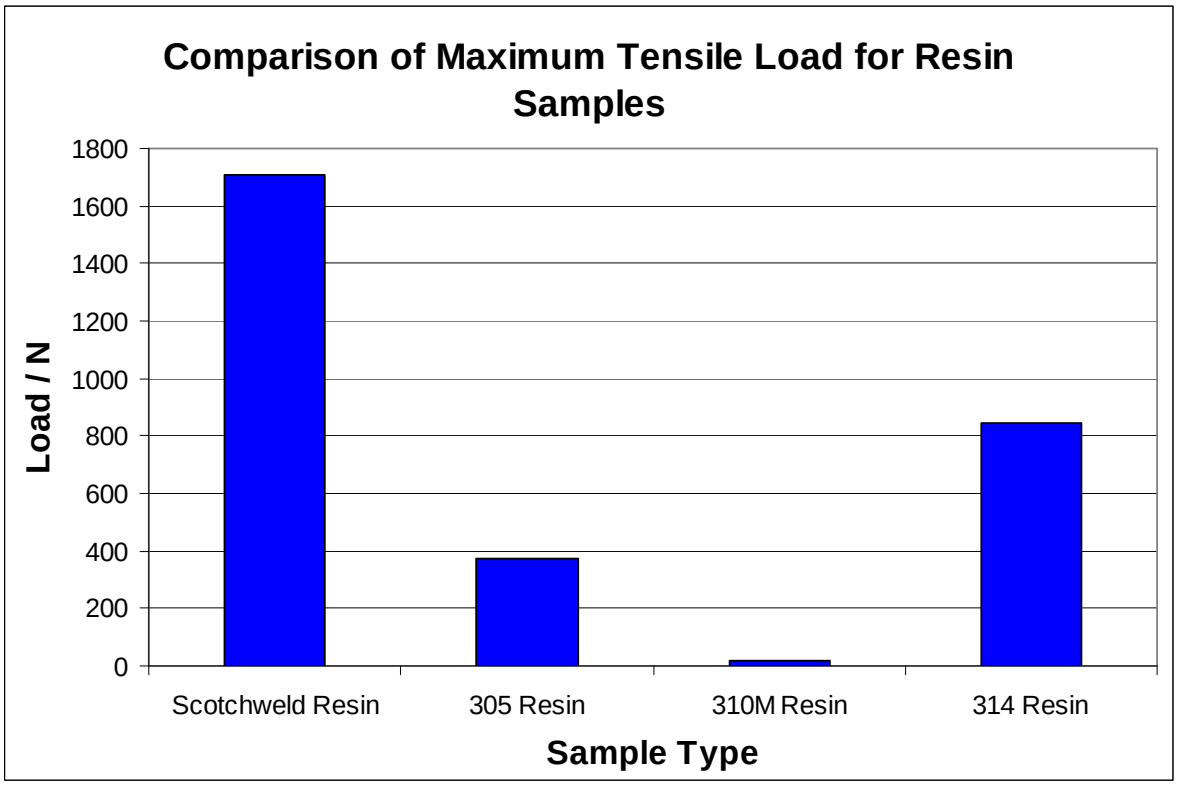

Figure 45: The maximum load applied for resin samples during tensile testing.

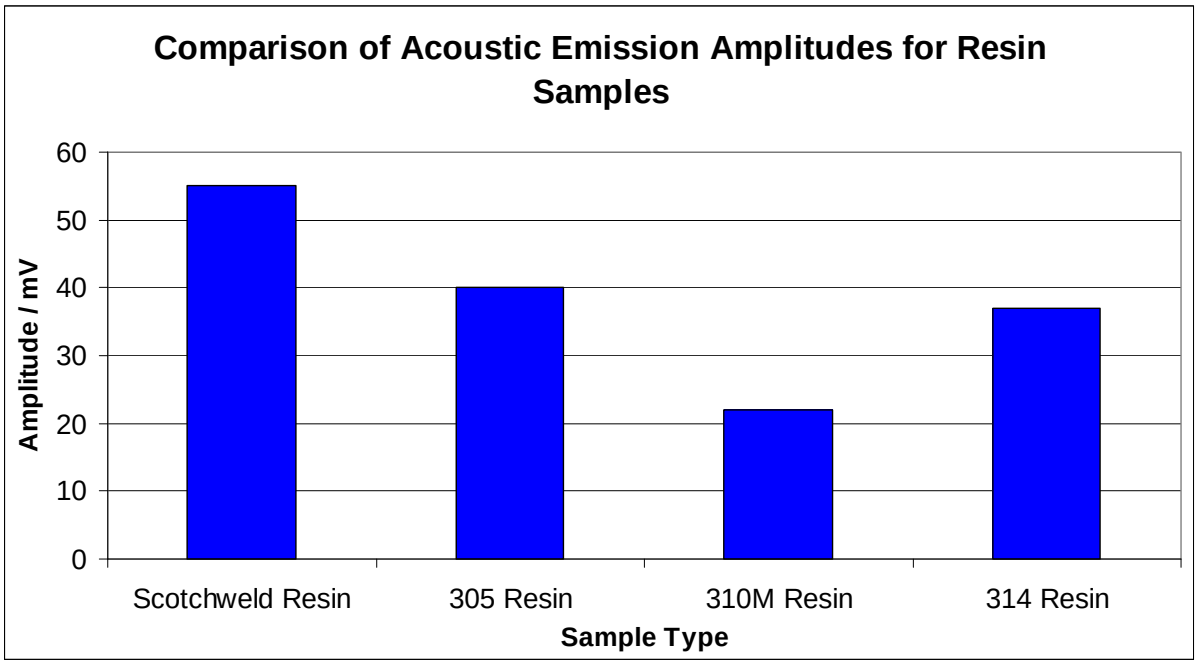

Figure 46: The amplitude of acoustic emission hits for resin samples during tensile testing.

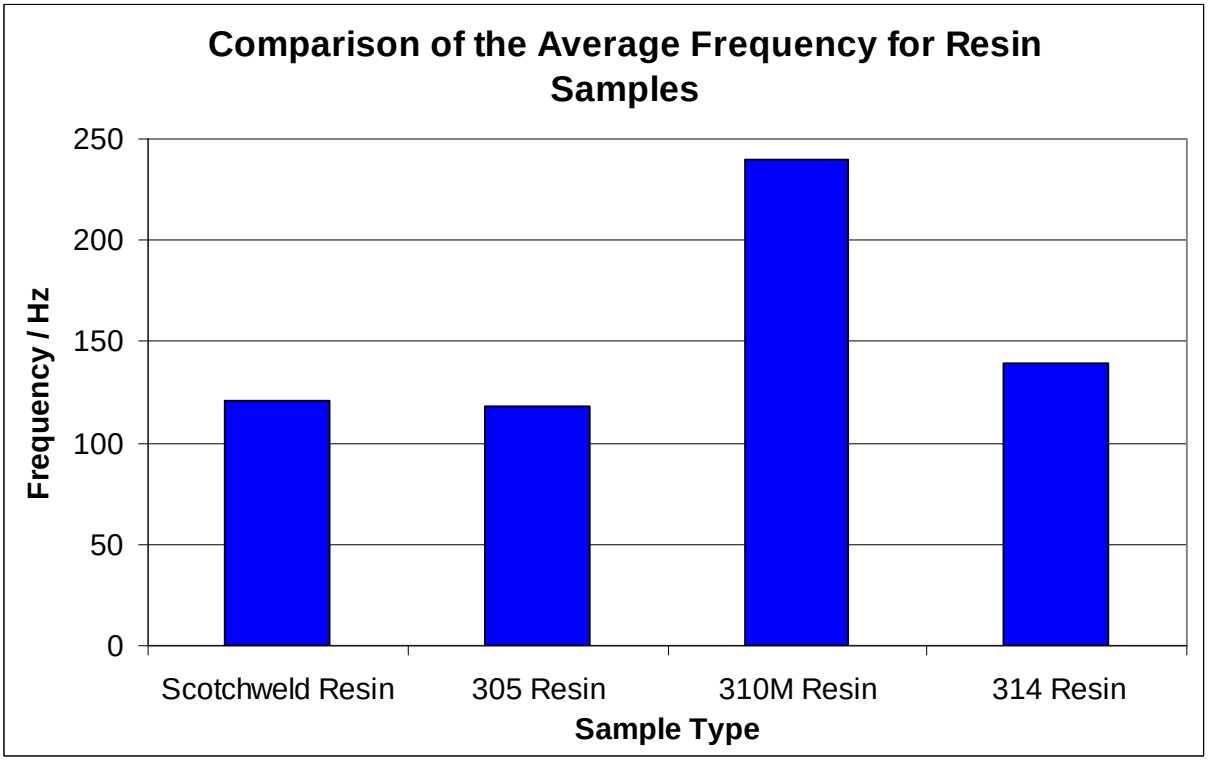

Figure 47: The average frequency of acoustic emission hits for resin samples during tensile testing.

6.3 Composite Samples

6.3.1 Mechanical Testing Results: Stress vs. Strain

The results for the mechanical testing of the composite samples have been presented with typical Stress vs. Strain traces for each sample type in Figures 48 and 49. Tables 13 and 14 summarise the average mechanical properties of the two types of composite sample.

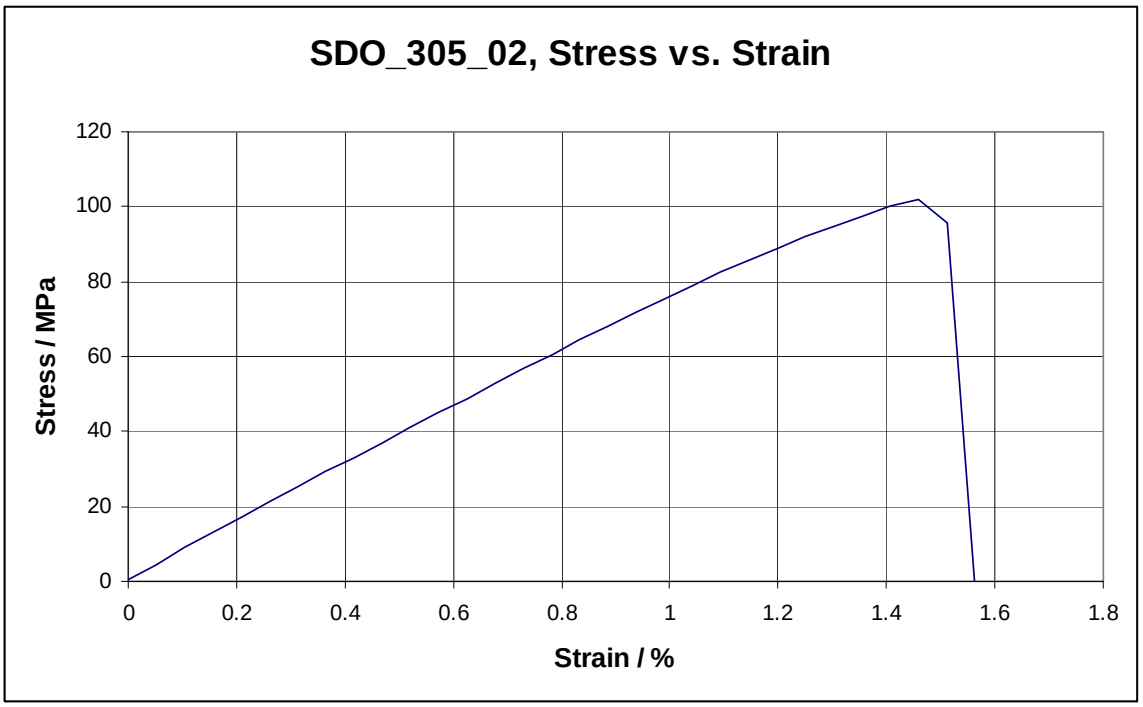

Figure 48: Stress vs. strain graph for a small diameter optical fibre / 305 resin composite sample.

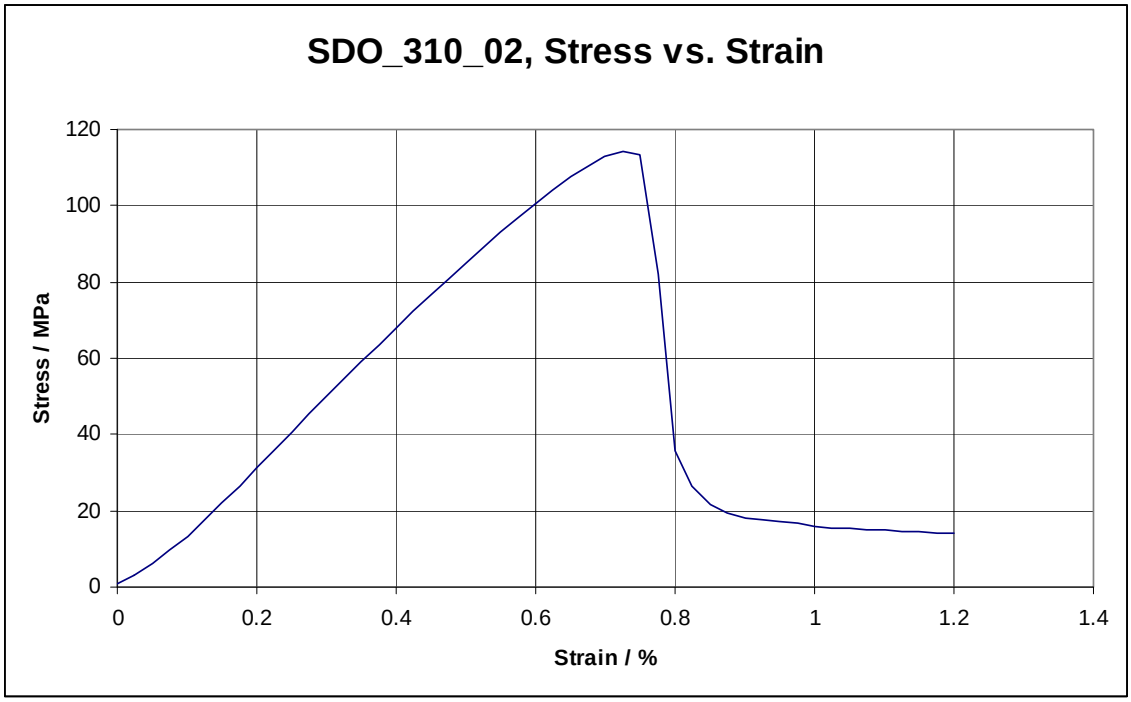

Figure 49: Stress vs. strain graph for a small diameter optical fibre / 310M resin composite sample.

Composite Type	Number of Samples	Time At Maximum Load (sec)		Maximum Load (N)		Extension at Maximum Load (mm)		Young's Modulus (GPa)
		Average	S.D.	Average	S.D.	Average	S.D.	Average
Epo Tek 305 / SDO Fibre	6	21	9.1	491.88	111.8	1.19	0.33	23.21
Epo Tek 310M / SDO Fibre	6	28	7.2	288.89	62.26	0.97	0.15	16.25

Table 13: A comparison of the average mechanical values for the composite samples.

Composite Type	Number of Samples	Young's Modulus (GPa) Average	Ultimate Tensile Strength (MPa) Average
Epo Tek 305 / SDO Fibre	6	23.21	244.93
Epo Tek 310M / SDO Fibre	6	16.25	144.44

Table 14: A comparison of further mechanical values for the composite samples.

The two sets of composite samples failed before the maximum load achieved by the SDO fibres as presented in Table 7, but were applied to greater maximum loads that the respective resins they were fabricated from. It would be expected for the composite samples to have a higher maximum load applied than that of the fibres. The SDO fibres also had a higher a greater percentage extension at the maximum applied load than that of the composite samples. The Young's modulus of the samples was considerably higher than the modulus of the neat resin samples for both types of composite. Table 14 presents the Young's modulus of the samples, the Epo Tek 305 / SDO Fibre had an average Young's modulus of 23.21 GPa, 15.99 GPa greater than the Young's modulus of Epo Tek 305. The Epo Tek 310M / SDO Fibres had a Young's modulus 11.63 GPa greater than neat Epo Tek 305.

The fabrication of the composite samples relied on a step at the end of the composite (Figure 25), the step in the sample proved to be a weak point. Failure in the sample was recorded at this point or this point was a site of initiation for failure for the majority of composite samples. Figure 44 is an example of such a failure, the decrease in stress after the Ultimate Tensile Stress (UTS) has

been reached stops at 90 MPa just under 50 % of the UTS. Whilst the extension of the sample continues the decrease in stress declines and then slowly increases.

6.3.2 Acoustic Emission Results

The results of the Acoustic Emission testing for the two composite samples are presented in Table 15.

Sample Type	Number of Samples	Number of Hits		Amplitude (mV)		Peak Frequency (kHz)		Average Frequency (kHz)	
		Average	S.D.	Average	S.D.	Average	S.D.	Average	S.D.
Epo Tek 305 / SDO Fibre	6	2140	1593	44.2	7.58	213.69	52.28	210.07	50.79
Epo Tek 310M / SDO Fibre	6	1118	593	34.9	4.32	174.83	41.87	231.73	23.08

Table 15: A comparison of the Acoustic Emission parameters for the composite samples.

The Epo Tek 305 / SDO fibre (SDO 305) and Epo Tek 310M / SDO (SDO 310) composites proved to be the toughest samples to test due to the small contact area of the composite and piezoelectric sensor. The average number of hits recorded for the SDO 305 samples was 2140, the average amplitude was 44 mV and was the most consistent recorded parameter. The average frequency was 210 kHz and the average peak frequency was 214 kHz but was the least consistent of the parameters with a SD of 52.2 kHz.

There were fewer hits recorded for the SDO 310 composites than the SDO 305 composites with an average of 1118 hits recorded per sample, this difference is in agreement with the neat resin samples where there were fewer hits for the Epo Tek 310 M samples than the Epo Tek 305 samples. An average amplitude of 34.9 mV was recorded with a SD of 4.32 mV. The SDO 310 composite samples had an average frequency of 231.7 kHz and a peak frequency of 174.8 kHz but had a SD of 24 %. The average frequency and peak frequency of the SDO 305 samples both had SD of 24 %, SD of this magnitude could be related to the contact of the piezoelectric sensor and the sensor.

To improve the repeatability and consistency of testing the contact between the piezoelectric sensor and the sample needs to be improved. The silicone gel was able to hold the sample in place but an improved method of using a temporary adhesive or the investigation into the use of smaller piezoelectric sensors should improve the contact between the sensor and sample. In turn the improvement in contact would help reduce the SD of the results especially when testing the frequency parameters.

6.3.3 Summary of Results for Composite Samples

Figure 50 provides a summary of the maximum load applied to the fibre samples. Figure 51 and 52 provide a summary of the amplitude and average frequency of the acoustic emission hits recorded respectively. The same parameters have been chosen to be presented for the same reaons as the figures presented in the summary of the fibre and resin results.

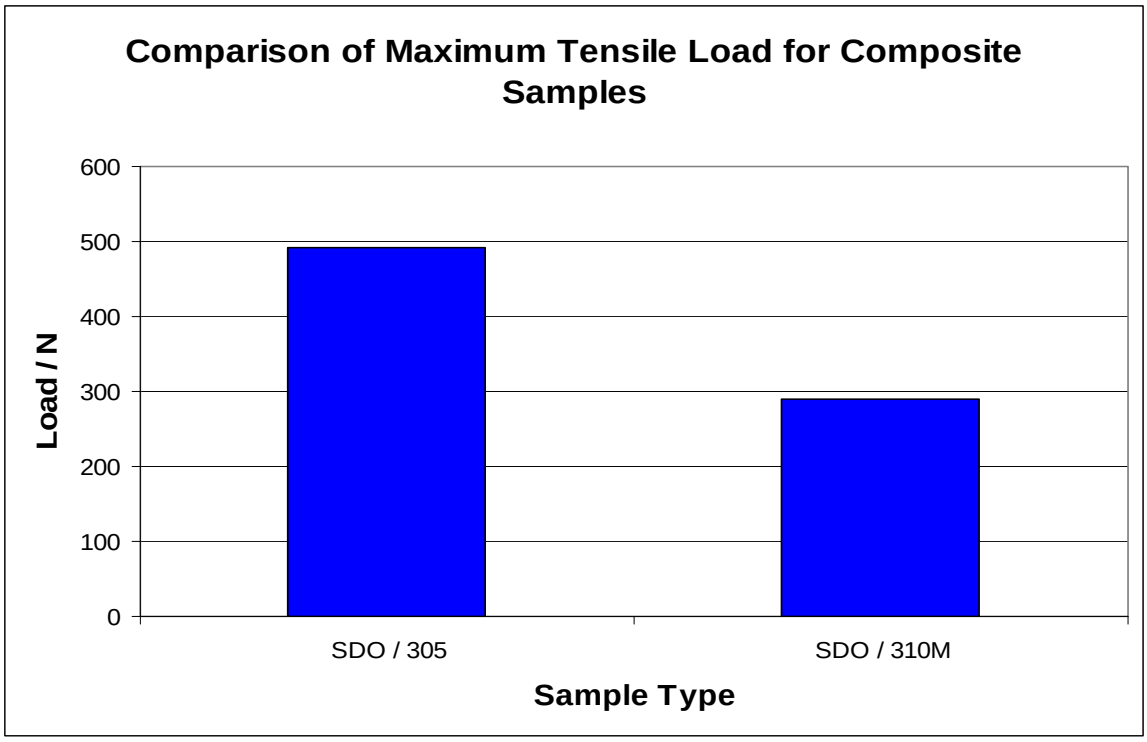

Figure 50: The maximum load applied for resin samples during tensile testing.

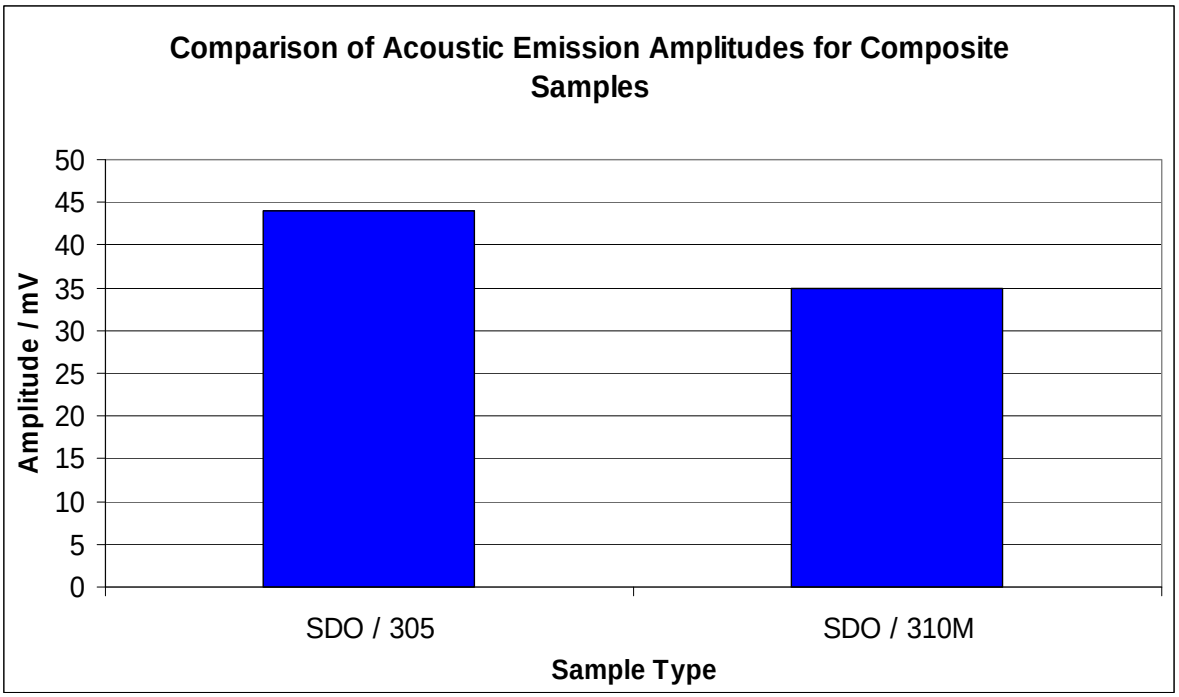

Figure 51: The amplitude of acoustic emission hits for composite samples during tensile testing.

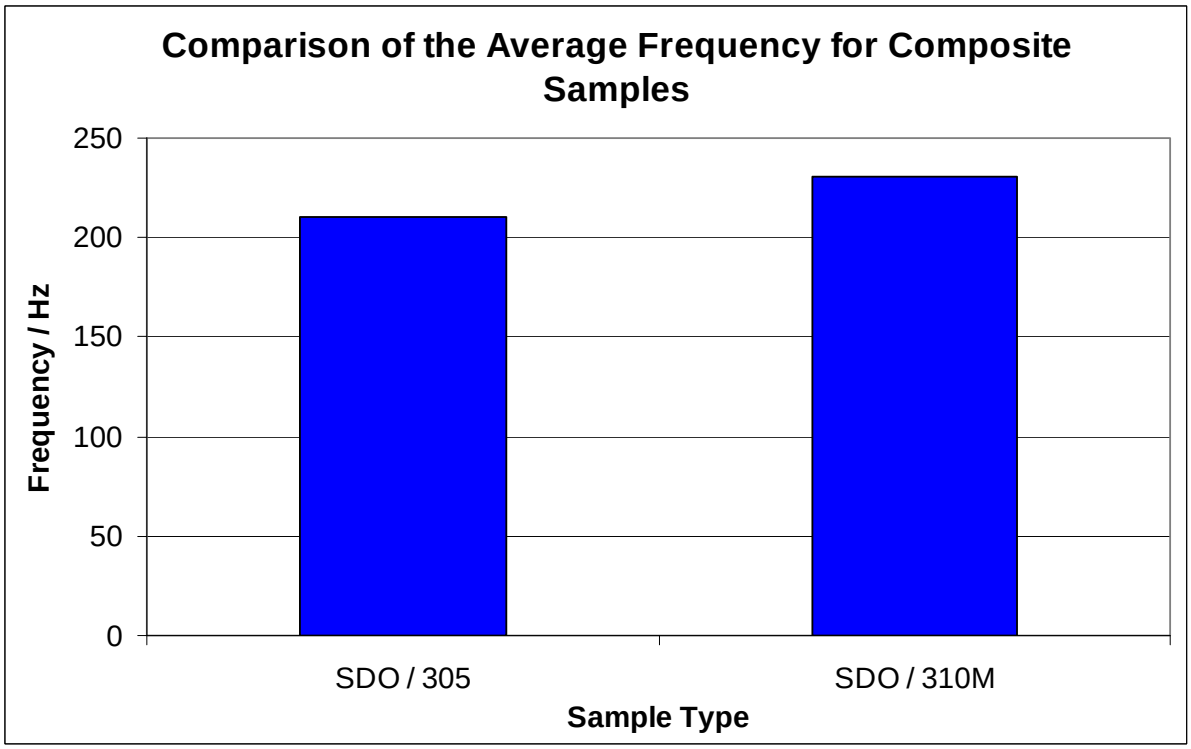

Figure 52: The average frequency of acoustic emission hits for composite samples during tensile testing.

6.4 Self Sensing Fibre Results

6.4.1 Self Sensing Fibre Analysis

The results for the self-sensing fibres have been presented in three parts. Figure 53 presents a typical plot for the change in normalised light intensity in comparison to the Load vs. Time trace from the tensile test. Table 16 presents the average changes in normalised light intensity to the changes in Load and time during the tensile test. Figures 54 – 56 are images from the end of the self-sensing fibre bundles captured at various stages during the tensile testing procedure.

SDO_3

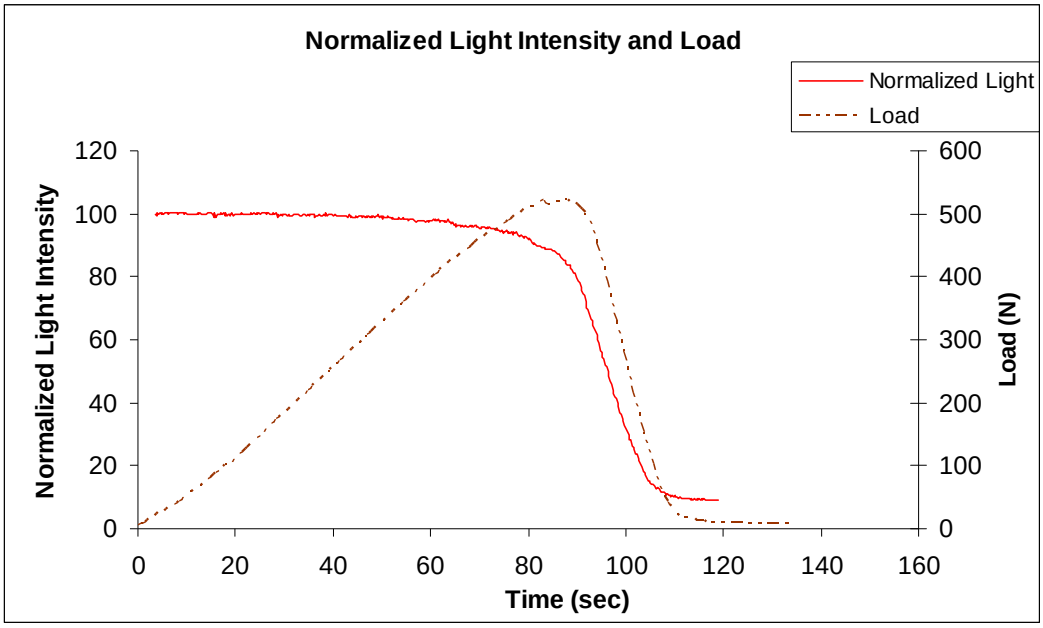

Figure 53: The change in normalised light intensity with a changing load during tensile testing.

Normalised Light Intensity (%)	Load		Time (sec.)
	(N)	(%)	
100	367.0	68.1	49.3
80	496.7	92.3	86.2
60	378.3	70.0	101.7
40	223.3	35.3	108.5
20	112.9	20.7	120.0

Table 16: The average change in light intensity compared to the change in load and duration of the tensile test for the SDO fibre samples.

6.4.2 Self-Sensing Fibre Images

SDO_4, Starting Image

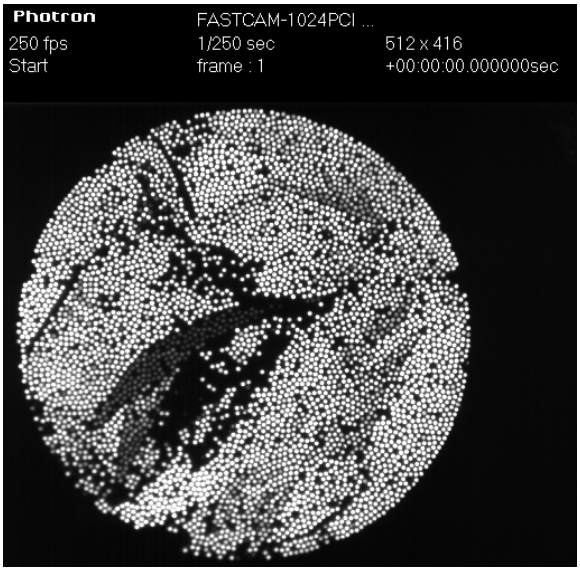

Figure 54: The initial image captured with the first AE hit for sample SDO_4.

SDO_4, 100 % Load

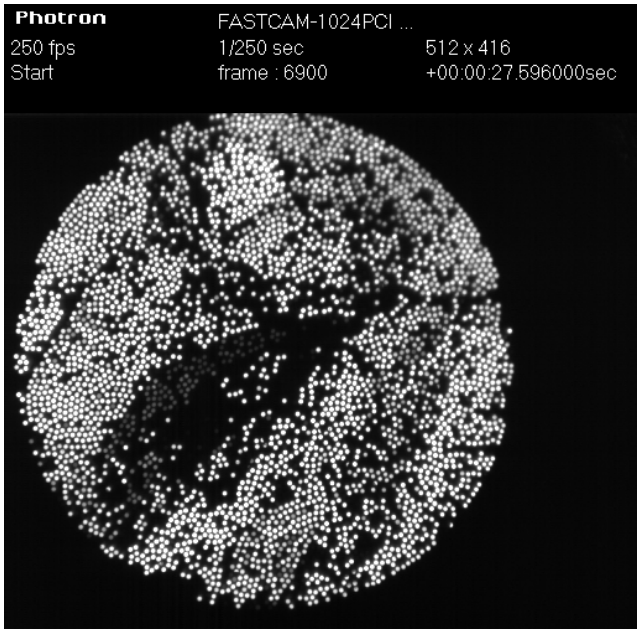

Figure 55: Image 6900 captured when maximum load was achieved during tensile testing of for sample SDO_4.

SDO_4, Final Image

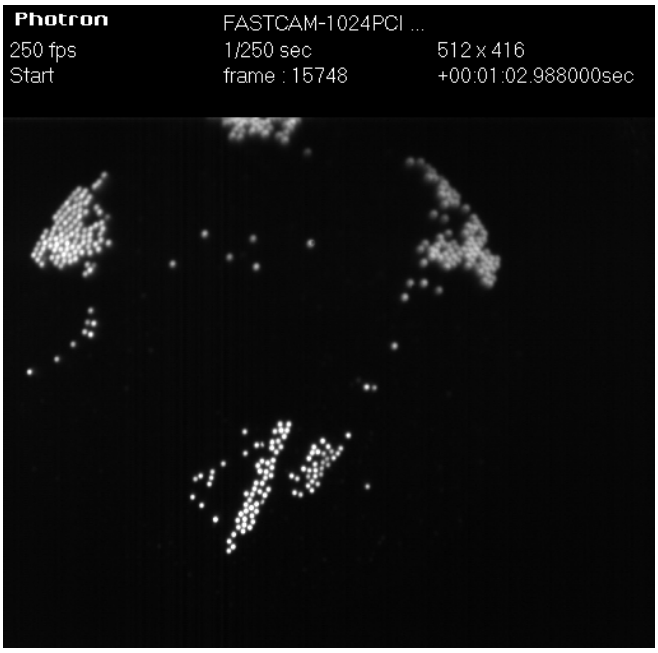

Figure 56: Image 15748 captured when 3.00 mm extension was achieved and the last image captured for sample SDO_4.

Qualitative results of the changing images have been presented, recording the initial image when the camera was triggered by the first AE hit is typified by the image recorded in Figure 54. Further images have been presented to demonstrate the changes from the start of recording to 100 % of the maximum load as in Figure 55 and then the final image recorded when the tensile test was recorded as presented in Figure 56.

Sample SDO_4 demonstrates the change in images recorded, Figure 55 is the image recorded when the load its maximum of 426 N. The images show minimal change from the first image to 50 % load, there is a larger change visible when the samples have reached their maximum load. This is in agreement with work completed by Kister *et al*. who stated that attenuation of reinforced fibre light guides began at 50 % of the failure load.

Graphical representation of the change in light intensity during the tensile test provides a quantative analysis. Hayes *et al*. presented graphical representation of the change in the light transmission characteristics before and after impact when using self-sensing fibres and embedded 50 µm optical fibres. Whilst it was possible to compare characteristics before and after impact Table 16 presents the average change in light intensity throughout the experiments whilst the SDO fibres were undergoing tensile testing.

National Instruments Vision Assistant v8.1 program was used to perform analysis of the recorded images throughout the tensile testing; this allowed the light intensity to be plotted against various parameters such as time, load, extension or AE Hits. As presented in Figure 53 data for the normalised light intensity was plotted against the time and load. Table 11 demonstrates the

average decrease in normalised light intensity was from 100 % to less then 20 %. Compared to the qualitative analysis where it is not possible to specify a start of attenuation of light intensity, analysis of the change in normalised light intensity with load from Table 11 suggests that attenuation of light intensity begins at an average of 84 % of the failure load. At this point the decrease in normalised light intensity occurs at a rate similar to the unloading rate. The light intensity consistently reached its minimum value at an average load of 55 N. These results are in agreement with Kister *et al*. that permanent damage in terms of fibre fracture can be detected using reinforced fibre light guides.

A major achievement of the mechanical testing process was the fabrication of the Top Hat end-tabs (Figure 16) for the fibre and composite samples. The design of the end-tabs ensured that the fibres in all samples were not crushed when the Instron grips were tightened, the fibres were set in the middle of the grips and the end-tabs were held in the correct position by pinning the corners. This allowed the maximum number of fibres to transmit light from the source to the end of the fibre. In turn this increased the number of fibres recorded by the camera and provided more data for data to be analysed and plotted against the changes in time and load as in Figure 53.

A further achievement of the testing of the self-sensing fibres was the equipment setup. By using the first Acoustic Emission recorded by the AEWin system as a trigger for the high speed camera to start recording it was ensured all changes in light intensity were recorded from the onset of damage.

7.0 CONCLUSION

Acoustic Emission characterisation of three fibre types was completed. The parameters of the AE hits were analysed, amplitude, average frequency and peak frequency were consistently recorded and proved to be accurate when compared with parameters analysed in previous literature. Four resin systems were successfully fabricated into samples for tensile testing and tested, Acoustic Emission characterisation was performed for the three aforementioned parameters and favourably agreed with Acoustic Emission analysis in previous literature. Successful fabrication of composite samples containing Small Diameter Optical fibres and Epo Tek 305 resin system and a further set using the alternative Epo Tek 310M resin system were tensile tested. Characterisation of Acoustic Emissions from the two composite types during tensile testing was completed and presented.

Analysis of the amplitude parameter proved to be the most consistent, the average frequency and peak frequency parameters were both accurate methods of detecting damage in the composite and provided substantial data for characterising Acoustic Emissions for all fibre, resin and composite sample. With the number of hits recorded and analysis of the parameters Acoustic Emission testing demonstrated its ability to be a highly reliable method of damage detection.

The use of Small Diameter Optical fibres acting as self-sensing fibres demonstrated the vast potential as an application for damage detection in composites. The ability to record tens of thousands of images and relate them to, changes in extension and load is a viable method of analysing damage. The use of analysis software such as National Instruments to monitor changes

in light intensity and flux with the changes of applied load can be regarded as a further advance in the use of self-sensing fibres to detect damage. Improving the number and quality of images whilst using alternative fibre types such as the Uncoated E-glass fibres and illumination methods will provide further opportunities to develop self-sensing fibres as a method of detecting damage in composites.

Comparison of the two methods has reinforced the use of piezoelectric sensors to record Acoustic Emissions as a comprehensive and accurate method of detecting damage within composite materials. Small Diameter Optical Fibres have demonstrated the wide range of possibilities and future applications that must be taken advantage of in the future. A combination of the methods as used when the recorded hits from Acoustic Emission testing triggered the camera to allow image analysis of the Small Diameter Optical fibres was very successful and an indication of the potential in combining the two methods. Further use of running the two methods in parallel will further the abilities of Acoustic Emission testing and increase and develop the use of Small Diameter Optical fibres to detect damage in composite materials.

8.0 FUTURE RESEARCH

The main area that has been highlighted for future research is the bonding of electrical resistance strain gauges and FBGs to the resin samples.

Work continuing investigations into developing techniques for surface-mounting / bonding FBG sensors with a known volume and thickness of adhesive has been reported in the paper: Finite element modelling of fibre Bragg grating strain sensors and experimental validation (Appendix 1). Similar testing procedures were implemented and results were correlated with Finite Element Analysis (FEA) to determine the effect of adhesive thickness on the strain measured by FBGs. It was experimentally and theoretically proven that the thickness of the adhesive has an effect on strain measurements by the FBG.

Following on from the research into the bonding of FBGs similar research into the bonding of electrical resistance strain gauges should be performed. By using a predetermined volume of solvent to ensure the strain gauge remains in place during the testing which would also be reproduceable for all samples could resolve the problem of the strain gauges peeling away from the sample surface during tensile testing.

9.0 APPENDICIES

Appendix 1

Finite element modeling of fibre Bragg grating strain sensors and experimental validation

Shoaib Malik, David Collins, Venkata Machavaram, Liwei Wang and Gerard F Fernando

Sensors and Composite Group, Department of Metallurgy and Materials,
University of Birmingham, Edgbaston, Birmingham, B15 2TT, UK

Abstract

Fiber Bragg grating (FBG) sensors continue to be used extensively for monitoring strain and temperature in and on engineering materials and structures. Previous researchers have also developed analytical models to predict the load-transfer characteristics of FBG sensors as a function of applied strain. The general properties of the coating or adhesive that is used to surface-bond the FBG sensor to the substrate has also been modeled using finite element analysis.

In this current paper, a technique was developed to surface-mount FBG sensors with a known volume and thickness of adhesive. The substrates used were aluminum dog-bone tensile test specimens. The FBG sensors were tensile tested in a series of ramp-hold sequences until failure. The reflected FBG spectra were recorded using a commercial instrument.

Finite element analysis was performed to model the response of the surface-mounted FBG sensors. In the first instance, the effect of the mechanical properties of the adhesive and substrate were modeled. This was followed by modeling the volume of adhesive used to bond the FBG sensor to the substrate. Finally, the predicted values obtained via finite element modeling were correlated to the experimental results. In addition to the FBG sensors, the tensile test specimens were instrumented with surface-mounted electrical resistance strain gauges.

Keywords: Damage detection, fibre reinforced composite, fibre Bragg gratings, optical fiber sensors

1. Introduction

The fibre-optic Bragg grating (FBG) sensors have been extensively used for single and multiplexed strain measurement in composite materials. Botsis (2004) reported fibre Bragg gratings sensors as tools to measure the internal elastic strain in various configurations such as bridging forces in center cracked composite, through the thickness strain distribution of a

laminated composite and residual stresses. He also highlighted two big issues associated with FBG as embedded strain sensors. Firstly, the obtained strains were actually strains that took place in the grating fibres, whilst the interest is strains of the host materials. Under a certain condition of loading and morphology around the FBG, the axial strain experienced by the gratings was assumed to be equal to the longitudinal strain in the vicinity of the surrounding host materials. Secondly, when the embedded FBGs were experienced in non-homogenous strain field, the interpretation of its response becomes complicated.

(Graham Duck, Guillaume Renaud, & Raymond Measures 1999) investigated the mechanical load transfer into an optical fibre due to a linear strain gradient. Both surface bonded and embedded cases were discussed in detail. The embedded configuration was modeled as an axisymmetric system consisting of two regions, representing the optical fibre sensor surrounded by the substrate material. The finite element analysis was performed to calculate the mechanical load transfer. Whereas the surface the surface mounted configuration was modeled as two stacked structural components bonded together with a thin adhesive layer.

[1]g.fernando@bham.ac.uk

1.	(McKenzie et al. 2000)	FBGs were used for health monitoring of bonded repair system.
2.	(R C Tennyson et al. 2001)	FBGs have been used to measure static and dynamic load on bridge decks and columns, including composite repairs for rehabilitation.
3.	(Hyun-Kyu Kang et al. 2003)	A simultaneous measurement of strain and temperature during and after cure of unsymmetrical cross-ply composite laminates was made using FBGs.
4.	(K.S.C.Kuanga et al. 2001)	FBGs have been embedded in different advanced composite. Distortion and broadening of the width of the FBG spectra were observed in several of the specimens. Due to strong non-uniformity of the strain field caused by local asymmetric loading of the sensor, pronounced splitting of the spectra into multiple peaks was noted for FBG sensors.
5.	(R.de Oliveira et al. 2004)	FBG were used for simultaneous detection of the strain and the acoustic emission due to damage in structures.
6.	(Hang-Yin Ling, Kin-Tak Lau, & Li Cheng 2004)	This work studied the dynamic strain measurement and delamination detection of composite structures using embedded multiplexed FBG sensors through experimental and theoretical approaches.
7.	(C.S.Shin & C.C.Chiang 2006)	Fatigue damage detection was done using FBG. It was found that the embedded fibre Bragg gratings have good potentials to detect the appearance of damage due to cyclic loading.
8.	(Jung-Ryul Lee & Hiroshi Tsuda 2005)	This work relates to development of novel fiber Bragg grating acoustic emission sensor for mechanical tests.
9.	(J.A.Guemes &	FBG were embedded in composite laminates. Peak splitting

	J.M.Mene´ ndez 2001)	phenomenon due to transverse loading was discussed.
10.	(J.Degrieck, W.De Waele, & P.Verleysen 2001)	FBGs were used to monitor strain in filament wound pressure vessel as embedded sensors, It was found that the measured strain from FBG is perfectly linear with applied load.
11.	(D.H.Kang, C.S.Hong, & C.G.Kim 2000)	This study investigated the fabrication of FBG with various grating lengths. A new method of fabricating FBG sensors with various grating lengths was devised.
12.	(Hiroaki Tsutsui et al. 2004)	In this work FBG sensors were used for detecting impact load and impact damage in stiffened composite panels.
13.	(K S C Kuang, W J Cantwell, & P J Scully 2002)	This paper describes the use of plastic optical fibre sensor for curvature and strain measurements in structures subjected to flexural and tensile loading conditions.
14.	(Rupali Suresh, SweeChuan Tjin, & Nam Quoc Ngo 2005)	This paper is about the development of a novel fibre Bragg grating (FBG) based shear force sensor for structural health monitoring of civil structure.
15.	(Kin-tak Lau et al. 2005)	FBGs were used to characterize delamination in glass fibre-reinforced epoxy (GF/EP) composite laminates using a static strain method. Three point bending test was employed and electric strain gauges were also used for comparison. Strain distribution of the beams was also calculated using finite element method. A corresponding change in FBG spectra due to delamination was achieved.
16.	(Sirkis & Lu 1995)	In their work they used a concentric cylinder geometry for modeling the inter-phase of embedded FBG in a unidirectional composite. Their paper addressed the properties of the adhesive used and its effect on the strain measurement, a reduction in transverse tensile and compressive strengths due to embedded FBGs was also reported.

Table 1: Fiber Bragg Gratings usage-a review

Summarizing the work presented in this paper is new in terms of change of adhesive thickness experimentally. FBG are in use for monitoring strain, temperature under different conditions (table 1), however the accuracy of the data obtained from them is still under research and consideration.

3. Experimental Procedures

3.1 Aluminum dumb-bell shaped samples:

Standard aluminum dumb-bell shaped samples were used. The sample is shown with dimensions in figure 1. Fibre Bragg gratings (FBG) were installed on one side and electric strain gauge on other side. These are more clearly shown and discussed at their relevant sections.

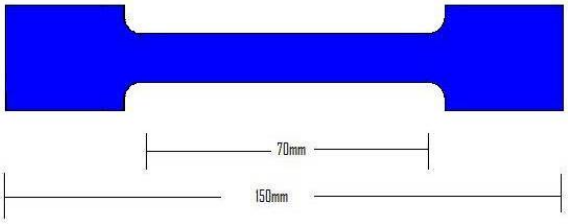

Figure 1: Aluminum dumb-bell shaped samples with dimensions.

3.2 Substrate ad Adhesive thickness

The step by step procedure for control of adhesive thickness is described as follows:

1. Firstly metal spacers of known height (50µm) are glued to metal sample.
2. FBG was then attached to the metal spacer first and secured in place using masking tape on both ends.
3. A silicon moat was built around the FBG to control the amount of adhesive. The silicon used was Silax from Replication Technologies Limited. A very fine layer of chemical was applied using a 0.5mm syringe. The moat was cured for 24 hours.
4. After the moat was cured the M-Bond 200 adhesive was carefully poured so that FBG was fully covered. It was then allowed to cure for one day at room temperature.
5. The numbers of metal spacers were varied in series of 2, 4, 8, 12 and 16 to achieve the desired heights of 100µm, 200 µm, 400 µm, 600 µm and 800 µm respectively on different samples.

All of this process is schematically illustrated in figure 2.

Figure (a):

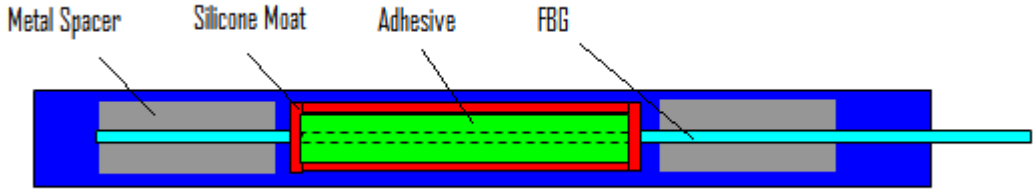

Figure (b):

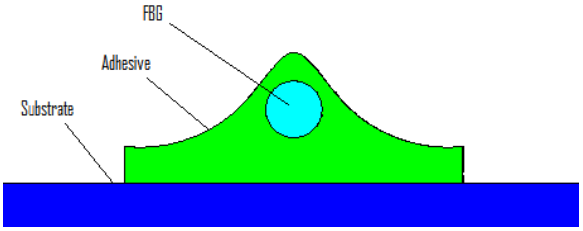

Figure (c):

Figures 2 (a, b and c) Schematic illustration: (a) Side view showing metal spacer and FBG lifted from the aluminum sample. (a) Top view showing moat and adhesive with FBG (c) Variable thickness (h of the adhesive on the aluminum substrate.

3.3 Electrical resistance strain gauges

General purpose electrical resistance strain gauges (ESRG) from Tokyo Sokki Kenkyujo Co. Ltd. were surface-mounted on the aluminum test specimen. The ESRG are attached on opposite side of sample where FBG is attached. Prior to bonding the strain gauges, the surface was degreased using iso-propanol (IPA) and dried. For the strain gauge data to be recorded ESRG were attached to the Cambridge Electronic Systems DMM4 electric strain gauge indicator. The surface of the contacts and strain gauge wires were first cleaned with M-Line resin solvent. The strain gauge wires were formed with a zigzag in them to allow the contacts and strain gauge to move apart during testing without breaking the circuit. The data was manually logged at different loads of 200N, 400N, 600N, 800N and 1000N. Figure 3 shows the aluminum sample and strain gauge.

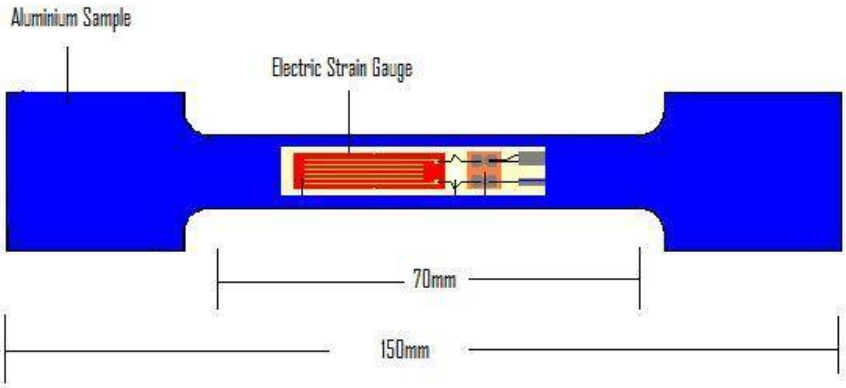

Figure 3: Schematic aluminum dumb bell shaped sample with electric strain gauge.

3.4 Fibre Bragg gratings

The Fibre Bragg Gratings (FBGs) were written onto a single mode fibre. Single mode fibres were chosen as there was less light loss when the fibre was bent during tensile tests. A 10 mega Joule laser shot 3000 shots at the fibre to write the grating. The Bragg wavelength of the FBG was recorded before it was attached. The reflection spectrum from the FBG was recorded using National Instruments Lab-view software in a ramp and hold method.

3.5 Tensile Testing

The test specimens were tensile tested on a screw-driven mechanical test machine (Instron 5566). The tests were performed at a cross-head displacement rate of 0.1 mm/min. The test specimen was loaded in a series of ramp-hold sequences where the load was increased from 200 to 1000N in steps of 200N. The strain data from the ERSG and the FBG were recorded during the hold-period. The data from the Instron machine was logged using Merlin software. The whole test setup was shown in figure 4.

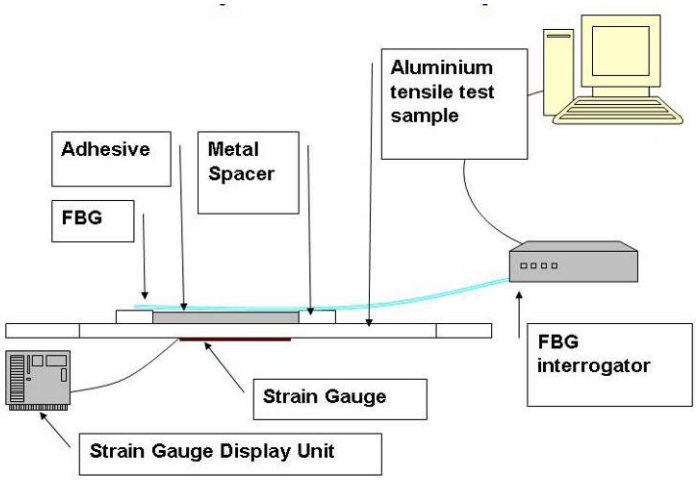

Figure 4: Test setup

3.6 Finite element analysis (FEA)

The commercial available code ANSYS version 11 was used to perform the FEA. Mesh was generated using element Solid-45 that has six degree of freedom at each of its six nodes. The boundary conditions are very close to the conditions during the test. The aluminum sample was constrained from one end and load is applied on the other end. Only half of the model is made due to symmetry. Figure 5 shows the FE model and the boundary conditions. Symmetry exists at the mid-plane FBG is modeled as a fiber with adhesive attached all around. Then the height of the FBG was altered as per experimental conditions.

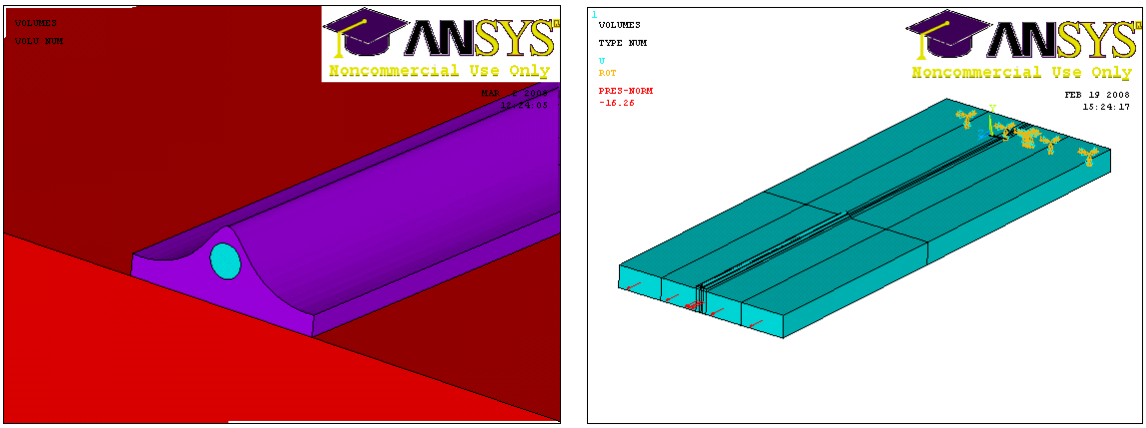

Figure 5: FE model (a) zoomed view with different colors representing distinct objects
(b) Boundary conditions: Red arrows shows the force applied on the face

4. Results and Discussions

4.1 Adhesive Thickness Control:

The micro graphs are shown in the figure 6 that shows the cross-sectional view of the FBG and adhesive with substrate. The height measured from the image was around 600µm.

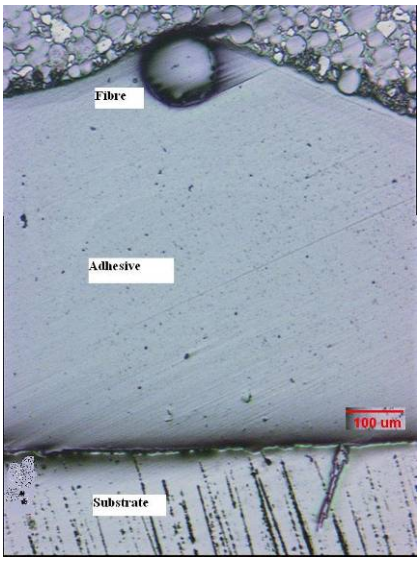

Figure 6: Microscopic view of fibre, adhesive and substrate showing the distance of fibre form substrate.

4.2 Tensile test Data

Typical load/extension and load/strain data for the aluminum sample with the surface-mounted strain sensors are shown in Figures 7 and 8. Figure 6 shows the graph when the metal sample is loaded till 1000N and then released. The arrow in the figure shows that the sample can still be loaded till failure. Figure 8 is ramp and hold graph for load and extension which shows that extension remains almost constant during holding the load.

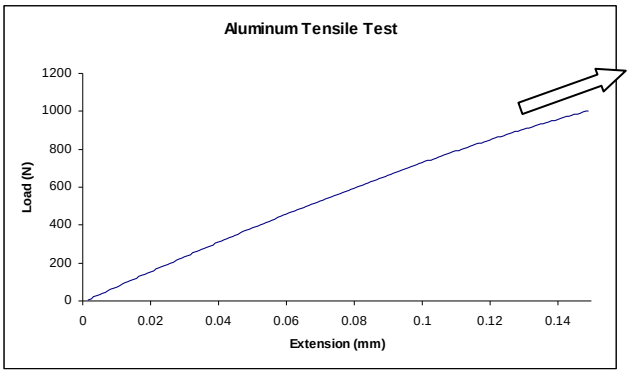

Figure 7: Typical load-extension trace for the aluminum tensile test

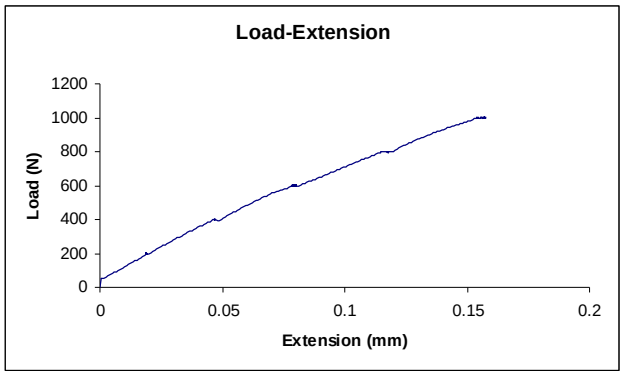

Figure 8: Load extension graph for ramp and hold

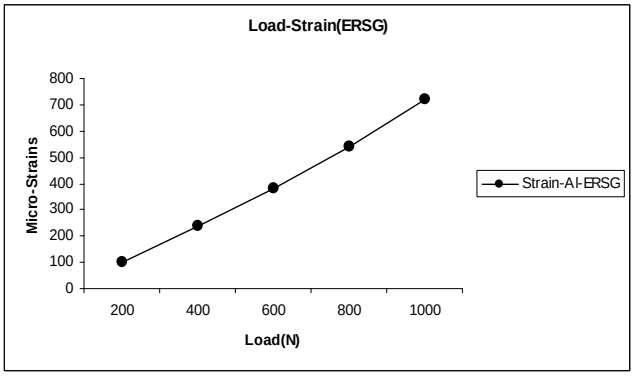

Figure 9: Load Strain (ERSG) graph.

4.3 Fibre Bragg Gratings (FBG)

The reflection spectrum of a free-and surface-mounted FBG is shown in Figure 10 and 11 respectively. Figure 11 shows the peak shift recorded at different load when the sample is tested. Table 2 summarizes the strain derived from FBG and electric strain gauges.

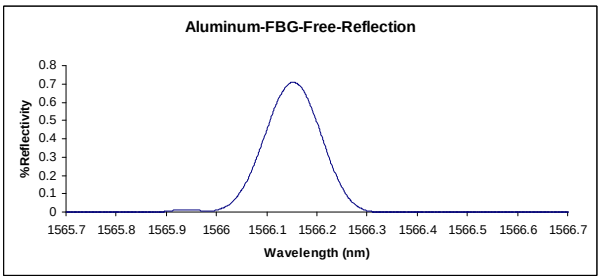

Figure 10: FBG spectra when FBG is in Free State.

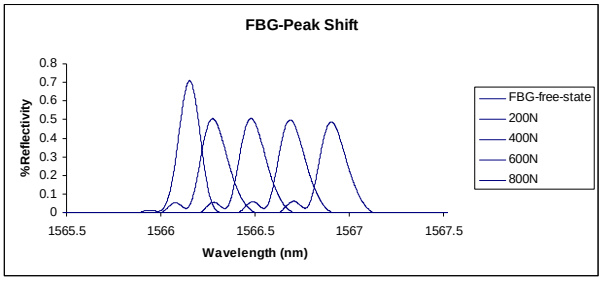

Figure 11: FBG peak shift at zero distance from substrate at different loads.

	FBG at zero distance		FBG at 100 µm distance		FBG at 200 µm distance		FBG at 400 µm distance		FBG at 600 µm distance		FBG at 800 µm distance	
Load (N)	Strain from FBG	Electric Strain Gauge	Strain from FBG	Electric Strain Gauge	Strain from FBG	Electric Strain Gauge	Strain from FBG	Electric Strain Gauge	Strain from FBG	Electric Strain Gauge	Strain from FBG	Electric Strain Gauge
200	144.93	103	128.02	113	121.01	109	115.47	118	106.27	142	77.17	141
400	306.76	238	277.77	260	269.53	260	251.94	271	240.51	274	168.82	263
600	458.94	384	417.86	416	408.1	427	405.68	405	396.35	460	214.04	391
800	599.84	543	556.34	595	547.34	581	544.93	521	520.47	637	367.27	492
1000	745.57	720	717.37	789	705.35	725	690.06	705	680.49	752	463.31	683

Table 2: FBG and Electric Strain gauge readings.

4.4 Finite Element Analysis (FEA)

The finite element analysis graphs were shown for an applied load of 200N. Figure 5(a) shows the displacement for the substrate, adhesive and fibre (not visible), the average stress on the substrate for an applied load of 200N is shown in figure 5 (b). Similarly figure 6 (a) and (b) shows the average stress graphs for adhesive and fibre respectively.
All the FEA results are summarized in Table 3.

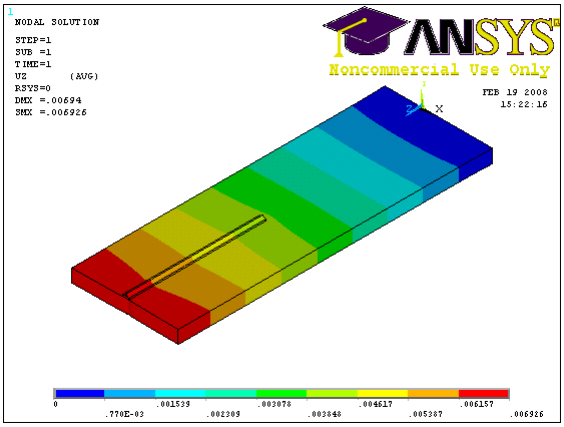

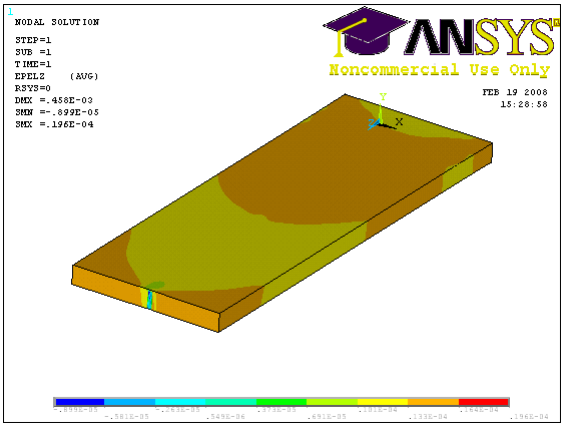

Figure 5: FE results (a) Full model (b) the substrate

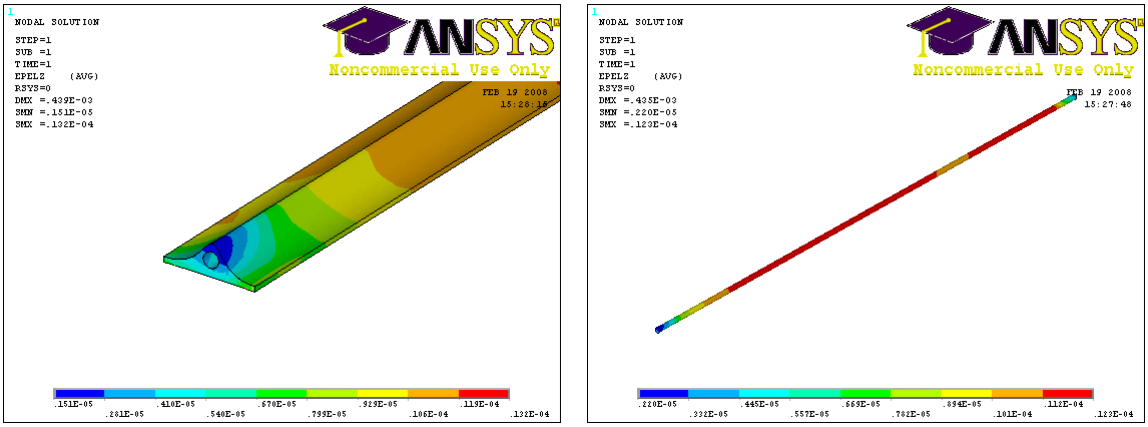

Figure 6: FE results (a) Adhesive (b) the fibre

		FBG at zero distance	FBG at 100 µm distance	FBG at 200 µm distance	FBG at 400 µm distance	FBG at 600 µm distance	FBG at 800 µm distance
Load (N)	Strain in aluminum	Strain in fibre	Strain from FBG	Strain from FBG	Strain from FBG	Strain from FBG	Strain from FBG
200	141.3	122.31	120.28	116.32	109.84	104.82	100.15
400	282.6	244.52	238.16	231.77	224.37	213.57	208.62
600	423.9	366.11	360.74	349.86	338.54	327.83	313.84
800	565.2	492.21	469.11	458.53	442.39	425.95	411.97
1000	706.5	650.33	601.93	591.36	569.58	549.9	534.33

Table 3: FEA results

4.5 Comparison of Results

The results from different modes of analysis were compared in figure 7 for FBG at 200µm and figure 8 for 800µm. It is clear that the strain values when the FBG is near substrate more closely matches with others.

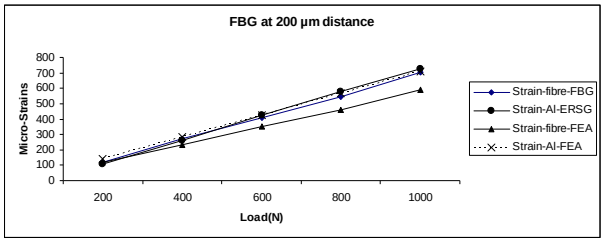

Figure 7: FBG at 200µm distance

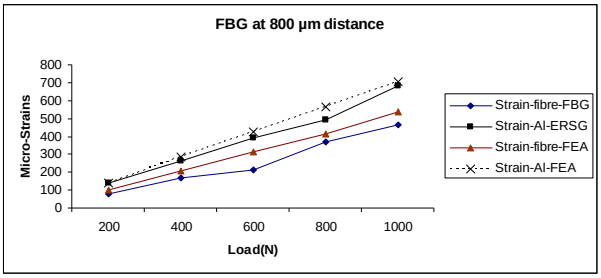

Figure 8: FBG at 800µm distance

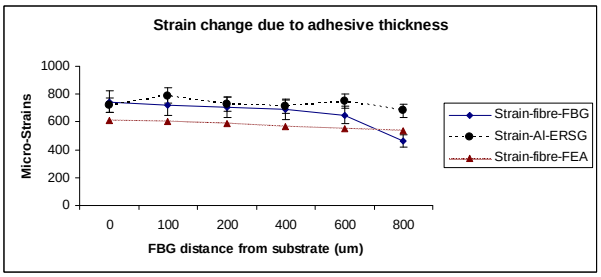

Figure 9: Strain change due to adhesive thickness

It is clear from the figure 9 that there is strain decay as the thickness of the adhesive increases. The FEA results prove the same phenomenon but the amount of decay is less than the actual experimental findings. This may be due to experimental errors or due to the amount of adhesive that is very hard to control practically.

5. Conclusions

It has been experimentally found and theoretically proved that the thickness of adhesive has its effect on the strain measured by FBG. The idea has been modeled using available FE code; the results from FEA are quite in favor of experimental findings.

6. Acknowledgments

The authors would like to acknowledge the support from EPSRC. A special word of thanks is for ANSYS Inc. USA for the software license at reduced academic rate.

7. References

1. C.S.Shin & C.C.Chiang 2006, "Fatigue damage monitoring in polymeric composites using multiple fiber bragg gratings", *International Journal of Fatigue 28*.

2. D.H.Kang, C.S.Hong, & C.G.Kim 2000, "Characteristics of Fiber Bragg Grating Sensors with Various Grating Lengths Embedded in Composite Materials", *Fiber Bragg Grating*.

3. Graham Duck, Guillaume Renaud, & Raymond Measures. The mechanical load transfer into a distributed optical fiber sensor due to a linear strain gradient: embedded and surface bonded cases. Smart Mater.Struct. 1999.
   Ref Type: Journal (Full)

4. Hang-Yin Ling, Kin-Tak Lau, & Li Cheng 2004, "Determination of dynamic strain profile and delamination detection of composite structures using embedded multiplexed fibre-optic sensors", *Composite Structures 66*.

5. Hiroaki Tsutsui, Akio Kawamata, Tomio Sanda1, 4., & NOBUO TAKEDA 2004, "Detection of impact damage of stiffened composite panels using embedded small-diameter optical fibers", *Meas.Sci.Technol.15*.

6. Hyun-Kyu Kang, Dong-Hoon Kang, Chang-Sun Hong, & Chun-Gon Kim1 2003, "Simultaneous monitoring of strain and temperature during and after cure of unsymmetric composite laminate using fibre-optic sensors", *Smart Mater.Struct.12*.

7. J.A.Guemes & J.M.Mene´ ndez 2001, "Response of Bragg grating fiber-optic sensors when embedded in composite laminates", *Composites Science and Technology 62*.

8. J.Degrieck, W.De Waele, & P.Verleysen 2001, "Monitoring of fibre reinforced composites with embedded optical fibre Bragg sensors, with application to filament wound pressure vessels", *NDT&E International 34*.

9. Jung-Ryul Lee & Hiroshi Tsuda 2005, "A novel fiber Bragg grating acoustic emission sensor head for mechanical tests", *Scripta Materialia 53*.

10. K S C Kuang, W J Cantwell, & P J Scully 2002, "An evaluation of a novel plastic optical fibre sensor for axial strain and bend measurements", *Meas.Sci.Technol.13*.

11. K.S.C.Kuanga, , .P.Whelanb, .Kenny, .J.Cantwella, & .R.Chalkera 2001, "Embedded fibre Bragg grating sensors in advanced composite materials", *Composites Science and Technology 61*.

12. Kin-tak Lau, Hang-Yin Ling, Li Cheng, & Wei Jin 2005, "Utilization of embedded optical fibre sensors for delamination characterization in composite laminates using a static strain method", *SMART MATERIALS AND STRUCTURES*.

13. McKenzie, R.Jones, I.H.Marshall, & S.Galea. Optical fibre sensors for health monitoring of bonded repair systems. Composite Structures 50 . 2000. Elsevier Science Ltd.
Ref Type: Journal (Full)

14. R C Tennyson, A A Mufti, S Rizkalla, G Tadros, & B Benmokrane 2001, "Structural health monitoring of innovative
bridges in Canada with fiber optic sensors", *SMART MATERIALS AND STRUCTURES 10*.

15. R.de Oliveira, O.Fraz~ao, J.L.Santos, & A.T.Marques 2004, "Optic fibre sensor for real-time damage detection in smart composite", *Computers and Structures 82*.

16. Rupali Suresh, SweeChuan Tjin, & Nam Quoc Ngo 2005, "Application of a new fiber Bragg grating based shear force sensor for monitoring civil structural components", *Smart Mater.Struct.14*.

17. Sirkis, J. S. & Lu, I. P. 1995, "On interphase modeling for optical fiber sensors embedded in unidirectional composite systems", *Journal of Intelligent Material Systems and Structures*, vol. 6, no. 2, pp. 199-209.

10.0 LIST OF REFERENCES

Abrya JC, Bocharda S, Chateauminois A, Salvia M and Giraud G. (1999) In situ detection of damage in CFRP laminates by electrical resistance measurements. *Composites Science and Technology*, 59, 92-935

Angelidis N and Irving PE. (2007) Detection of impact damage in CFRP laminates by means of electrical potential techniques. *Composites Science and Technology*, 67, 594–604

Angelidis N, Khemiri N and Irving PE. (2005) Experimental and finite element study of the electrical potential technique for damage detection in CFRP laminates. *Smart Mater. Struct*. 14, 147–154

Angelidis N, Wei CW and Irving PE. (2004) The electrical resistance response of continuous carbon fibre composite laminates to mechanical strain. *Composites: Part A*, 35, 1135–1147

Avdelidis NP, Hawtin BC and Almond BN. (2003) Transient thermography in the assessment of defects of aircraft composites. *NDT&E International*, 36, 433–439

Aymerich F & Meili S (2000) Ultrasonic evaluation of matrix damage in impacted composite laminates. *Composites: Part B*, 31, 1–6

Barre S. (1994) On the use of acoustic emission to investigate damage mechanisms in glass–fibre-reinforced polypropylene. *Composites Science Technology*, 52, 369–76.

Belbin GR. (1985) Thermoplastic structural composites a challenging opportunity. *Materials & Design*, 6, 9-17

Burke SK, Cousland SM and Scala CM. (1994) Non-destructive characterisation of advanced composite materials. Mater Forum, 18, 85–109.

Cantwell W J. and Morton J. (1985) Detection of Impact Damage in CFRP Laminates *Composite Structures*, 3, 241-257

Chang SM, Muramatsu H, Nakamura C and Miyake J. (2000) The principle and applications of piezoelectric crystal sensors. *Materials Science and Engineering C*, 12, 111–123

Chen R, Bradshaw T, Burns J, Cole P, Jarman P, Pedder D, Theobald R and Fernando GF. (2006) Linear location of acoustic emission using a pair of novel fibre optic sensors. *Meas. Sci. Technology*. 17, 2313–2318

Cole MJ, Loh WH, Laming RI, Zervas MN and Barcelos S. (1995) Moving fibre/phase mask-scanning beam technique for enhanced flexibility in producing fibre gratings with uniform phase mask. *Electronic Letters*, 31, 1488-1490.

Cole PT. (1985) Using Acoustic Emission (AE) to Locate and Identify Defects in Composite Structures. *Composite Structures*, 3, 59-267

Dong L and Mistry J. (1998) Acoustic emission monitoring of composite cylinders. *Composite Structures*, 40, 43-53,

Drouillard TF. (1996) A history of acoustic emission. *Journal of Acoustic Emission*, 14, 1-34

Dunham GH and Edie DD. (1992) Model of stabilisation for PAN based carbon fibre precussor bundles. *Carbon*, 30, 435-450.

Edie DD. (1997) The effect of processing on the structure and properties of carbon fibre. *Carbon*, 36, 345-362

Feldman D. (1990) Some considerations on thermosetting polymers as matrices for composites. *Programme of Polymer Science*, 15, 603-628

Ford RA. (2004)Semi-finished thermoplastic composites-realising their potential. *Materials and Design*, 25, 631–636

Gabriel O, Shonaike and Matsuo T. (1995) Fabrication and mechanical properties of glass fibre reinforced thermoplastic elastomer composite. *Composite Structures*, 32, 445-451

Gautschi, G. (2002) Piezoelectric Sensorics Force, Strain, Pressure, Acceleration and Acoustic Emission Sensors, Materials and Amplifiers. *Springer,* 200

Giraldia de M. ALF, Bartolia JR, Velascob JI and Mei LHI. (2005)Glass fibre recycled poly(ethylene terephthalate) composites: mechanical and thermal properties. *Polymer Testing*, 24, 507–512

Groot PJ, Wijnen PA & Janssen BF. (1995) Real-time frequency determination of acoustic emission for different fracture mechanisms in carbon/epoxy composites. *Composites Science Technology*, 55, 405–412

Hare DA and Moore, Sr. TC. (2000) Characteristics of Extrinsic Fabry-Perot Interferometric (EFPI) Fiber-Optic Strain Gages. *NASA/TP-2000-210639*

Harris B. (1999) "Engineering Composite Materials" 2nd Ed. *OM Communications Ltd, London*.

Haselbach W and Lauke B. (2003) Acoustic emission of debonding between fibre and matrix to evaluate local Adhesion. *Composites Science and Technology*, 63, 2155–2162

Hayes S, Liu T, Brooks D, Monteith S, Ralph B, Vickers S and Fernando GF. (1997) In-situ self-sensing fibre reinforced composites. *Smart Mater. Struct.* 6, 432–440.

Hill KO & Meltz G. (1997) Fibre Bragg Grating and Technology Fundamentals and Overview *Journal of Light wave Technology*, 15, 1263-1276

Hill KO, Fujii F, Johnson DC and Kawasaki BS. (1978) Photosensitivity on optical fiber waveguides: application to reflection filter fabrication *Applied Physics Letters*, 32, 647–649.

Hill KO, Malo B, Bilodeau F, Johnson DC, and Albert J. (1993) Bragg gratings fabricated in monomode photosensitive optical fibre by U.V exposure through a phase mask. *Applied Physics Letters*, 62, 566-568

Hofer B. (1987) Fibre optic damage detection in composite structures. *Composites*, 18, 309-316

http://ir.gknplc.com/presentations/pdfs/aerospace_graham_chisnall.pdf. 30/11/2007 15:01:00

Huang NC and Liu XY. (1994) Debonding and fiber pull-out in reinforced composites. *Theoretical and Applied Fracture Mechanics*, 21, 157-176

Hull D and Clyne TW. (1996) An Introduction to Composite Materials. *Cambridge University Press*, 9-36

Hung YY. (1996) Shearography for Non-destructive Evaluation of Composite Structures. *Optics and Lasers in Engineering*, 24, 161-182

Hung YY. (1999) Applications of digital shearography for testing of composite structures. *Composites: Part B*, 30, 765–773

Hunga YY and Ho HP. (2005) Shearography: An optical measurement technique and applications. *Materials Science and Engineering*, 49, 61–87

Imieli´nskaa K, Castaingsc M, Wojtyrab R, Harasa J, Le Clezioc E and Hostenc B. (2004) Air-coupled ultrasonic C-scan technique in impact response testing of carbon fibre and hybrid: glass, carbon and Kevlar/epoxy composites. *Journal of Materials Processing Technology*, 157–158, 513–522

Introduction to Acoustic Emission Testing. http://www.ndt-ed.org/EducationResources/CommunityCollege/Other%20Methods/AE/AE_Index.htm. 14/03/2007 10:46

Johnson M and Gudmundson P. (2001) Broad-band transient recording and characterization of acoustic emission events in composite laminates. *Composites Science and Technology*, 61, 1367–1378

Kister G, Ralph B and Fernando GF. (2004) Damage detection in glass fibre-reinforced plastic composites using self-sensing E-glass fibres. *Smart Mater. Struct*. 13, 1166–1175

Kister G, Wang L, Ralph B and Fernando GF. (2003) Self-sensing E-glass fibres. *Optical Materials*, 21, 713–727

Lafarie-Frenot MC, Henaff-Gardin C and Gamby D. (2001)Matrix cracking induced by cyclic ply stresses in composite laminates. *Composites Science and Technology*, 61, 2327–2336

Leng J. and Asundi A. (2003) Strucural health monitoring of smart composite materials by using EFPI and FBG sensors. *Sensors and Actuators*, 103, 330-340

Leps G, Bohse J and May M. (1986) Acoustic emission on rubber-modified and filled thermoplastic materials. *NDT International Volume*, 19, 387-394

Marin-Francha P, Martin T, Tunnicliffe DC and Das-Gupta DK. (2002) PTCa/PEKK piezo-composites for acoustic emission detection. *Sensors and Actuators A*, 99, 236–243

Marschall K and Gautschi GH. (1994) In-Process Monitoring with Piezoelectric Sensors. *J. Mater. Process. Technol*. 44, 345-352

McConnell VP. (2000) Application of composites in sporting goods. *Comprehensive Composite Materials*, 6, 787-809

Meyer GW, Pak SJ, Lee YJ and McGrath JE. (1995)New high-performance thermosetting polymer matrix material systems. *Polymer*, 36, 2303-2309

Mimura K and Ito H. (2002) Characteristics of epoxy resin cured with in situ polymerized curing agent. Polymer, 43, 7559–7566

Moulson AJ and Herbert JM. (1992) Electroceramics: Materials. Properties. Applications. *Chapman & Hall*

Nam-Jeong L and Jang J. (2000) The effect of fibre-content gradient on the mechanical properties of glass-fibre-mat/polypropylene composites. *Composites Science and Technology*, 60, 209-217

Neffgen B. (1985) Epoxy resins in the building industry - 25 years of experience. *The International Journal of Cement Composites and Lightweight Concrete*, 7, 253 – 260

Okafor AC, Otieno AW, Dutta A and Rao VS. (2001) Detection and characterisation of high-velocity impact damage in advanced composite plates using multi-sensing techniques. *Composite Structures*, 54, 289-297

Pan N, Su Z, Ye L, Zhou L and Lu Y. (2006)A quantitative identification approach for delamination in laminated composite beams using digital damage fingerprints (DDFs). *Composite Structures*, 75, 559–570

Pevzner P, Weller T, and Berkovits A. (2005) A novel fiber Bragg grating acoustic emission sensor head for mechanical tests. *Scripta Materialia,* 53, 1181–1186

Pevzner P, Weller T, and Berkovits A. (2005) Use of heat emitted by broken optic fibers: A new approach for damage detection in composites. *Engineering Failure Analysis*, 12, 860–874

Poumellec B, Niay D. M., and Bayon J.F. (1996) The UV-induced refractive index grating in Ge: SiO2 preforms: Additional CW experiments and the macroscopic origin of the change in index. *J. Phys. D, Appl. Phy*., 29, 1842–1856.

Prakash, R. (1980) Non-destructive testing of composites. *Composites*, 11, 217-224

Rae PJ, Brown EN and Orler EB. (2007)The mechanical properties of poly (ether-ether-ketone) (PEEK) with emphasis on the large compressive strain response. *Polymer,* 48, 598-615

Ramirez-Jimenez CR, Papadakis N, Reynolds N, Gan TH, Purnell P & Pharaoh M. (2004) Identification of failure modes in glass/polypropylene composites by means of the primary frequency content of the acoustic emission event. *Composites Science and Technology,* 64, 1819–
1827

Rao YJ, Yuan SF, Zeng XK, Lian DK, Zhu Y, Wang JP, Huang SL, Liu TY, Fernando GF, Zhang L and Bennion I. (2002) Simultaneous strain and temperature measurement of advanced 3-D braided composite materials using an improved EFPI/FBG. *Optics and Lasers in Engineering,* 38, 557–566

Schuler R, Joshi SP and Schulte K. (2001) Damage detection in CFRP composites using electrical conductivity mapping. *Composite Science and Technology*, 61, 921-930

Seo DC and Lee JL (1999) Damage detection of CFRP laminates using electrical resistance measurement and neural network. *Composite Structures*, 47, 525-530

Shen L, Li J, Liaw BM, Delale F and Chung JH. (2006) Modelling and Analysis of the Electrical Resistance Measurement of Carbon Fiber Polymer-Matrix Composites. *Composite Science and Technology*, 10.1016/j.compscitech.2006.12.020

Short D & Summerscales J. (1984) Amplitude distribution acoustic emission signatures of unidirectional fibre composite hybrid materials. *Composites,* 15, 200-207

Short GJ, Guild FJ and Pavier MJ. (2002) Delaminations in flat and curved composite laminates subjected to compressive load. *Composite Structures*, 58, 249–258

Stenzenberger HD. (1993) Recent developments of thermosetting polymers for advanced composites. *Composite Structures*, 24, 219-231

Sung-Choong W & Nak-Sam C. (2007) Analysis of fracture process in single-edge-notched laminated composites based on the high amplitude acoustic emission events. *Composites Science and Technology*, 67, 1451–1458

Surgeon M and Wevers M. (1999) One sensor linear location of acoustic emission events using plate wave theories. *Materials Science and Engineering A*, 265, 254–261

Taylor HF. (2002) Fiber optic sensors based upon the Fabry–Perot interferometer, *Fiber Optic Sensors*, 41-71

Todoroki A, Tanaka Y and Shimamura Y. (2002) Delamination monitoring of graphite/epoxy laminated composite plate of electric resistance change method. *Composites Science and Technology*, 62, 1151–1160

Todoroki A, Tanaka Y and Shimamura Y. (2005) Electrical resistance change method for monitoring delaminations of CFRP laminates: effect of spacing between electrodes. *Composites Science and Technology*, 65, 37–46

Toh SL, Chau FS, Shim VPW, Tay CJ and Shang HM. (1990) Applications shearography in non-destructive testing of composite plates. *Journal of Materials Processing Technology*, 23, 267-275

Toubal L, Karama M and Lorrain B. (2006) Damage evolution and infrared thermography in woven composite laminates under fatigue loading. *International Journal of Fatigue*, 28, 1867–1872

Tsuda H and Lee JR. (2007) Strain and damage monitoring of CFRP in impact loading using a fiber Bragg grating sensor system. *Composites Science and Technology*, 67, 1353–1361

Tsuda H. (2006) Ultrasound and damage detection in CFRP using fiber Bragg grating sensors. *Composites Science and Technology*, 66, 676–683

Wang L, Kister G, Ralph B, Talbot JDR and Fernando GF. (2004) Conventional E-glass fibre light guides: self-sensing composite based on sol–gel cladding. *Smart Mater. Struct.* 13, 73–81

Wang S and Chung DDL. (2006) Self-sensing of flexural strain and damage in carbon fiber polymer-matrix composite by electrical resistance measurement. *Carbon*, 44, 2739–2751

Wevers M. (1997) Listening to the sound of materials: acoustic emission for the analysis of material behaviour. *NDT&E International*, 30, 99-106,

www.netcomposites.com/?st=1+sc=1+s=12, 26/05/2007 20:06

Yeun-Ho Y, Jin-Ho C, Jin-Hwe K and Dong-Hyun K. (2006) A study on the failure detection of composite materials using an acoustic emission. *Composite Structures*, 75, 163–169

Zhang Z, Breidt C, Chang L and Friedrich K. (2004) Wear of PEEK composites related to their mechanical performances. *Tribology Internationa*l, 37, 271–277

Zhou G and Sim LM. (2002) Damage detection and assessment in fibre-reinforced composite structures with embedded fibre optic sensors—review. *Smart Mater. Struct*. 11, 925-939